Development and applications of a new database of soil physical properties for the Kansas Mesonet

by

Nathaniel Parker

B.Sc., Kwame Nkrumah University of Science and Technology, Ghana, 2014
M.Sc., Ghent University, Belgium, 2017

AN ABSTRACT OF A DISSERTATION

submitted in partial fulfillment of the requirements for the degree

DOCTOR OF PHILOSOPHY

Department of Agronomy
College of Agriculture

KANSAS STATE UNIVERSITY
Manhattan, Kansas

2021

Abstract

In this dissertation, we investigated three central questions to improve mesoscale soil moisture monitoring using the Kansas Mesonet. Our first question was: i) Can we improve the accuracy of soil moisture measurements and related soil water processes by characterizing site-specific soil physical properties? We developed a comprehensive database of site- and depth-specific soil physical properties for the Kansas Mesonet. We analyzed a total of 320 soil samples collected from four sensor depths at 40 stations of the Kansas Mesonet monitoring soil moisture and soil temperature. The resulting database comprises 14 site and depth-specific soil hydraulic properties and three soil thermal properties for 40 stations of the Kansas Mesonet. In addition, the database of soil physical properties allowed us to identify an improved calibration model for the soil moisture sensors used by the Kansas Mesonet. Our second question was: ii) Can we re-construct precipitation events using changes in rootzone soil water storage to improve operational quality control and quality assurance of precipitation observations in mesoscale networks? Co-located hourly soil moisture and precipitation observations from May 2017 to December 2020 at 30 Kansas Mesonet stations were analyzed to test whether the rootzone can be used as a natural rain gauge. Precipitation events were back-calculated from soil moisture as the sum of hourly differences in profile soil water storage. The proposed soil moisture approach correctly flagged 82% of the precipitation events. Precipitation amounts and timing obtained from in situ soil moisture were more accurate than using precipitation observations from the nearest station when the nearest neighbor station was at a distance of >15 km. Our third question was: iii) Are traditional and modern laboratory methods for measuring soil water retention curves compatible? We compared water retention curves developed for a total of 24 soil samples from five different textural classes using traditional instrumentation (tension tables, pressure

cells, and pressure plate) and modern instrumentation (precision tensiometers and a dew point water potential meter). Both traditional and modern methods resulted in similar water contents at saturation, field capacity, and permanent wilting point, but the traditional method had residual water content 125% higher than modern methods.

Development and applications of a new database of soil physical properties for the Kansas Mesonet

by

Nathaniel Parker

B.Sc., Kwame Nkrumah University of Science and Technology, Ghana, 2014
M.Sc., Ghent University, Belgium, 2017

A DISSERTATION

submitted in partial fulfillment of the requirements for the degree

DOCTOR OF PHILOSOPHY

Department of Agronomy
College of Agriculture

KANSAS STATE UNIVERSITY
Manhattan, Kansas

2021

Approved by:

Major Professor
Dr. Andres Patrignani

Copyright

© Nathaniel Parker 2021.

Abstract

In this dissertation, we investigated three central questions to improve mesoscale soil moisture monitoring using the Kansas Mesonet. Our first question was: i) Can we improve the accuracy of soil moisture measurements and related soil water processes by characterizing site-specific soil physical properties? We developed a comprehensive database of site- and depth-specific soil physical properties for the Kansas Mesonet. We analyzed a total of 320 soil samples collected from four sensor depths at 40 stations of the Kansas Mesonet monitoring soil moisture and soil temperature. The resulting database comprises 14 site and depth-specific soil hydraulic properties and three soil thermal properties for 40 stations of the Kansas Mesonet. In addition, the database of soil physical properties allowed us to identify an improved calibration model for the soil moisture sensors used by the Kansas Mesonet. Our second question was: ii) Can we re-construct precipitation events using changes in rootzone soil water storage to improve operational quality control and quality assurance of precipitation observations in mesoscale networks? Co-located hourly soil moisture and precipitation observations from May 2017 to December 2020 at 30 Kansas Mesonet stations were analyzed to test whether the rootzone can be used as a natural rain gauge. Precipitation events were back-calculated from soil moisture as the sum of hourly differences in profile soil water storage. The proposed soil moisture approach correctly flagged 82% of the precipitation events. Precipitation amounts and timing obtained from in situ soil moisture were more accurate than using precipitation observations from the nearest station when the nearest neighbor station was at a distance of >15 km. Our third question was: iii) Are traditional and modern laboratory methods for measuring soil water retention curves compatible? We compared water retention curves developed for a total of 24 soil samples from five different textural classes using traditional instrumentation (tension tables, pressure

cells, and pressure plate) and modern instrumentation (precision tensiometers and a dew point water potential meter). Both traditional and modern methods resulted in similar water contents at saturation, field capacity, and permanent wilting point, but the traditional method had residual water content 125% higher than modern methods.

Table of Contents

List of Figures x
List of Tables xiv
Acknowledgments xvii
Chapter 1 - General Introduction 1
References 5
Chapter 2 - A New Database of Soil Physical Properties for the Kansas Mesonet 9
Abstract 9
Introduction 10
Materials and Methods 11
Field sampling campaign 11
Soil hydraulic properties 13
General soil physical properties 15
Soil thermal properties 16
Soil chemical properties and soil color 17
In situ validation of soil moisture 18
Results and Discussion 20
General soil physical properties 20
Soil hydraulic properties 23
Soil thermal properties 30
Soil chemical properties and soil color 34
In situ validation of soil moisture 37
Conclusions 40
References 42
Chapter 3 - Reconstructing Precipitation Events Using Co-located Soil Moisture Information 47
Abstract 47
Introduction 48
Materials and Methods 52
Concept and assumptions 52
Precipitation and soil moisture dataset 54

Computation of changes in soil water storage 56
Comparison with nearest-neighbor interpolation approach 59
Results and Discussion 59
Testing of model assumptions 59
Distribution of precipitation events 63
Qualitative analysis 64
Quantitative analysis 67
Conclusions 77
Acknowledgments 78
References 79
Chapter 4 - Revisiting Laboratory Methods for Measuring Soil Water Retention Curves 86
Abstract 86
Introduction 87
Materials and methods 90
Soil sampling 90
Laboratory soil water retention measurements 90
Results and Discussion 95
General soil physical properties 95
Osmotic potential and verified matric potential of pressure plate-equilibrated samples at -1500 kPa 97
Traditional versus modern techniques 99
Soil hydraulic parameters 101
Plant available water capacity 103
Conclusions 106
References 107
Chapter 5 - General Conclusions 110
Appendix A - Supplemental Materials for Chapter 2 113
Appendix B - Supplemental Materials for Chapter 3 115

List of Figures

Figure 2.1 Map showing the location of the 62 stations of the Kansas Mesonet as of December 2020. Filled triangles represent the 40 stations with soil moisture sensors that were sampled in this study and open circles represent the remaining stations without soil moisture sensors. 12

Figure 2.2 Flowchart of laboratory measurements in the development of the soil physical properties database for the Kansas Mesonet. The yellow-colored boxes represent the points at which thermal properties were measured. Note that some variables like field soil moisture and effective soil saturation are measured at the beginning of the process, but can only be determined near the end of the process when information about the oven-dry mass of the sample is available. 13

Figure 2.3 Distribution of USDA soil textural classes of the collected samples across 40 stations of the Kansas Mesonet. Abbreviated textural classes are sand (S), loamy sand (L S), sandy loam (S L), sandy clay loam (S C L), sandy clay (S C), clay loam (C L), silt loam, silty clay (Si C), and silty clay loam (Si C L). 20

Figure 2.4 Graphical correlation matrix of a selected number of measured soil physical properties for the Kansas Mesonet (N= 160). 27

Figure 2.5 Measured soil water retention curve (markers) and fitted van Genuchten soil water retention model (lines) for the soil profiles at the Overbrook, Ashland Bottoms, Rossville, and Lake City stations. Abbreviated textural classes are silty clay (Si Clay), silty clay loam (Si C L), silt loam (Si L), and sandy loam (Sandy L). The highest RMSE of 0.022 cm^3 cm^{-3} was observed at 20 cm depth in the Lake City station and the lowest RMSE of 0.002 cm^3 cm^{-3} was observed at 5 cm depth in the Ashland Bottoms station. 29

Figure 2.6 Measured versus predicted A) thermal conductivity using the Johansen (1975) model and B) volumetric heat capacity using De Vries (1963) additive model for the 320 soil samples collected at stations of the Kansas Mesonet. The thermal conductivity predictions were made using a total of 428 observations (at -33 and -70 kPa) and the volumetric heat capacity predictions were made using a total of 1107 observation points (at saturation, -33 kPa, -70 kPa, and oven-dryness). The saturation and oven-dry thermal conductivity values were not included in Figure 2.6A because they represent the maximum and minimum points

used in the normalization of the Johansen model. Positive MBE represents overestimation and negative bias represents underestimation by model. 32
Figure 2.7 Pattern of soil organic matter content at the top 5 cm depth across the state of Kansas. The figure shows increasing soil organic matter across the state of Kansas from west to east. 34
Figure 2.8 Relationship between soil organic matter and soil color expressed in the CIELAB color space in terms of light- and darkness (L^*) under A) wet conditions (L^*_{wet}) and B) Oven-dry conditions (L^*_{dry}). The lower the L^* value, the darker the soil color. Both figures show that soil color gets darker as organic matter content increases, regardless of the soil moisture status. 36
Figure 2.9 Observed volumetric soil water content (θ) based on the thermogravimetric method versus θ of the CS655 soil water reflectometers at the time of sampling obtained using A) the factory default calibration equation of Topp et al. (1980), and separate laboratory sensor calibration coefficients derived in an independent study based on the linear models by B) Ledieu et al. (1986), C) Evett et al. (2005), and D) Kargas and Soulis (2019). The dashed line represents the 1:1 line. 38
Figure 3.1 Distribution of the 47 stations of the Kansas Mesonet considered in this study. Filled triangles represent stations with precipitation and soil moisture records (N=30) and open circles represent stations with precipitation and without soil moisture records (N=17) that were considered for the nearest neighbor approach. 55
Figure 3.2 Example illustrating changes in profile soil moisture during A) 5-hour precipitation event at the Parsons station of the Kansas Mesonet from 14 May 2018 23:00 to 15 May 2018 03:00 Central Standard Time (CST), and B) the corresponding cumulative precipitation measured by the station pluviometer (P_{obs}) and the cumulative precipitation reconstructed using changes in soil water storage (ΔS). Times (t) are expressed in hours relative to the start of the precipitation event. Soil water content at time t = -1 h represents the water content of the soil profile at an hour before the start of the precipitation event and t = 6 h represents the soil water content at an hour after the end of the precipitation event. 57
Figure 3.3 Distribution of A) relative humidity and B) vapor pressure deficit precipitation event for 2497 hourly precipitation events across 30 stations of the Kansas Mesonet from 15 May 2017 to 31 December 2020. C) Example of the lower vapor pressure deficit (VPD) during a

precipitation event recorded at the Hays station of the Kansas Mesonet on 19 June 2020. Times are reported in Central Standard Time (CST). 61
Figure 3.4 A) histogram of precipitation amount, and B) histogram of precipitation intensity for the 2497 precipitation events in the resulting dataset across 30 stations of the Kansas Mesonet from 15 May 2017 to 31 December 2020. Rainfall intensity was classified as light (rainfall intensity <2.5 mm h^{-1}), moderate (rainfall intensity ≥2.5 to <10 mm h^{-1}), and heavy (rainfall intensity >10 mm h^{-1}) according to the classification by the World Meteorological Organization. The x-axes of the figures were truncated for visual clarity. 63
Figure 3.5 Examples of precipitation events that were effectively captured by the proposed approach based on changes in soil water storage, but that were missed due to a malfunctioning pluviometer at A) the Gypsum station on 22 April 2019 00:00 to 03:00 CST and at B) the Lake City station for July. Both figures comprise hourly results that have been aggregated into daily intervals for visual clarity. We also retrieved the precipitation total for the same dates obtained from the U.S. National Weather Service (NWS) 4-km multi-sensor gridded product that in both cases provided an independent precipitation observation. P_{obs} is the observed precipitation at the station and ΔS is the observed change in soil profile water storage at the station. Rain gauges in both stations were fixed during a time without rainfall. 66
Figure 3.6 Comparison of rain gauge observation to predicted precipitation using A) change in soil water storage for all precipitation events (N = 2497), B) change in soil water storage for precipitation events lower than the antecedent soil water deficit (N = 1716), and C) nearest neighbor interpolation for precipitation events exceeding 7.6 mm from 15 May 2017 to 31 December 2020. The soil moisture approach used precipitation events across 30 stations monitoring soil moisture while the nearest neighbor approach used 2497 precipitation events across all 47 stations of the Kansas Mesonet, including stations with and without soil moisture sensors. Dash lines represent the 1:1 line and solid lines represent fitted linear regressions (in both cases the linear model had $p<0.001$). 67
Figure 3.7 Example of precipitation underestimation by the proposed approach based on changes in soil water storage caused by near-saturation conditions due to several consecutive precipitation events at the Ottawa 2SE station. Pobs is the observed precipitation and ΔS is the change in soil profile water storage. 69

Figure 3.8 Time series of observed (Pobs) and predicted cumulative precipitation from changes in soil water storage (ΔS) (A and C) and the corresponding profile soil water content dynamics (B and D) for overestimated precipitation events. The top row illustrates an example for a sandy loam at the Lake City station from 5 July 2019 22:00 to 6 July 2019 03:00 CST and the bottom row illustrates an example for a silty clay loam soil at the Ashland Bottoms station from 29 June 2017 04:00 to 29 June 2017 09:00 CST. Soil water content at time t = -1 h represents the water content of the soil profile at an hour before the start of the precipitation event and t = 7 h represents the soil water content at an hour after the end of the precipitation event. 71
Figure 3.9 Timing of precipitation events within the same storm for a station of the Kansas Mesonet with close nearest neighboring stations (A, Ashland Bottoms) and a station with distant nearest neighboring stations (B, Woodson). The figure highlights that changes in soil water storage may constitute a better alternative to estimate both the amount and timing of precipitation events in stations with distant nearest neighbors compared to using information from nearest neighboring stations. Times are reported in Central Standard Time (CST). ... 76
Figure 4.1 Representative of measured (symbols) and fitted (lines) soil water retention curves determined using the combination of suction table, pressure cell, and pressure plate (traditional) and a combination of mini-tensiometers and dewpoint potential meter (modern) laboratory techniques in A) 10AB silty clay loam, B) 07W silty clay, C) 09W clay, D) 01W clay loam, and E) 15R sandy loam. Triangular symbols and solid lines represent the traditional techniques, while circles and dotted lines represent the modern techniques..... 99

List of Tables

Table 2.1 Number of samples per soil textural class (N) and textural class mean of percent sand, percent clay, percent silt, particle density (ρs), bulk density (ρb), total porosity (Ø), effective saturation (θ_e), and median saturated hydraulic conductivity (K_s). Values in parenthesis are the standard deviation. Abbreviated textural classes are clay loam (C loam), sandy clay loam (S C L), sandy loam (Sandy L), silt loam (Si Loam), silty clay (Si Clay), and silty clay loam (Si C L). 22

Table 2.2 Number of samples per soil textural class (N) and textural class mean of water contents at -10 kPa (θ-10), -33 kPa (θ-33), and -1500 kPa (θ-1500), and plant available water capacity (PAWC) calculated with upper limit taken at -10 kPa ($PAWC_{-10}$) and -33 kPa ($PAWC_{-33}$). Values in the bracket are standard deviations. Abbreviated textural classes are clay loam (C loam), sandy clay loam (S C L), sandy loam (Sandy L), silt loam (Si Loam), silty clay (Si Clay), and silty clay loam (Si C L). 25

Table 2.3 Number of samples per soil textural class (N), textural class mean fitted hydraulic parameters of the van Genuchten (1980) model for the Kansas Mesonet soils. θs, is saturation water content, θ_r is residual water content, and α relates to the inverse of air-entry pressure, and n is a measure of pore size distribution. θ_s, and θ_r, are also results from the fitting exercise. Values in the bracket are standard deviations. Abbreviated textural classes are clay loam (C loam), sandy clay loam (S C L), sandy loam (Sandy L), silt loam (Si Loam), silty clay (Si Clay), and silty clay loam (Si C L). 28

Table 2.4 Number of samples per soil textural class (N) and textural class mean of soil thermal conductivity (λ) and volumetric heat capacity (C) at saturation, at -33 kPa, at -70 kPa, and oven-dry conditions. Values in bracket are standard deviation. Abbreviated textural classes are clay loam (C loam), sandy clay loam (S C L), sandy loam (Sandy L), silt loam (Si Loam), silty clay (Si Clay), and silty clay loam (Si C L). 31

Table 2.5 Number of samples per soil moisture sensor depth (N) and mean depth-specific soil chemical properties. Values in bracket are standard deviation. OM represents organic matter content, TC is total carbon, TN is total nitrogen, pHBuf is buffer pH, P is phosphorus, K is potassium, Ca is calcium, Mg is magnesium, and Na is sodium. 35

Table 2.6 Number of samples per soil moisture sensor depth (*N*) and depth-specific soil color expressed in the CIELAB color space. Values in bracket are standard deviation. Values for *L** represent lightness in color from black (0) to white (100), *a** represents a variation from green (−) to red (+), and *b** represents a variation from blue (−) to yellow (+). 36
Table 2.7 In situ validation of the CS655 soil water reflectometer sensor using common models for estimating volumetric water content from the apparent dielectric permittivity using coefficients (a, b, c, and d) derived from an independent laboratory sensor calibration in a separate study. The optimized coefficients were obtained from the least-squares fitting of the models to the water contents of the in-situ soil samples at the time of sampling. *r* represents the coefficient of correlation, RMSE represents the root mean squared error, and MBE represents the mean bias error. Negative MBE represents underestimation and positive MBE represents overestimation. 39
Table 3.1 Qualitative evaluation of precipitation detection by soil moisture using 2497 hourly observations that exceeded 7.6 mm from 30 stations of the Kansas Mesonet..... 64
Table 3.2 Comparison of precipitation estimation error between the proposed soil moisture approach (SM) and the nearest neighbor interpolation approach (NN) for all precipitation events greater than 7.6 mm at each of the 30 stations of the Kansas Mesonet that monitors rootzone soil moisture. The predicted precipitation from soil moisture was computed as the sum of hourly changes in soil water storage + interception value of 7.6 mm. 74
Table 4.1 Sample location and measured textural class, percent sand, percent clay, percent silt, organic matter (OM), bulk density (ρb), total porosity (Ø), saturated hydraulic conductivity (Ks), osmotic potential (ψos), and verified matric potential of samples equilibrated at -1500 kPa in the dewpoint water potential meter (ψ_{verify}). Abbreviated textural classes are clay loam (C L), silty clay loam (Si C L), silty clay (Si C), clay (C), and sandy loam (S L)..... 96
Table 4.2 Fitted hydraulic parameters of the van Genuchten (1980) model derived from the water retention measurements for the soil samples using traditional (suction table, pressure cell, and pressure plate) and modern (mini-tensiometers and dew point potential meter) laboratory techniques. θ_s, is saturation water content, θ_r is residual water content, and α relates to the inverse of air-entry pressure, and n is a measure of pore size distribution. θ_s, and θ_r, are also results from the fitting exercise. Abbreviated textural classes are clay loam (C L), silty clay loam (Si C L), silty clay (Si C), clay (C), and sandy loam (S L). 101

Table 4.3 Water contents at field capacity (θ-10), permanent wilting point (θ-1500), and plant available water capacity (PAWC), and difference in plant available water capacity (ΔPAWC) estimated from the water retention measurements for the soil samples using traditional (suction table, pressure cells, and pressure plate) and modern (mini-tensiometers and dew point potential meter) laboratory techniques. θ_s, is saturation water content, θ_r is residual water content, and α relates to the inverse of air-entry pressure, and n is a measure of pore size distribution. θ_s, and θ_r, are also results from the fitting exercise. Abbreviated textural classes are clay loam (C L), silty clay loam (Si C L), silty clay (Si C), clay (C), and sandy loam (S L). 105

Acknowledgments

My ultimate gratitude goes to the almighty God for how far he has brought me. My special thanks go to my major advisor, Dr. Andres Patrignani, for granting me the opportunity to be his student and also for his amazing supervision, encouragement, and constructive criticisms. I also acknowledge my supervisory committee members, Dr. Gerard J. Kluitenberg, Dr. Eduardo Alvarez Santos, and Dr. Behzad Ghanbarian for their guidance and constructive feedbacks. My heartfelt appreciation to the students and visiting scholars in the KSU Soil Water Lab for their help during the field work and laboratory work of my studies. Special thanks to my beloved wife Alice Ariziku and my lovely sons, Nathaniel Parker Jr. and Jayden Nhyira Parker for their unflinching love, support and prayers. Many thanks to my family in Ghana, my church, and my friends for all their prayers, encouragement, and support in achieving this great milestone. I owe it all to them.

Chapter 1 - General Introduction

Mesoscale *in situ* networks are an emerging hub of climate and near real-time environmental observations that are becoming widely used for research in meteorology, hydrology, and agriculture. A mesoscale network refers to a collection of monitoring stations with a horizontal spatial extent of a few to several hundred kilometers (American Meteorological Society, 2021) that are used to study climate trends and support natural hazard forecasting of mesoscale phenomena like wildfires, severe thunderstorms, flash flooding, and droughts. Currently, the United States of America has the largest number of mesoscale networks in the world with about 30 mesoscale networks having a combined total >2300 observation sites across the country (Quiring et al., 2016). The mesoscale networks in the US comprise both national and statewide networks. The national networks include the Soil Climate Analysis Network (Schaefer et al., 2007) with 190 stations and the U.S. Climate Reference Network (Bell et al., 2013) with 114 stations across the country. At the state level, the two networks with the highest station density are the New York State Mesonet (Brotzge et al., 2020) that has 126 stations across 141,297 km^2, and the Oklahoma Mesonet (McPherson et al., 2007) that has 129 stations across 181,038 km^2. In the Southern Great Plains, the Kansas Mesonet (Patrignani et al., 2020a) is currently the second-largest mesoscale network after the Oklahoma Mesonet with 62 stations that covers an area of 213,100 km^2, which makes the Kansas Mesonet the most important infrastructure for environmental monitoring in the state of Kansas, and an essential component in research and outreach efforts. In this dissertation, we investigated three central questions to improve mesoscale soil moisture monitoring and applications of soil moisture and temperature observations from the Kansas Mesonet:

i) In 1986, the Kansas State Research and Extension started the Kansas Mesonet with a total of 13 weather stations that were distributed across the agricultural research stations of Kansas State University. The Kansas Mesonet has expanded over the years and currently has 62 stations distributed across the state of Kansas with at least one station in every two counties (Patrignani et al., 2020b). The Kansas Mesonet monitors standard climate variables in addition to soil moisture and soil temperature at intervals of 5 minutes, which is then aggregated into hourly and daily intervals (Patrignani et al., 2020a). The climate variables from the Kansas Mesonet are routinely used for agricultural extension programs and also for research studies in agriculture (Barkley et al., 2014; Tack et al., 2015; Lollato et al., 2020), meteorology (Miller et al., 2020)**,** and hydrology (Brookfield et al., 2018). However, unlike the atmospheric variables, applications of the soil variables in fostering understanding of soil water and surface energy dynamics at the mesoscale level have been limited by a lack of site-specific information on soil physical properties co-located with the soil moisture and soil temperature observations. Can we improve the applications of the soil moisture and soil temperature observations from the Kansas Mesonet by developing a database of soil physical properties for each station? Can the accuracy of soil moisture measurements be enhanced by characterizing soil physical properties?

ii) Precipitation monitoring in mesoscale environmental networks is typically carried out using tipping-bucket, weighing-bucket, and siphon rain gauges that are automated using electronic data loggers (McPherson et al., 2007; Shulski et al., 2018; Patrignani et al., 2020a). However, sporadic instrument breakdowns and clogging of the rain collector in automated rain gauges could result in missing precipitation records (Shafer et al., 2000; Michaelides et al., 2009). Missing precipitation records could consequently affect the results of hydrologic studies that use precipitation as input (Tan and Yang, 2020). Missing precipitation records at a targeted

station are typically replaced by interpolating the precipitation records of the stations surrounding the targeted station (i.e. replacement using the same variable from different stations). Commonly used spatial interpolation methods for replacing missing precipitation events varies from simple methods such as nearest neighbor and Thiessen polygon (Mair and Fares, 2011; Bárdossy and Pegram, 2014) to more complex and sophisticated methods such as ordinary kriging and geographically weighted regression (di Piazza et al., 2011). However, the naturally high variability of precipitation events in terms of space and timing of precipitation events at different locations implies that even sophisticated spatial interpolation methods could lead to errors in the estimated missing precipitation events, especially at sub-daily intervals (e.g. hourly) (Ciach and Krajewski, 2006; Cristiano et al., 2017). On the other hand, it is practically challenging to run a real-time precipitation quality control onboard station dataloggers using gridded precipitation products from remote sensing sources (e.g. radars, satellite sensors). To operationally run a real-time precipitation quality control at the stations that resolve the uncertainties related to spatial interpolation methods, can we use concurrent changes in situ soil moisture (i.e. a different variable from the same station) as an operational quality control approach to detect missing precipitation events in mesoscale networks? Can we quantify the changes in soil water storage during precipitation events to replace missing precipitation records at the same station?

iii) While completing the soil physical property database for the Kansas Mesonet, we became curious about the compatibility between different laboratory methods for measuring soil water retention. Measurement of called soil water retention curve (also called soil water characteristics curve) is important in studies that rely on the energy state of water in the soil such as simulation of soil water fluxes (Skaggs; Wyatt et al., 2017)**,** modeling transport of pollutants

(Gärdenäs et al., 2005), and quantifying plant available water (Parker et al., 2021)**.** Water retention curve over the entire moisture range is typically measured by combining at least two different instrumentations due to the non-existence of one instrumentation that is capable of measuring water retention over the entire moisture range (Bittelli and Flury, 2009; Schelle et al., 2013; Parker et al., 2021). For almost a century now, the most popular instrumentation for measuring soil water retention in the laboratory is the pressure plate (Richards and Fireman, 1943; Richards, 1948, 1965), and thus the pressure plate has somewhat become the traditional water retention instrumentation in soil physics laboratories. Due to the long existence of the pressure plate, most of the commonly used models for predicting soil water characteristics in the literature were developed based on water retention measurements using the pressure plate (Arya and Paris, 1981; Schaap et al., 2001; Saxton and Rawls, 2006). However, the pressure plate is reported to produce inaccurate results at low matric potentials $\leq$ -1500 kPa due to problems such as lack of equilibration (Creswell et al., 2008), and poor contact between soil samples and the pressure plate (Gee et al, 2002). On the other hand, newer instrumentations such as the evaporation method based on mini-tensiometers and the dewpoint method based on water potential meter, which is now available in commercial quantities, are suggested to address the issues associated with the pressure plate (Bittelli and Flury, 2009; Schelle et al., 2013). However, there are still unanswered questions or concerns regarding the level of compatibility between full water retention curves measured using the pressure plate and water retention curves measured using the newer methods. Therefore, this study investigated some of the lingering questions, specifically: What is the level of compatibility between a full water retention curve measured using the pressure plate (i.e. traditional method) and a full water retention curve measured using the newer methods based on mini-tensiometers and water potential meter (i.e. modern methods)?

If the methods are not compatible, to what degree do the differences between the methods propagate into the estimation of plant available water?

References

American Meteorological Society, 2021: Mesoscale. Glossary of Meteorology, https://glossary.ametsoc.org/wiki/Mesoscale. Accessed on October 21, 2021.

Arya, L.M., and J.F. Paris. 1981. A Physicoempirical Model to Predict the Soil Moisture Characteristic from Particle-Size Distribution and Bulk Density Data. Soil Science Society of America Journal 45(6): 1023–1030.

Bárdossy, A., and G. Pegram. 2014. Infilling missing precipitation records - A comparison of a new copula-based method with other techniques. Journal of Hydrology 519(PA): 1162–1170. doi: 10.1016/j.jhydrol.2014.08.025.

Barkley, A., J. Tack, L.L. Nalley, J. Bergtold, R. Bowden, et al. 2014. Weather, disease, and wheat breeding effects on Kansas wheat varietal yields, 1985 to 2011. Agronomy Journal 106(1): 227–235. doi: 10.2134/agronj2013.0388.

Bell, J.E., M.A. Palecki, C.B. Baker, W.G. Collins, J.H. Lawrimore, et al. 2013. U.S. Climate Reference Network Soil Moisture and Temperature Observations. Journal of Hydrometeorology 14(3): 977–988. doi: 10.1175/JHM-D-12-0146.1.

Bittelli, M., and M. Flury. 2009. Errors in water retention curves determined with pressure plates. Soil Science Society of America Journal 73(5): 1453–1460. doi: 10.2136/sssaj2008.0082.

Brookfield, A.E., M.C. Hill, M. Rodell, B.D. Loomis, R.L. Stotler, et al. 2018. In Situ and GRACE-Based Groundwater Observations: Similarities, Discrepancies, and Evaluation in the High Plains Aquifer in Kansas. Water Resources Research 54(10): 8034–8044. doi: 10.1029/2018WR023836.

Brotzge, J.A., J. Wang, C.D. Thorncroft, E. Joseph, N. Bain, N. Bassill, N. Farruggio, J.M. Freedman, K. Hemker Jr, D. Johnston, and E. Kane, 2020: A technical overview of the New York State Mesonet standard network. Journal of Atmospheric and Oceanic Technology, 37(10), 1827–1845.

Ciach, G.J., and W.F. Krajewski. 2006. Analysis and modeling of spatial correlation structure in small-scale rainfall in Central Oklahoma. Advances in Water Resources 29(10): 1450–1463. doi: 10.1016/j.advwatres.2005.11.003.

Cresswell, H.P., T.W. Green, and N.J. McKenzie. 2008. The Adequacy of Pressure Plate Apparatus for Determining Soil Water Retention. Soil Science Society of America Journal 72(1): 41–49. doi: 10.2136/sssaj2006.0182.

Cristiano, E., M. ten Veldhuis, and N. van de Giesen. 2017. Spatial and temporal variability of rainfall and their effects on hydrological response in urban areas – a review. Hydrology and Earth System Sciences 21(7): 3859–3878. doi: 10.5194/hess-21-3859-2017.

Gärdenäs, A.I., J.W. Hopmans, B.R. Hanson, and J. Šimůnek. 2005. Two-dimensional modeling of nitrate leaching for various fertigation scenarios under micro-irrigation. Agricultural Water Management 74(3): 219–242. doi: 10.1016/j.agwat.2004.11.011.

Gee, G.W., A.L. Ward, Z.F. Zhang, G.S. Campbell, and J. Mathison. 2002. The Influence of Hydraulic Nonequilibrium on Pressure Plate Data. Vadose Zone Journal 1(1): 172–178. doi: 10.2113/1.1.172.

Lollato, R.P., G.P. Bavia, V. Perin, M. Knapp, E.A. Santos, et al. 2020. Climate-risk assessment for winter wheat using long-term weather data. Agronomy Journal 112(3): 2132–2151. doi: 10.1002/agj2.20168.

Mair, A., and A. Fares. 2011. Comparison of Rainfall Interpolation Methods in a Mountainous Region of a Tropical Island. Journal of Hydrologic Engineering 16(4): 371–383. doi: 10.1061/(ASCE)HE.1943-5584.0000330.

McPherson, R.A., C.A. Fiebrich, K.C. Crawford, R.L. Elliott, J.R. Kilby, et al. 2007. Statewide monitoring of the mesoscale environment: A technical update on the Oklahoma Mesonet. Journal of Atmospheric and Oceanic Technology 24(3): 301–321. doi: 10.1175/JTECH1976.1.

Michaelides, S., V. Levizzani, E. Anagnostou, P. Bauer, T. Kasparis, et al. 2009. Precipitation: Measurement, remote sensing, climatology and modeling. Atmospheric Research 94(4): 512–533. doi: 10.1016/j.atmosres.2009.08.017.

Miller, R.L., C.L. Ziegler, and M.I. Biggerstaff. 2020. Seven-doppler radar and in situ analysis of the 25-26 June 2015 Kansas MCS during PECAN. Monthly Weather Review 148(1): 211–240. doi: 10.1175/MWR-D-19-0151.1.

Parker, N., W.M. Cornelis, K. Frimpong, E. Oppong Danso, E. Bessah, et al. 2021. Short-term effects of rice straw biochar on hydraulic properties and aggregate stability of an Acrisol. Soil Research: 1–31.

Patrignani, A., M. Knapp, C. Redmond, and E. Santos. 2020a. Technical overview of the kansas mesonet. Journal of Atmospheric and Oceanic Technology 37(12): 2167–2183. doi: 10.1175/JTECH-D-19-0214.1.

Patrignani, A., N. Mohankumar, C. Redmond, E.A. Santos, and M. Knapp. 2020b. Optimizing the spatial configuration of mesoscale environmental monitoring networks using a geometric approach. Journal of Atmospheric and Oceanic Technology 37(5): 943–956. doi: 10.1175/JTECH-D-19-0167.1.

di Piazza, A., F. lo Conti, L. v. Noto, F. Viola, and G. la Loggia. 2011. Comparative analysis of different techniques for spatial interpolation of rainfall data to create a serially complete monthly time series of precipitation for Sicily, Italy. International Journal of Applied Earth Observation and Geoinformation 13(3): 396–408. doi: 10.1016/j.jag.2011.01.005.

Quiring, S.M., T.W. Ford, J.K. Wang, A. Khong, E. Harris, et al. 2016. The North American soil moisture database development and applications. Bulletin of the American Meteorological Society 97(8): 1441–1460. doi: 10.1175/BAMS-D-13-00263.1.

Richards, L.A. and Fireman, M., 1943. Pressure-plate apparatus for measuring moisture sorption and transmission by soils. Soil Science, 56(6):395-404.

Richards, L.A. 1948. Porous plate apparatus for measuring moisture retention and transmission by soil. Soil Science 66(2): 105–110. doi: 10.1097/00010694-194808000-00003.

Richards, L.A. 1965. Physical condition of water in soil. Methods of Soil Analysis, Part 1: Physical and Mineralogical Properties, Including Statistics of Measurement and Sampling: 128–152. doi: 10.2134/agronmonogr9.1.c8.

Saxton, K.E., and W.J. Rawls. 2006. Soil Water Characteristic Estimates by Texture and Organic Matter for Hydrologic Solutions. Soil Science Society of America Journal 70(5): 1569–1578. doi: 10.2136/sssaj2005.0117.

Schaap, M.G., F.J. Leij, and M.T. van Genuchten. 2001. Rosetta: A computer program for estimating soil hydraulic parameters with hierarchical pedotransfer functions. Journal of Hydrology 251(3–4): 163–176. doi: 10.1016/S0022-1694(01)00466-8.

Schaefer, G.L., M.H. Cosh, and T.J. Jackson. 2007. The USDA Natural Resources Conservation Service Soil Climate Analysis Network (SCAN). Journal of Atmospheric and Oceanic Technology 24(12): 2073–2077. doi: 10.1175/2007JTECHA930.1.

Schelle, H., L. Heise, K. Jänicke, and W. Durner. 2013. Water retention characteristics of soils over the whole moisture range: A comparison of laboratory methods. European Journal of Soil Science 64(6): 814–821. doi: 10.1111/ejss.12108.

Shafer, M.A., C.A. Fiebrich, D.S. Arndt, S.E. Fredrickson, and T.W. Hughes. 2000. Quality assurance procedures in the Oklahoma Mesonetwork. Journal of Atmospheric and Oceanic Technology 17(4): 474–494. doi: 10.1175/1520-0426(2000)017<0474:QAPITO>2.0.CO;2.

Shulski, M., S. Cooper, G. Roebke, and al Dutcher. 2018. The Nebraska Mesonet: Technical overview of an automated state weather network. Journal of Atmospheric and Oceanic Technology 35(11): 2189–2200. doi: 10.1175/JTECH-D-17-0181.1.

Skaggs, R.W. 1978. A water management model for shallow water table soils.

Solone, R., M. Bittelli, F. Tomei, and F. Morari. 2012. Errors in water retention curves determined with pressure plates: Effects on the soil water balance. Journal of Hydrology 470–471: 65–74. doi: 10.1016/j.jhydrol.2012.08.017.

Tack, J., A. Barkley, and L. Lanier Nalley. 2015. Estimating Yield Gaps with Limited Data: An Application to United States Wheat. American Journal of Agricultural Economics 97(5): 1464–1477. doi: 10.1093/ajae/aau157.

Tan, M.L., and X. Yang. 2020. Effect of rainfall station density, distribution and missing values on SWAT outputs in tropical region. Journal of Hydrology 584(September 2019): 124660. doi: 10.1016/j.jhydrol.2020.124660.

Wyatt, B.M., T.E. Ochsner, C.A. Fiebrich, C.R. Neel, and D.S. Wallace. 2017. Useful Drainage Estimates Obtained from a Large-Scale Soil Moisture Monitoring Network by Applying the Unit-Gradient Assumption. Vadose Zone Journal 16(6): vzj2017.01.0016. doi: 10.2136/vzj2017.01.0016.

Chapter 2 - A New Database of Soil Physical Properties for the Kansas Mesonet

This work will be submitted to the *Vadose Zone Journal*

Nathaniel Parker, Christopher Redmond, Gerard J. Kluitenberg, and Andres Patrignani

Abstract

This study developed a comprehensive database of soil hydraulic and soil thermal properties to expand the applications of soil moisture and temperature observations from the Kansas Mesonet. The database comprises 14 site and depth-specific soil hydraulic properties (sand, clay, and silt contents; bulk density; particle density; total porosity; effective saturation; saturated hydraulic conductivity; and water retention at six matric potentials) and three soil thermal properties (thermal conductivity; volumetric heat capacity; and thermal diffusivity) for the 40 Kansas Mesonet stations that monitor soil moisture and soil temperature. Eight USDA soil textural classes (six fine and two coarse textures) were found in the Kansas Mesonet. Silty clay loam, silt loam, and silty clay dominated the fine soils while sandy loam and sandy clay loam were the only coarse soils captured. All the measured soil properties showed low variation within soil texture, except the saturated hydraulic conductivity, which varied from a median of 0.520 ±308 cm d^{-1} in clay soil to 47.1 ±119 cm d^{-1} in sandy loam soil. The uncertainty in the Kansas Mesonet soil moisture measurements improved by 29% using sensor calibration equations compared to the factory default sensor equation. Our soil physical property database offers new prospects to use the Kansas Mesonet soil moisture and temperature observations for agricultural and hydrological applications such as drought monitoring, drainage, and groundwater recharge estimations, and also for other applications in civil engineering and urban planning.

Introduction

The Kansas Mesonet is a mesoscale environmental monitoring network that was established by the Kansas State University Research and Extension in 1986. The Kansas Mesonet consists of 62 automated stations distributed across an area of 213,000 km^2 and has an average distance between neighboring stations of about 35 km (Patrignani et al., 2020b). Each station of the Kansas Mesonet is instrumented with research-grade sensors that record atmospheric and soil variables, including soil moisture and soil temperature (Patrignani, et al. 2020a). Soil moisture and soil temperature are monitored at 5-minute, hourly, and daily intervals at 5, 10, 20, and 50 cm depths using soil water reflectometers (model CS655, Campbell Scientific, Inc.) and soil temperature probes (model CS107, Campbell Scientific Inc.). The soil temperature record at 5 and 10 cm depth spans a period of 35 years, while the soil moisture record based on the current sensor layout dates back to May 2017.

Information from the Kansas Mesonet are routinely used for outreach activities through agricultural climate updates (climate.k-state.edu/ag/updates) and for research applications including climate risk assessment for crops (Barkley et al., 2014; Lollato et al., 2020), analysis of mesoscale convective systems (Miller et al., 2020), estimating crop yield gaps (Tack et al., 2015; Lollato et al., 2017), examining factors influencing the value of farm land (Tsoodle et al., 2006), determining the efficiency of alternative irrigation technologies on groundwater levels (Pfeiffer and Lin, 2014), estimating groundwater volumes from satellite-based models (Brookfield et al., 2018), and simulating regional-scale surficial ecohydrological processes (Steward et al., 2011).

While the number of agricultural and hydrological applications that use meteorological data is expanding, the lack of site-specific soil physical properties limits the use of soil moisture and soil temperature observations for studying and advancing our understanding of the

components of the soil water balance and the surface energy balance at the mesoscale level. Thus, there is a need for developing a comprehensive database of site-specific soil physical properties for the Kansas Mesonet. The objectives of this study were to determine site-specific soil hydraulic and thermal properties for stations of Kansas Mesonet equipped with soil moisture sensors. To illustrate an example application of the resulting dataset, we conducted a network-wide validation of the soil water reflectometers used by the Kansas Mesonet.

To our knowledge, only a few mesoscale networks have determined and made publicly available databases of site-specific soil physical properties, which include the databases of the North Carolina EcoNet, the Oklahoma Mesonet, and the US Climate Reference Network. In the case of the US Climate Reference Network and the North Carolina EcoNet, new soil databases were aimed at providing co-located ancillary soil physical properties to support soil moisture observations (Pan et al., 2012; Wilson et al., 2016). Similarly, the Oklahoma Mesonet soil database was aimed at improving the accuracy of soil moisture observations from heat dissipation sensors through better estimates of soil hydraulic parameters (Scott et al., 2013). While these databases contain detailed soil hydraulic properties, we are not aware of any soil physical property database also containing detailed information on soil thermal properties.

Materials and Methods

Field sampling campaign

From September 2018 to November 2019, we visited 40 stations of the Kansas Mesonet equipped with soil moisture sensors (Figure 2.1). At each station, we collected duplicate undisturbed soil cores at 5, 10, 20, and 50 cm depth at about 1 m from the permanent array of soil moisture sensors to avoid disturbing the sensing area. The duplicate soil samples were

adjacent at about 1 m from each other. Undisturbed cores were collected using a soil core sampler (model C, Eijkelkamp Agrisearch Equipment) that had stainless steel rings with a volume of 100 cm^3 (51 mm height and 50 mm i.d.). Before starting the soil sampling process, the top 2 cm of the soil were removed to eliminate any dense root system at or near the soil surface that could interfere with the sampling process (Scott et al., 2013). After collecting each soil sample, we measured the depth of the bore hole left in the soil and we compared it to the length of the soil sample to check for the occurrence of compaction. Rings with undisturbed soil were then covered with two plastic lids to prevent water loss and were placed in a carrying case to prevent disturbance during transportation to the laboratory. The mass of each core was measured within 12 hours of field sampling to record the field soil water content at the time of sampling. During lab analyses, soil samples were kept in a refrigerator at 6 ºC to reduce the rate of chemical reactions and microbial activity that could affect the soil's physical properties.

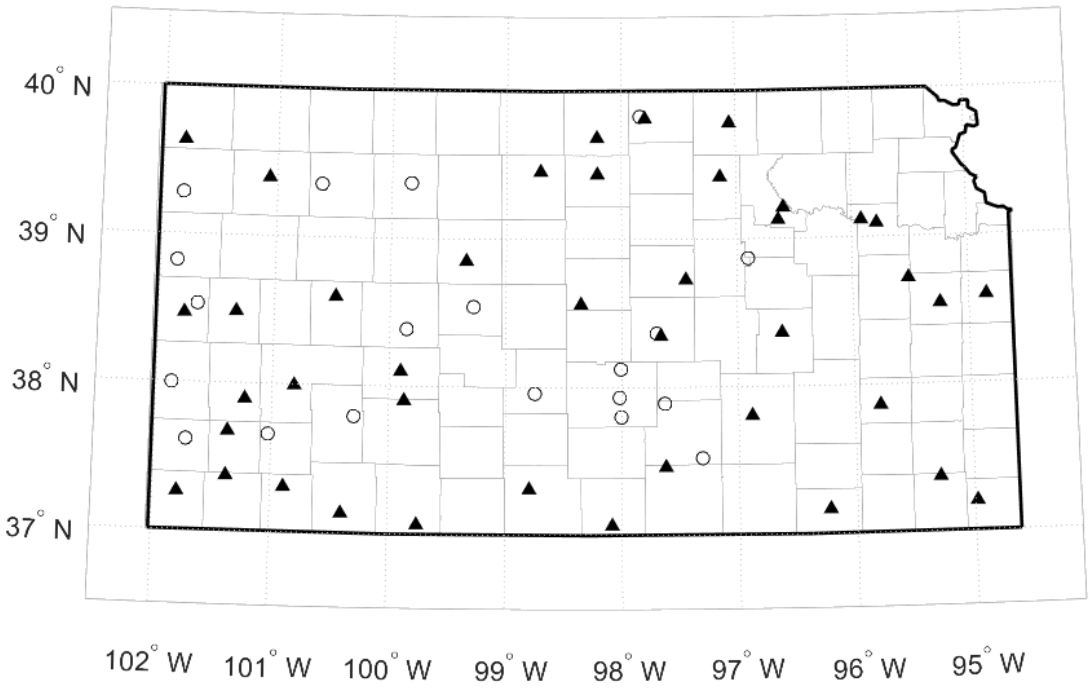

Figure 2.1 Map showing the location of the 62 stations of the Kansas Mesonet as of December 2020. Filled triangles represent the 40 stations with soil moisture sensors that were sampled in this study and open circles represent the remaining stations without soil moisture sensors.

Soil hydraulic properties

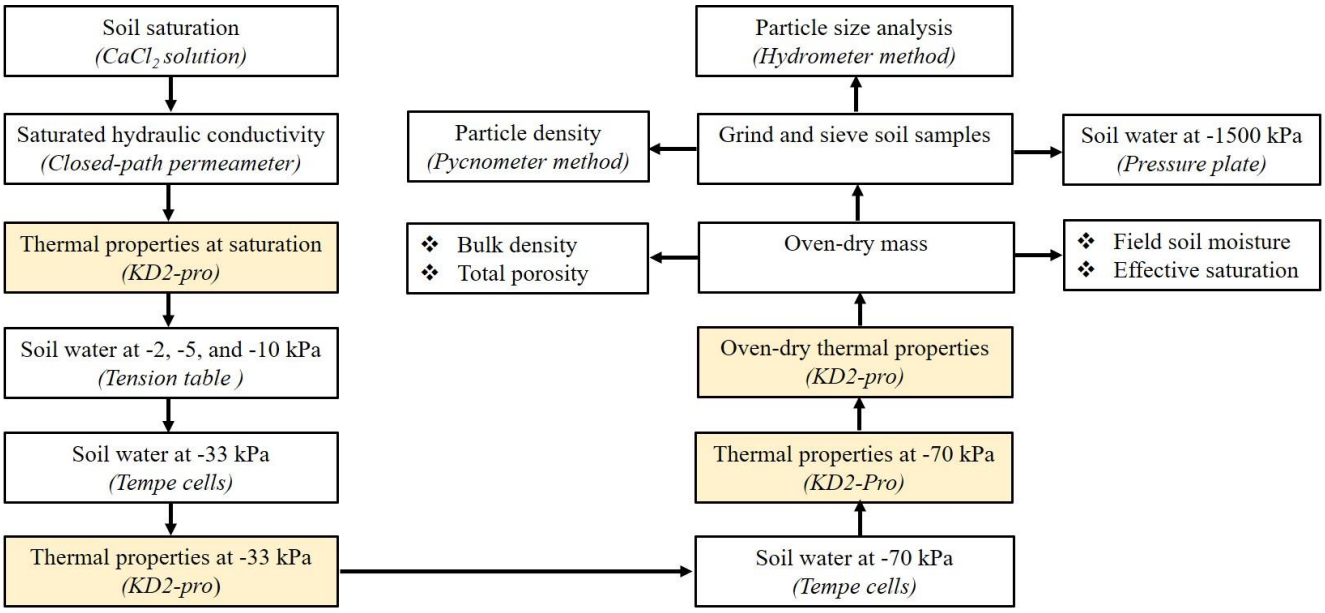

Figure 2.2 Flowchart of laboratory measurements in the development of the soil physical properties database for the Kansas Mesonet. The yellow-colored boxes represent the points at which thermal properties were measured. Note that some variables like field soil moisture and effective soil saturation are measured at the beginning of the process, but can only be determined near the end of the process when information about the oven-dry mass of the sample is available.

Soil saturation and saturated hydraulic conductivity

Soil samples were saturated in a 5 mM $CaCl_2$ solution with ¾ of the ring height submersed in the solution (Reynolds and Elrick, 2002) (Figure 2.2). To prevent soil loss during the saturation process, a piece of cheesecloth was affixed with a rubber band to the face of the sample ring in the $CaCl_2$ solution. The soil samples were left in the solution for a minimum of five days until they reached saturation. Samples that did not reach saturation after five days were placed under vacuum for 48 hours to facilitate saturation. Saturated hydraulic conductivity (K_{sat}) of the soil samples was determined with the constant head method (Reynolds and Elrick, 2002) using a close-path permeameter (Eijkelkamp Agrisearch Equipment) (Figure 2.2). In the case of soils with extremely low permeability, we used the falling head method (Reynolds and Elrick,

2002). Both K_{sat} measurements using the constant head and falling head methods were performed following the procedure detailed in the operational manual of the permeameter at a temperature of 21 ºC ±1 ºC.

Soil water retention curve

Soil water retention curves were determined by first measuring the volumetric water content at tensions of -2, -5, and -10 kPa using a tension table (model 08.01, Eijkelkamp Agrisearch Equipment) (Figure 2.2). Samples were left in the tension table until hydraulic equilibrium, which was confirmed by two consecutive days with a mass change <0.2%. A standard soil of known mass at hydraulic equilibrium (i.e. check soil sample) was included with every batch of water retention measurement in the tension table. Then, the undisturbed soil samples were placed in pressure cells (Tempe cell, Soil Moisture Equipment Corp.) connected to a controlled air pressure system to determine soil water retention at -33 and -70 kPa (Dane and Hopmans, 2002). After measuring soil matric potential at -70 kPa, the undisturbed samples were oven-dried at 105 ºC for 48 hours, ground using a soil grinder (model 5K533A, Dayton Electric Manufacturing Co.), sieved through a 2 mm-sieve (ASTM E-11, Humboldt Manufacturing Co.), and then stored in paper envelopes inside plastic containers at room temperature. The last step consisted of determining water retention at -1500 kPa by placing approximately 15 g of the disturbed (pre-sieved) soil into a pressure plate extractor (model 1500F2, Soil Moisture Equipment Corp.) (Dane and Hopmans, 2002). A check soil sample was included with every batch of water retention measurement at -1500 kPa in the pressure plate extractor. Samples were left in the pressure plate extractor for a minimum of 21 days or until no water outflow was evidenced from the vessel for five consecutive days. Soil samples were oven-dried at 105ºC for 48 hours to determine the gravimetric soil water content.

Location- and depth-specific soil water retention curves were generated by fitting the van Genuchten (1980) model to observations of volumetric water content and soil matric potential using least-squares in Matlab R2020b (Mathworks). The model is given as:

$$\frac{\theta - \theta_r}{\theta_s - \theta_r} = [1 + (-\alpha\psi_m)^n]^{-m} \qquad [1]$$

where θ ($cm^3\ cm^{-3}$) is the volumetric water content, θ_s ($cm^3\ cm^{-3}$) is saturated water content, θ_r ($cm^3\ cm^{-3}$) is residual water content, ψ_m (kPa) is matric potential, α (kPa^{-1}) is a parameter related to the inverse of air-entry pressure, *n* is a parameter related to the pore size distribution, and *m* was assumed to equal to 1–1/*n* (Schaap et al., 2001).

General soil physical properties

Particle size analysis

The fraction of sand (0.05 to 2 mm), silt (0.002 to 0.05 mm), and clay (<0.002 mm) were determined using the hydrometer method (Gavlak et al., 2005) (Figure 2.2). Briefly, the analysis consisted of placing 40 ± 0.05 g of pre-sieved and oven-dried soil into 250-ml plastic jars with 100 ml of 0.08 M sodium hexametaphosphate solution that was used as a dispersing agent. Samples were agitated for 16 hours using a linear shaker and then transferred to 1-liter cylinders that were topped with de-ionized water at room temperature. Samples were manually agitated using a perforated plunger and the suspension density was measured at the 40 s mark using a Buoyoucos hydrometer (ASTM 152-H, Humboldt Manufacturing Co.). The agitation and first reading of the suspension density were repeated twice. A second reading of the suspension density was carried at around seven hours from the end of the agitation based on the laboratory temperature (~22 ºC). A separate subsample of about 15 g was oven-dried at 105 ºC to correct

for any water gained by the pre-sieved soil samples while in storage. Similar to the previous analyses, a check soil sample of known soil texture was included with every batch.

Bulk density, Particle density, Total porosity

Bulk density was determined using the core method, which consisted of dividing the mass of the oven-dry soil by the ring volume (Grossman and Reinsch, 2002) (Figure 2.2). On the other hand, particle density was measured using the pycnometer method, which consisted of placing 10 ± 0.05 g of ground oven-dried soil into a Gay-Lussac pycnometer, that was then filled with degassed de-ionized water (Flint and Flint, 2002). The degassing process consisted of boiling 1 liter of de-ionized water for about 10 minutes on a hot plate and then allowing it to cool down at room temperature. Similar to particle size analysis, an additional 6 g of soil was used to correct for the initial mass of water in the oven-dried soil. The total porosity of the soils was computed using the measured values for both bulk density and particle density using the equation:

$$\emptyset = 1 - \frac{\rho_b}{\rho_s} \qquad [2]$$

where Ø ($cm^3\ cm^{-3}$) is total porosity, ρ_b ($g\ cm^{-3}$) is bulk density, and ρ_s ($g\ cm^{-3}$) is measured particle density.

Soil thermal properties

Soil thermal conductivity, volumetric heat capacity, and soil thermal diffusivity were measured during the determination of the soil water retention curves at saturation, -33 kPa, -70 kPa, and oven-dryness using a KD2-Pro thermal properties analyzer with a dual needle of 1.3 mm diameter each and 6 mm needle spacing (model SH-1, Decagon Devices Inc.) (Figures 2.2).

The three soil thermal properties were obtained from a single measurement with the KD2-Pro, allowing us to make a single measurement per soil core and minimize sample disturbance. The KD2 was vertically inserted into the center of the soil samples through the KD2-Pro needle spacer and was let to reach thermal equilibrium with the sample for five minutes before taking the measurements. After oven drying the samples, the existing needle holes shrunk and became partially sealed, so we used a tabletop vertical milling machine (model 5410, Sherline Products Inc.) to carefully re-drill the holes using a drill bit with 1.3 mm diameter to ensure close contact between the needles and the soil. In this study, we did not use any thermal grease.

Soil chemical properties and soil color

Soil chemical properties were analyzed for one section of the soil cores from each sensor depth at each mesonet station. The soil analysis was done in the Kansas State University Soil Testing Lab using samples that were oven-dried at 60 ^{o}C until a constant mass, ground, and passed through 2 mm sieves. The properties analyzed comprise organic matter content, soil pH, total carbon, total nitrogen, pH buffer, and phosphorus, potassium, calcium, magnesium, and sodium contents. The soil organic matter content was analyzed by loss on ignition, pH was analyzed using 1:1 (soil: water), phosphorus was analyzed by Mehlich - 3, total nitrogen was analyzed by dry combustion, and the exchangeable cations were determined by atomic absorption spectrometry. All the chemical analyses mentioned above were performed following the procedures in the protocol book on Methods of Soil Analysis (Sparks et al., 1996).

Soil color was determined for one section of our soil cores in terms of dry color and wet color using a Nix Pro 2 color sensor (Nix Sensor Ltd.). The soil color was presented in CIELAB color space, which represents a color with three values: L^* for lightness from black (0) to white (100), a^* from green (−) to red (+), and b^* from blue (−) to yellow (+) (McLaren, 1976). Before

the measurements, we downloaded and installed a sensor-compatible software (Nix Pro Color Sensor software version 2.6.4) from Apple's App Store, which allowed us to operate the color sensor via Bluetooth. For the dry measurements, we placed 4 g of oven-dry and pre-sifted soil into a 15-ml steel cup, leveled the soil to entirely cover the bottom of the steel cup using a rubber stopper, placed the color sensor on the surface of the soil in the cup, and then scanned the soil color using the Nix Pro. After the dry measurement, we mixed 1 g of deionized water (25%wt) with the dry soil to obtain a uniformly wet soil, leveled the soil surface with the rubber stopper, and then covered the soil with a lid for the water to redistribute in the soil for at least 12 h but <48 h. After the water redistribution, we placed the color sensor on the surface of the wet soil in the cup and then scanned the soil color with the sensor software to obtain the wet soil color. During both the wet and dry measurements, three readings were taken at different points in the steel cup and then averaged to obtain the representative soil color. In addition, we minimized measurement errors by ensuring that no external light passed underneath the interface between the color sensor and the soil surface.

In situ validation of soil moisture

Soil water reflectometers, like other sensors based on electromagnetic principles, rely on functions relating the dielectric permittivity to the volumetric water content. The CS655 uses the model proposed Topp et al. (1980) as the factory default equation, which is given as:

$$\theta = 4.3 \times 10^{-6} {K_a}^3 - 5.5 \times 10^{-4} {K_a}^2 + 2.92 \times 10^{-2} K_a - 5.3 \times 10^{-2} \quad [3]$$

where θ (cm^3cm^{-3}) is volumetric water content and K_a (unitless) is the soil's apparent bulk dielectric permittivity. Equation (3) has been extensively tested and usually provides acceptable errors in coarse texture and loam soils. However, the Topp model is well known for

overestimating volumetric water content in fine-textured soils at moderate to high volumetric water contents (Evett et al., 2005; Caldwell et al., 2018; Kargas and Soulis, 2019). New multivariate models that include EC_b can reduce errors associated with EC_b and temperature effects on the dielectric permittivity, hence, a site-specific validation was conducted to determine the uncertainty of the Kansas Mesonet soil moisture observations (Figure 2.2). In addition, we also validated three common empirical linear models developed for the same type of sensors (CS655 water reflectometer). The models are based on Ledieu et al. (1986), which is given as:

$$\theta = a + b\sqrt{K_a} \qquad [4]$$

where θ (cm^3cm^{-3}) is volumetric water content and K_a (unitless) is soil apparent bulk dielectric permittivity, and a and b are empirical coefficients; Evett et al. (2005), which is given as:

$$\theta = a + b\sqrt{k_a} + c\sqrt{EC_b} \qquad [5]$$

where EC_b (dS m^{-1}) is the bulk electrical conductivity and a, b, and c are empirical coefficients; and Kargas and Soulis (2019), which is given as:

$$\theta = a + b\sqrt{k_a} + cEC_b \qquad [6]$$

We used values for coefficients *a*, *b*, and *c* determined from laboratory sensor calibration in an independent study using a dataset of ~300 observations and nine soil textural classes to validate equations 4 – 6. For this validation, the observed volumetric water content was estimated as the average of both soil cores at each station and sensor depth at the time of sampling. We also compared the accuracy of the independent laboratory sensor calibration coefficients to the accuracy of the least squares-fitted coefficients a, b, and c in equations 4 – 6, to determine the discrepancy between independent laboratory sensor calibration and field-based sensor calibration in site-specific soils.

Results and Discussion

The database of soil physical properties for the Kansas Mesonet spanned a total of 40 stations with duplicate samples for each of the four sensor depths, resulting in a total of 320 samples (40 sites x 4 depths x 2 cores).

General soil physical properties

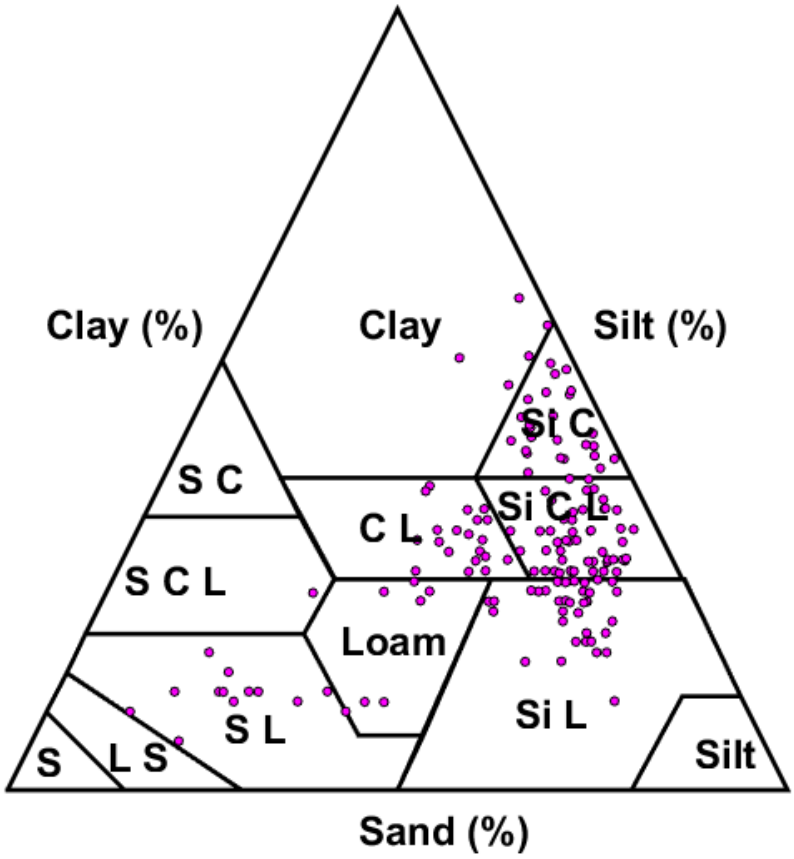

Figure 2.3 Distribution of USDA soil textural classes of the collected samples across 40 stations of the Kansas Mesonet. Abbreviated textural classes are sand (S), loamy sand (L S), sandy loam (S L), sandy clay loam (S C L), sandy clay (S C), clay loam (C L), silt loam, silty clay (Si C), and silty clay loam (Si C L).

The soils of the Kansas Mesonet represented eight out of the twelve soil textural classes except for sand, loamy sand, sandy clay, and silt (Figure 2.3). Silty clay loam was the predominant soil texture of the dataset, representing 33% of the total number of samples,

followed by silt loam soils (23%) and silty clay soils (16%) (Table 2.1). Sandy clay loam and sandy loam soils were the least represented soil textural classes across the Kansas Mesonet, representing <10% of the total number of samples in our dataset. Overall, soils had a sand content that ranged from 6 to 66%, a clay content that ranged from 12 to 57%, and a silt content that ranged from 22 to 61% (Table 2.1). The database was predominantly represented by fine soils with 93% of the samples having greater than 20% clay content. Stations of the Kansas Mesonet with the highest clay content were found in eastern Kansas, where the soil parent materials originated from loess deposits (Gunal and Ransom, 2005). Stations with the highest sand content like Lakin, Lake City, and Meade stations are located in southwestern Kansas, where the soil parent materials originated from alluvial deposits of the Ogallala formation and dunes from the Arkansas and Cimarron river valleys (Layzell et al., 2016). The range of soil particle sizes in our database was narrower compared to the range of particle sizes in the Oklahoma Mesonet, where there were 10 to 82% sand, 7 to 53% clay, and 5 to 60% silt (Scott et al., 2013). Also, the predominant textural classes in the Oklahoma Mesonet were clay, clay loam, and loam soils, each representing 16% of the soils, whereas loamy sand and sandy clay were the least represented texture in the Oklahoma Mesonet each representing 1% of the soils.

The average particle density by soil textural class ranged from 2.61 g cm^{-3} (SD = 0.09 g cm^{-3}) in silt loam soils to 2.69 g cm^{-3} (SD = 0.05 g cm^{-3}) in sandy loam and loam soils (Table 2.1), a range that is similar to the particle density of quartz with a typical value of 2.65 g cm^{-3} (Lipiec et al., 2007; Derakhshani et al., 2015). The particle density of our soils showed a negative correlation with soil organic matter content (r = -0.43) and ranged from 2.84 g cm^{-3} at 10 cm depth in the Tribune station with 2% organic matter to 2.23 g cm^{-3} at 20 cm depth in the Garden City station with 3% organic matter. The trend in decreasing particle density with

increasing soil organic matter content has been reported in other studies in North America. For instance, in a study that analyzed 54 soil horizons sampled from 18 soil profiles across North America, soil particle density varied from 2.75 g cm^{-3} at 0% organic matter content and decreased with increasing organic matter to 2.31 g cm^{-3} at 23% organic matter content (McBride et al., 2012). Also, a 22-year study in a Rayne silt loam soil in Ohio reported that forest, pasture, and no-till land management systems resulted in a particle density of 1.79 to 2.35 g cm^{-3} due to their high organic matter build-up, whereas soil tillage with a moldboard plow, resulted in a soil particle density of 2.52 g cm^{-3} due to disruption of organic matter build-up (Blanco-Canqui et al., 2006). The association of soil particle density with organic matter content occurs typically when the organic matter fraction in the soil, which has a lower particle density (~1.48 g cm^{-3}) than the particle density of the mineral fraction (~ 2.65 g cm^{-3}), is not removed from soil samples before the analysis of particle density (Flint and Flint, 2002; McBride et al., 2012).

Table 2.1 Number of samples per soil textural class (N) and textural class mean of percent sand, percent clay, percent silt, particle density (ρs), bulk density (ρb), total porosity (Ø), effective saturation (θ_e), and median saturated hydraulic conductivity (K_s). Values in parenthesis are the standard deviation. Abbreviated textural classes are clay loam (C loam), sandy clay loam (S C L), sandy loam (Sandy L), silt loam (Si Loam), silty clay (Si Clay), and silty clay loam (Si C L).

Textural class	*N*	Sand	Clay	Silt	ρ_s	ρ_b	Ø	θ_e	K_s
		%	%	%	g cm^{-3}	g cm^{-3}	cm^3 cm^{-3}	cm^3 cm^{-3}	cm d^{-1}
Clay	10	7 (5)	57 (4)	36 (4)	2.68 (0.04)	1.40 (0.09)	0.48 (0.03)	0.46 (0.05)	0.52 (308)
C loam	40	26 (3)	32 (3)	42 (4)	2.65 (0.07)	1.41 (0.09)	0.47 (0.04)	0.43 (0.04)	18.7 (172)
Loam	15	39 (9)	20 (8)	41 (4)	2.69 (0.03)	1.44 (0.13)	0.47 (0.04)	0.40 (0.05)	41.0 (70)
S C L	2	48 (0)	25 (0)	27 (0)	2.65 (0.02)	1.54 (0.15)	0.42 (0.05)	0.39 (0.07)	0.46 (0.49)
Sandy L	24	66 (7)	12 (3)	22 (7)	2.69 (0.05)	1.67 (0.11)	0.38 (0.04)	0.34 (0.04)	47.1 (119)
Si Loam	72	16 (4)	23 (4)	61 (5)	2.61 (0.09)	1.36 (0.11)	0.48 (0.04)	0.45 (0.05)	13.9 (709)
Si Clay	52	6 (4)	46 (4)	48 (5)	2.63 (0.07)	1.35 (0.14)	0.49 (0.05)	0.47 (0.05)	1.5 (7211)
Si C L	104	10 (4)	32 (3)	58 (4)	2.62 (0.07)	1.33 (0.15)	0.49 (0.05)	0.46 (0.05)	32.1 (2845)

The average bulk density by textural class ranged from 1.33 g cm^{-3} (SD = 0.15 g cm^{-3}) in silty clay loam to 1.67 g cm^{-3} (SD = 0.11 g cm^{-3}) in sandy loam soils (Table 2.1). The bulk

density range of the soils in our database is similar to the bulk density of soils reported in other environmental networks such as the North Carolina ECONet, where bulk density ranged from 1.10 to 1.69 g cm^{-3} (Pan et al., 2012), the Oklahoma Mesonet with a range in bulk density across 117 stations of 1.48 to 1.67 g cm^{-3} (Scott et al., 2013), and the US Climate Reference Network with bulk density ranging between 1.30 to 1.53 g cm^{-3} (Wilson et al., 2016). The bulk density showed a negative correlation with soil organic matter (r = -0.64, p <0.00001) and clay content (r = -0.28, p = 0.0004), and also showed a positive correlation with sand content (r = 0.60, p <0.00001) (Figure 2.4), which is consistent with the observations in the literature (Saxton and Rawls, 2006; Botula et al., 2012). As expected, the sandy loam soil presented ~20% higher bulk density than the fine-textured soils in our database (Table 2.1), which is also consistent with other studies in the literature (Rawls et al., 1982; Reynolds et al., 2009; Schelle et al., 2013). Opposite to bulk density, the total porosity of the sandy loam was up to 29% lower than the porosity of the fine-textured soils. The average total porosity by textural class varied from 0.38 cm^3 cm^{-3} (SD = 0.04 cm^3 cm^{-3}) in sandy loam soils to 0.49 cm^3 cm^{-3} (SD = 0.05 cm^3 cm^{-3}) in silty clay and silty clay loam soil (Table 2.1), which is similar to the typical soil porosity range of 0.39 to 0.50 cm^3 cm^{-3} reported for soils across 32 states in the contiguous U.S. (Rawls et al., 1982), although the study by Rawls et al. (1982) did not include any soil from the state of Kansas.

Soil hydraulic properties

As expected, the effective saturation for individual samples was slightly below total porosity values since soil samples even under laboratory conditions rarely attain full saturation due to air entrapment in soil micropores (Klute, 1965). The average effective saturation by

textural class varied from 0.34 cm^3 cm^{-3} (SD = 0.04 cm^3 cm^{-3}) in sandy loam soils to 0.47 cm^3 cm^{-3} (SD = 0.05 cm^3 cm^{-3}) in silty clay soils (Table 2.1).

Overall, the median textural class K_s in our database ranged from 0.520 to 47.1 cm d^{-1} (Table 2.1). The highest saturated hydraulic conductivities were observed in sandy loam and loam soils, with maximum values reaching ~260 cm d^{-1}. The lowest hydraulic conductivities were observed in clay and sandy clay loam soils, with values as low as 0. 116 cm d^{-1}, which is close to the evaporation correction factor of 0.086 cm d^{-1} that is applied to the K_s method (Table 2.1). The higher K_s in sandy loam and loam soils and the lower K_s in clay and sandy clay soils observed in our study is consistent with observations of K_s across soils from 32 states in the contiguous U.S. (Rawls et al., 1982). Occasionally, large K_s values occurred in some of our soil samples from the top 5 cm depth due to preferential flow and macropores. For instance, a silty clay soil sample for the Overbrook station at 5 cm depth that had cracks and root channels resulted in a K_s of 43,098 cm d^{-1} (Figure A1A in Appendix A). During the soil sampling at the Overbrook station, we observed in multiple soil profiles that the top 30 cm soil of the site had an angular blocky structure with cracks, hence the extremely high K_s value recorded at 5 cm depth was representative of the surface soil at the station. Also, macropores from worm activity and root channels in a silty clay loam soil at 5 cm depth collected at the Miami station resulted in a K_s of 9,500 cm d^{-1} (Figure A1B in Appendix A). High variability in K_s due to soil preferential flow was also reported in a previous study in Ontario that measured K_s in clay loam soils of a no-till agricultural field in which soil cracks resulted in K_s spanning five orders of magnitude from 2 to >10,000 cm d^{-1} (Reynolds et al., 2000). The wide range in K_s highlights the importance of measuring site-specific saturated hydraulic conductivity rather than estimating K_s from models since existing K_s models typically do not capture the effect of soil structure (Zhang and Schaap,

2019). The wide variability of K_s due to the influence of soil structure even in soils of the same texture suggests that either it is not a good idea to average K_s by soil textural class or it is better to represent textural class K_s by the median value (as we did in this study) to avoid a few samples with extremely large K_s values from masking the K_s values of the remaining samples.

Table 2.2 Number of samples per soil textural class (N) and textural class mean of water contents at -10 kPa (θ-10), -33 kPa (θ-33), and -1500 kPa (θ-1500), and plant available water capacity (PAWC) calculated with upper limit taken at -10 kPa ($PAWC_{-10}$) and -33 kPa ($PAWC_{-33}$). Values in the bracket are standard deviations. Abbreviated textural classes are clay loam (C loam), sandy clay loam (S C L), sandy loam (Sandy L), silt loam (Si Loam), silty clay (Si Clay), and silty clay loam (Si C L).

Textural class	*N*	θ_{-10}	θ_{-33}	θ_{-1500}	$PAWC_{-10}$	$PAWC_{-33}$
		$cm^3\ cm^{-3}$	$cm^3\ cm^{-3}$	$cm^3\ cm^{-3}$	$cm^3\ cm^{-3}$	$cm^3\ cm^{-3}$
Clay	10	0.44 (0.05)	0.43 (0.06)	0.31 (0.05)	0.13 (0.03)	0.11 (0.03)
C loam	40	0.39 (0.03)	0.34 (0.03)	0.21 (0.04)	0.18 (0.04)	0.13 (0.04)
Loam	16	0.36 (0.05)	0.27 (0.05)	0.13 (0.06)	0.23 (0.05)	0.14 (0.04)
S C L	2	0.36 (0.05)	0.33 (0.06)	0.16 (0.01)	0.19 (0.06)	0.16 (0.07)
Sandy L	24	0.29 (0.05)	0.21 (0.03)	0.09 (0.02)	0.21 (0.06)	0.12 (0.02)
Si Loam	72	0.40 (0.03)	0.34 (0.05)	0.16 (0.05)	0.25 (0.05)	0.18 (0.06)
Si Clay	52	0.43 (0.04)	0.40 (0.05)	0.26 (0.06)	0.17 (0.07)	0.14 (0.07)
Si C L	104	0.41 (0.04)	0.35 (0.04)	0.20 (0.04)	0.21 (0.05)	0.15 (0.05)

The water content at the permanent wilting point (i.e. θ_{-1500}) showed a positive (r = 0.84) correlation with the clay content and a negative (r = -0.58) correlation with sand content in our soils (Figure 2.4), which agrees well with previous studies that evaluated pedotransfer functions for predicting soil water retention from easily observable variables (Botula et al., 2012). The average θ_{-1500} increased with clay content from 0.09 $cm^3\ cm^{-3}$ in sandy loam to 0.31 $cm^3\ cm^{-3}$ in the clay soil (Table 2.2). Interestingly, θ_{-1500} exhibited a weak positive correlation with soil organic matter with an r = 0.13 (Figure 2.4). The weak correlation between θ_{-1500} and organic matter may be explained by the strong dependence of particle surface area rather than soil

structure on soil water retention at matric potentials close to -1500 kPa. Water content at field capacity (i.e. upper limit for plant available water) is typically measured either at a matric potential of -10 kPa (θ_{-10}) (van Lier, 2017; Parker et al., 2021) or -33 kPa (θ_{-33}) (Rawls et al., 1982; Saxton and Rawls, 2006; van Lier, 2017). Both measured θ_{-10} and θ_{-33} positively correlated with clay content and organic matter and negatively correlated with sand content (Figure 2.4), which is not surprising since clay and organic matter promotes soil aggregation (Bronick and Lal, 2005), which in turn affects soil water retention at the wet-end of the retention curve. In addition, both θ_{-10} and θ_{-33} positively correlated with θ_{-1500}, suggesting that θ_{-1500} could be estimated using θ_{-10} and θ_{-33}. In our study, the textural class average θ_{-10} ranged from 0.29 to 0.44 $cm^3\ cm^{-3}$ while the textural class average θ_{-33} ranged from 0.21 to 0.43 $cm^3\ cm^{-3}$ (Table 2.2). The loam and sandy loam soils recorded the highest discrepancy between θ_{-10} and θ_{-33} (0.10 $cm^3\ cm^{-3}$), while the least discrepancy was observed in the clay soil (0.01 $cm^3\ cm^{-3}$). The resulting textural class average plant available water capacity estimated using θ_{-10} ranged from 0.13 to 0.25 $cm^3\ cm^{-3}$, while the average plant available water capacity estimated using θ_{-33} ranged from 0.11 to 0.18 $cm^3\ cm^{-3}$ (Table 2.2). This implies that estimated plant available water capacity can change up to 43% in sandy loam soils and 39% in loam soils depending on the selected matric potential to denote field capacity. On the other hand, clay, sandy clay loam, and silty clay soils are less sensitive to the choice of an upper limit with discrepancies of 15% for clay, 16% for sandy clay loam, and 17% for silty clay (Table 2.2). The discrepancy in estimated plant available water capacity due to the choice of an upper limit suggests the need to either better document the matric potential values of the upper limit in research studies or use alternative approaches based on negligible drainage rates (Nachabe, 1998).

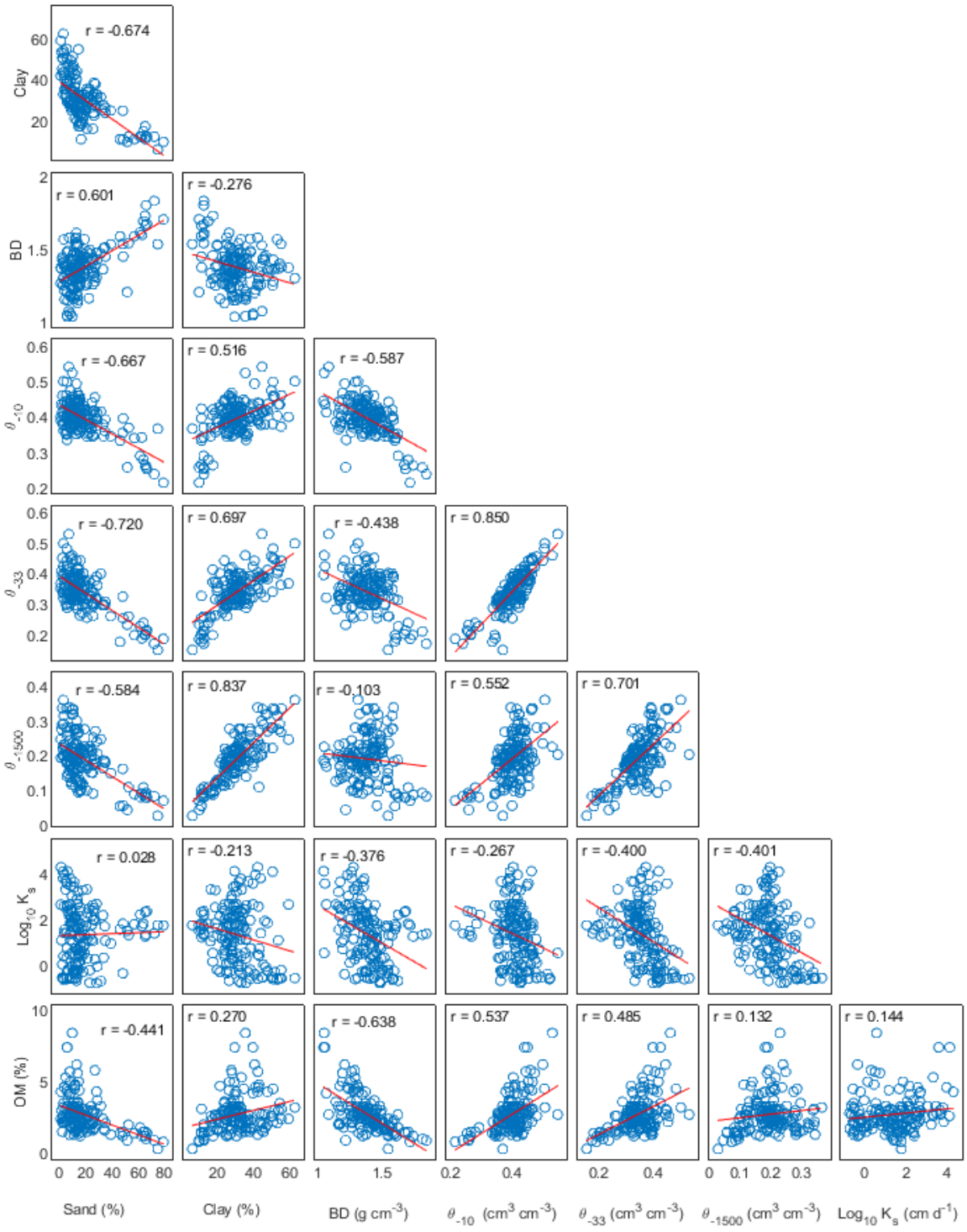

Figure 2.4 Graphical correlation matrix of a selected number of measured soil physical properties for the Kansas Mesonet (N= 160).

Table 2.3 Number of samples per soil textural class (N), textural class mean fitted hydraulic parameters of the van Genuchten (1980) model for the Kansas Mesonet soils. θs, is saturation water content, θ_r is residual water content, and α relates to the inverse of air-entry pressure, and n is a measure of pore size distribution. θ_s, and θ_r, are also results from the fitting exercise. Values in the bracket are standard deviations. Abbreviated textural classes are clay loam (C loam), sandy clay loam (S C L), sandy loam (Sandy L), silt loam (Si Loam), silty clay (Si Clay), and silty clay loam (Si C L).

Textural class	*N*	θ_s	θ_r	α	n
		$cm^3\ cm^{-3}$	$cm^3\ cm^{-3}$	kPa^{-1}	-
Clay	10	0.46 (0.05)	0.10 (0.09)	0.05 (0.07)	1.15 (0.05)
C loam	40	0.43 (0.04)	0.08 (0.09)	0.19 (0.25)	1.26 (0.14)
Loam	16	0.40 (0.06)	0.07 (0.05)	0.11 (0.11)	1.60 (0.50)
S C L	2	0.37 (0.05)	0.03 (0.02)	0.03 (0.03)	1.25 (0.10)
Sandy L	24	0.34 (0.04)	0.03 (0.03)	0.20 (0.21)	1.41 (0.35)
Si loam	72	0.44 (0.05)	0.06 (0.07)	0.15 (0.23)	1.41 (0.30)
Si clay	52	0.47 (0.04)	0.10 (0.10)	0.24 (0.35)	1.20 (0.11)
Si C L	104	0.46 (0.05)	0.08 (0.08)	0.23 (0.31)	1.31 (0.40)

Fitted textural class average soil hydraulic parameters of the van Genuchten (1980) model derived from the measured water retention curves varied from 0.34 to 0.47 $cm^3\ cm^{-3}$ for saturated water content (θ_s), 0.03 to 0.10 $cm^3\ cm^{-3}$ for residual water content (θ_r), 0.05 to 0.24 cm^{-1} for α, and 1.15 to 1.60 for n (Table 2.3). The fitted θ_s were similar to the measured effective saturation of the soils and were slightly lower (4 to 12%) than the observed total porosity (Table 2.1). On the other hand, θ_r was lower than the water content at the permanent wilting point in all soil textural classes (Table 2.2). Clay and silty clay soils had the highest θ_r = 0.10 $cm^3\ cm^{-3}$, while the sandy loam and sandy clay loam soils had the lowest θ_r = 0.03 $cm^3\ cm^{-3}$ (Table 2.3), which is consistent with the trend observed in other studies in US soils (Rawls et al., 1982; Schaap et al., 2001; Scott et al., 2013). Soil water retention curves developed using depth-specific van Genuchten hydraulic parameters agreed with the measured water retention curves with an RMSE range of 0.0023 – 0.022 $cm^3\ cm^{-3}$. Figure 2.5 shows representative depth-specific

soil water retention curves developed using van Genuchten parameters derived for four Mesonet stations with soil profiles dominated by silty clay, silty clay loam, loam, and sandy loam. The lowest station RMSE was 0.002 cm^3 cm^{-3} recorded in the silty clay loam soil at 5 cm depth in Ashland Bottoms station (Figure 2.5B), whereas the highest RMSE was 0.022 cm^3 cm^{-3} recorded in the sandy loam soil at 20 cm depth in Lake city station (Figure 2.5L).

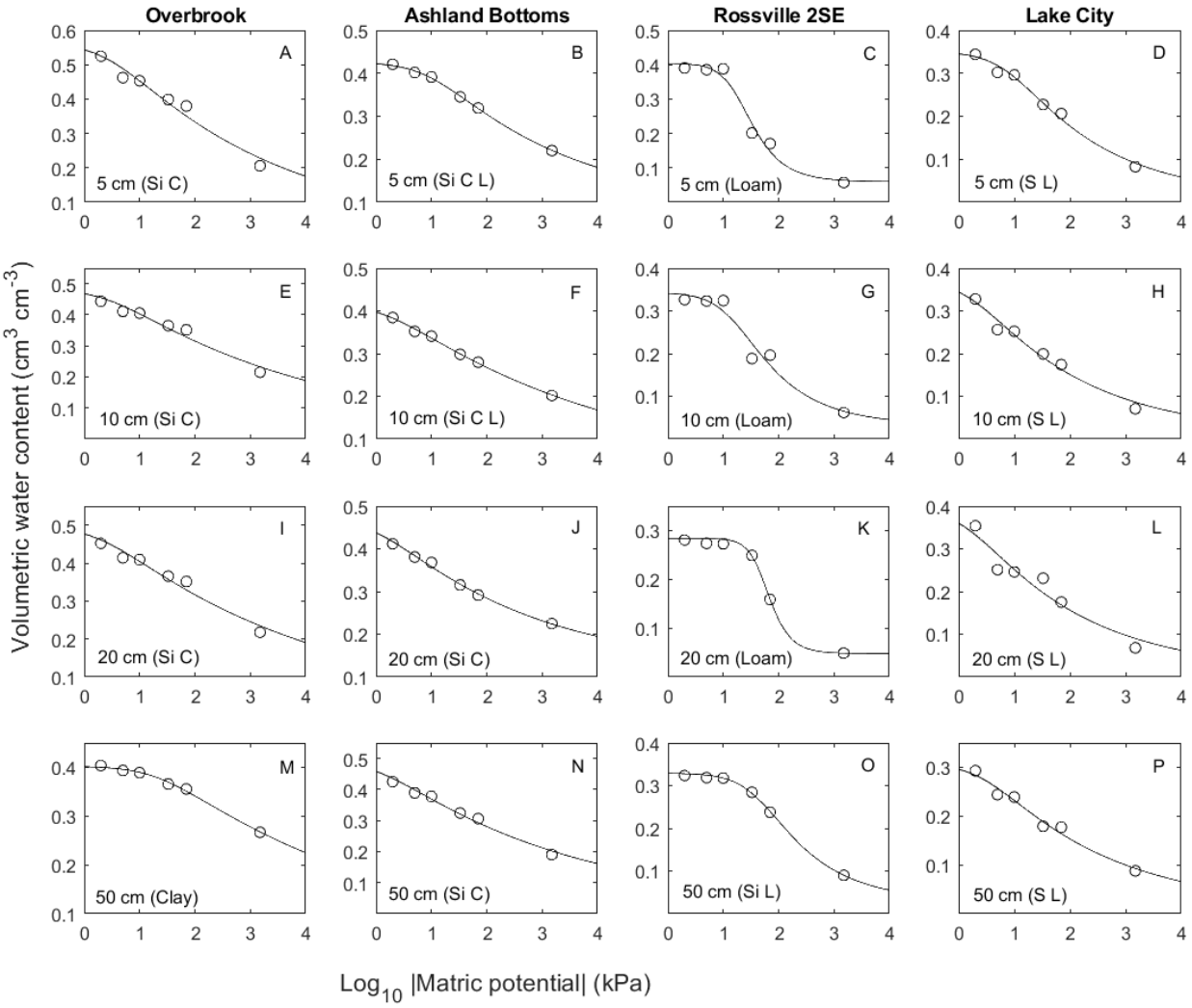

Figure 2.5 Measured soil water retention curve (markers) and fitted van Genuchten soil water retention model (lines) for the soil profiles at the Overbrook, Ashland Bottoms, Rossville, and Lake City stations. Abbreviated textural classes are silty clay (Si Clay), silty clay loam (Si C L), silt loam (Si L), and sandy loam (Sandy L). The highest RMSE of 0.022 cm^3 cm^{-3} was observed at 20 cm depth in the Lake City station and the lowest RMSE of 0.002 cm^3 cm^{-3} was observed at 5 cm depth in the Ashland Bottoms station.

Soil thermal properties

A unique feature of the database in our study is the measurement of soil thermal properties, comprising thermal conductivity and volumetric heat capacity across a wide range of soil types and volumetric water contents. Soil thermal conductivity decreased with decreasing (i.e., more negative) matric potential and varied from 1.30 to 2.0 W $m^{-1}K^{-1}$ at soil saturation to 0.41 to 0.69 W $m^{-1}K^{-1}$ at oven-dryness across eight textural classes (Table 2.4). The decrease in thermal conductivity with decreasing matric potential was due to the reduction of soil moisture, which decreases the contact area between the soil solids for heat conduction (Johansen, 1975; Ochsner et al., 2001; Lu et al., 2007). Soil thermal conductivity is primarily driven by soil water content, air-filled porosity, and bulk density due to their effect on the area of contact between soil particles (Ochsner et al., 2001; Tian et al., 2020). This implies that soil thermal conductivity increases with increasing water content and (or) increasing bulk density, whereas thermal conductivity also decreases with increasing air-filled porosity (Ochsner et al., 2001). In our soils, the coarse soils (sandy loam and sandy clay loam) had higher thermal conductivities than the fine-textured soils from saturation up to matric potential of -70 kPa, despite the coarse soils having comparatively lower water contents than the fine soils at the same matric potentials while having a similar air-filled porosity value at the same potentials, suggesting that the higher bulk density of the coarse soils (Table 2.1) had a major influence on the thermal conductivity of our soils than the water content did. The dry thermal conductivity, however, was similar in all the soils except in the sandy clay loam and the clay soils, which recorded slightly higher thermal conductivity values (Table 2.4). The similar dry thermal conductivity values might be due to the residual water content (Table 2.3) of the fine soils possibly offsetting the effect of bulk density on oven-dry soil thermal conductivity.

Table 2.4 Number of samples per soil textural class (N) and textural class mean of soil thermal conductivity (λ) and volumetric heat capacity (C) at saturation, at -33 kPa, at -70 kPa, and oven-dry conditions. Values in bracket are standard deviation. Abbreviated textural classes are clay loam (C loam), sandy clay loam (S C L), sandy loam (Sandy L), silt loam (Si Loam), silty clay (Si Clay), and silty clay loam (Si C L).

Textural class	*N*	λ_{sat}	λ_{-33}	λ_{-70}	λ_{dry}	C_{sat}	C_{-33}	C_{-70}	C_{dry}
		$Wm^{-1}K^{-1}$	$Wm^{-1}K^{-1}$	$Wm^{-1}K^{-1}$	$Wm^{-1}K^{-1}$	$MJ\ m^{-3}K^{-1}$	$MJ\ m^{-3}K^{-1}$	$MJ\ m^{-3}K^{-1}$	$MJ\ m^{-3}K^{-1}$
Clay	10	1.30 (0.1)	1.26 (0.1)	1.25 (0.1)	0.58 (0.1)	2.75 (0.4)	2.41 (0.5)	2.39 (0.4)	1.33 (0.3)
C loam	36	1.47 (0.1)	1.34 (0.1)	1.27 (0.2)	0.50 (0.2)	2.69 (0.3)	2.31 (0.4)	2.13 (0.3)	1.34 (0.2)
Loam	16	1.52 (0.1)	1.43 (0.2)	1.35 (0.1)	0.41 (0.1)	2.59 (0.3)	2.14 (0.3)	1.92 (0.3)	1.14 (0.1)
S C L	2	1.89 (0.3)	1.88 (0.1)	1.83 (0.1)	0.69 (0.0)	2.90 (0.2)	2.36 (0.5)	2.42 (0.2)	1.81 (0.2)
Sandy L	24	2.00 (0.2)	1.70 (0.2)	1.64 (0.2)	0.51 (0.1)	2.61 (0.3)	2.10 (0.3)	2.02 (0.3)	1.27 (0.2)
Si Loam	72	1.46 (0.2)	1.34 (0.3)	1.32 (0.3)	0.41 (0.1)	2.64 (0.3)	2.25 (0.3)	1.99 (0.3)	1.27 (0.2)
Si Clay	52	1.31 (0.1)	1.24 (0.1)	1.21 (0.1)	0.48 (0.2)	2.78 (0.3)	2.36 (0.4)	2.27 (0.4)	1.30 (0.3)
Si C L	104	1.32 (0.1)	1.21 (0.2)	1.15 (0.2)	0.43 (0.1)	2.78 (0.3)	2.37 (0.3)	2.16 (0.3)	1.36 (0.3)

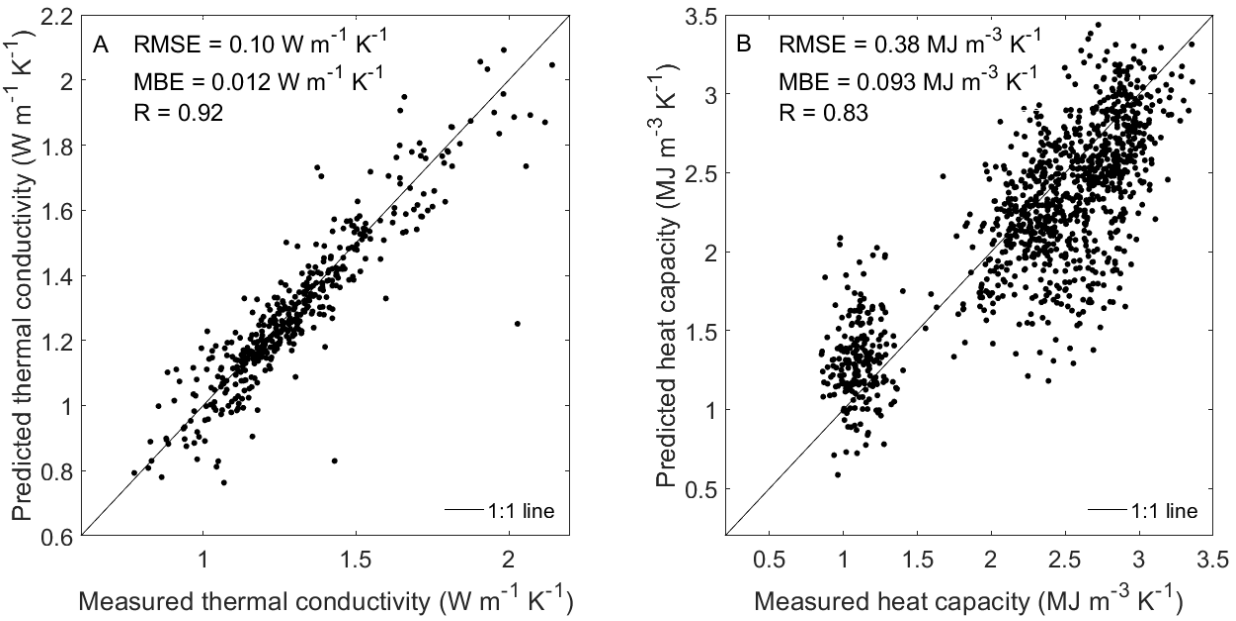

Figure 2.6 Measured versus predicted A) thermal conductivity using the Johansen (1975) model and B) volumetric heat capacity using De Vries (1963) additive model for the 320 soil samples collected at stations of the Kansas Mesonet. The thermal conductivity predictions were made using a total of 428 observations (at -33 and -70 kPa) and the volumetric heat capacity predictions were made using a total of 1107 observation points (at saturation, -33 kPa, -70 kPa, and oven-dryness). The saturation and oven-dry thermal conductivity values were not included in Figure 2.6A because they represent the maximum and minimum points used in the normalization of the Johansen model. Positive MBE represents overestimation and negative bias represents underestimation by model.

Due to the difficult nature of in situ measurements of soil thermal properties, researchers typically rely on models as a function of water content or other easily measurable soil variables (Lu et al., 2007). Hence, we validated a simple thermal conductivity model that assumes a linear relationship between the normalized soil thermal conductivity and the relative soil saturation based on the saturation and oven-dry thermal conductivities (Johansen 1975). The predicted soil thermal conductivity using the Johansen model across 428 soil samples at -33 and -70 kPa using resulted in an overall RMSE of 0.10 W m^{-1} K^{-1} and a bias of 0.012 W m^{-1} K^{-1} (Figure 2.6A). The error of the Johansen model in our study falls within the range of RMSE 0.073 to 0.203 W m^{-1} K^{-1} reported in previous studies (Farouki, 1981; Lu et al., 2007; Zhang et al., 2018). The good

accuracy and the simplicity of the Johansen model appear as a promising alternative for predicting soil thermal conductivity along with the entire soil moisture range.

Similar to the thermal conductivity, the soil volumetric heat capacity decreased with decreasing matric potential across the soil textural classes and varying from 2.59 to 2.90 MJ m^{-3} K^{-1} at saturation to 1.14 to 1.81 MJ m^{-3} K^{-1} at oven-dryness (Table 2.4). Sandy clay loam had the highest values for volumetric heat capacity at all the matric potentials while the remaining soil textures recorded similar volumetric heat capacity values at all the matric potentials. We also observed that volumetric heat capacity increased linearly with increasing volumetric water content in the various soil textures. Based on the linear relationship between volumetric heat capacity and volumetric water content, we validated de Vries (1963) additive model for estimating volumetric heat capacity of soils using the volume fractions and volumetric heat capacities of water and soil solids. Overall, the de Vries model overestimated the observed volumetric heat capacity with a bias of 0.093 MJ m^{-3} K^{-1} (Figure 2.6B). The RMSE between predicted and observed volumetric heat capacity was 0.38 MJ m^{-3} K^{-1}. The widely scattered points around the 1:1 line might be due to measurement error and variation in the volumetric heat capacity of soil minerals (C_m) across the soil textural classes because we represented C_m with a value of 1.92 MJ m^{-3} K^{-1} (de Vries, 1963) in all the soils, regardless of the soil texture, in the model validation because there is no well-defined value for C_m in the literature. Different values have been reported in the literature for C_m, including 1.92 MJ m^{-3} K^{-1} (de Vries, 1963), 2.13 and 2.39 MJ m^{-3} K^{-1} (Bristow and White, 1994), and 2.0 and 2.5 (Ochsner et al., 2001). However, upon testing C_m values ranging from 1.92 to 2.5 MJ m^{-3} K^{-1} in the de Vries (1963) model, the C_m value of 1.92 MJ m^{-3} K^{-1} resulted in the best overall estimates of volumetric heat capacity in our soils (RMSE of 0.38 MJ m^{-3} K^{-1}). To the best of our knowledge, this is the first published

database of soil physical properties for a mesoscale in situ network that includes soil thermal properties, enabling new opportunities for mesoscale research of coupled heat and water transport.

Soil chemical properties and soil color

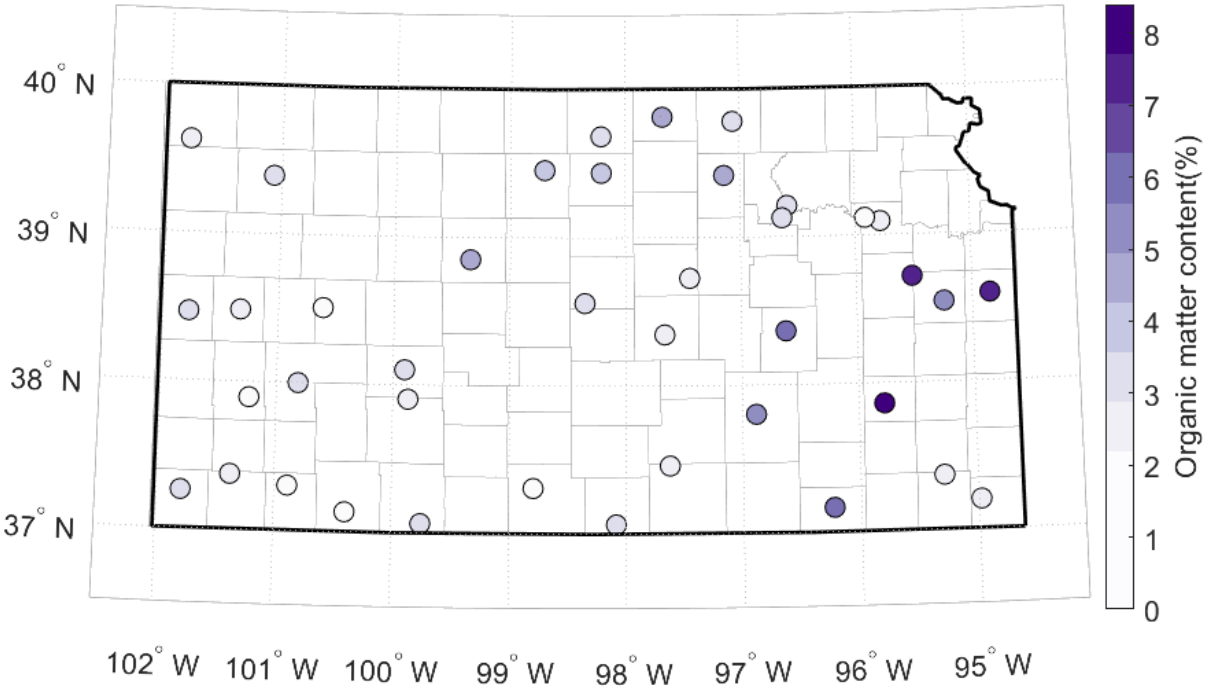

Figure 2.7 Pattern of soil organic matter content at the top 5 cm depth across the state of Kansas. The figure shows increasing soil organic matter across the state of Kansas from west to east.

Overall, the top 5 cm soils in the Kansas Mesonet showed a pattern of increasing organic matter content across the state from west to east, ranging from 1.5 to 8.4% (Figure 2.7). The observed pattern of soil organic matter across Kansas is consistent with the annual precipitation gradient across the state, which varies from ~400 mm in western Kansas to ~1200 mm in eastern Kansas (Lin et al., 2017). The organic matter content of our soils also decreased with soil depth with an average of 3.5 ± 1.6% at 5 cm depth to 1.9 ±0.6% at 50 cm depth (Table 5). The trend of decreasing organic matter with soil depth in our soils is expected because the surface soil layer is

where organic matter accumulation and decomposition occurs. As expected, the soil total carbon showed a similar pattern to the soil organic matter content since organic carbon is a component of soil organic matter (Table 2.5). The total nitrogen and pH of our soils were similar in all the soil depths analyzed. Overall, our soils were neutral with a depth-specific average pH of approximately 7, which could be attributed to the high amount of organic matter (≥ 2%) and available basic cations (K, Ca, Mg, Na) in our soils (Table 2.5) that regulates the soil pH.

Table 2.5 Number of samples per soil moisture sensor depth (N) and mean depth-specific soil chemical properties. Values in bracket are standard deviation. OM represents organic matter content, TC is total carbon, TN is total nitrogen, pHBuf is buffer pH, P is phosphorus, K is potassium, Ca is calcium, Mg is magnesium, and Na is sodium.

Depth	N	OM	TC	TN	pH	pHBuf	P	K	Ca	Mg	Na
cm		%	%	%			ppm	ppm	ppm	ppm	ppm
5	40	3.5 (1.6)	2.0 (0.9)	0.2 (0.1)	6.6 (0.8)	6.9 (0.4)	34	467	2713	328	46
10	40	2.8 (1.1)	1.6 (0.6)	0.1 (0.1)	6.7 (0.8)	6.9 (0.4)	25	405	2758	342	49
20	40	2.5 (1.0)	1.3 (0.5)	0.1 (0.0)	6.8 (0.9)	6.9 (0.4)	19	368	3017	409	58
50	40	1.9 (0.6)	1.0 (0.4)	0.1 (0.0)	7.3 (0.9)	7.1 (0.4)	14	385	3750	620	126

The soils analyzed in this study showed a similar color at the top 50 cm soil profile with similar wet and dry values for L^*, a^*, and b^* (Table 2.6). The L^* value, which represent the blackness of color (0 for black and 100 for white) (McLaren, 1976), varied from 27.3 ± 3.6 at the top 5 cm depth to 32 ±5.8 at 50 cm depth under wet condition, whereas at oven-dryness, L^* varied from 47.7 ± 4.9 at the top 5 cm depth to 51.9 ±9 at 50 cm depth (Table 2.6). The pattern of lower L^* in the top 5 cm soil layer than the deeper soil layers implies that the surface soil layer was darker than the deeper layers, which aligns with the pattern of soil organic matter variation with depth in our soils (Table 2.5). Similar to the organic matter distribution, the soil blackness increased across the state of Kansas from west to east (Figure A2 in Appendix A). Overall, the soil blackness (L^*) showed a negative correlation with soil organic matter content,

regardless of soil moisture condition (Figure 2.8). The observed negative relationship between the *L** and organic matter in our study agrees with the observations in previous studies (Spielvogel et al., 2004; Liles et al., 2013), which suggests soil organic matter is a useful variable for predicting soil color.

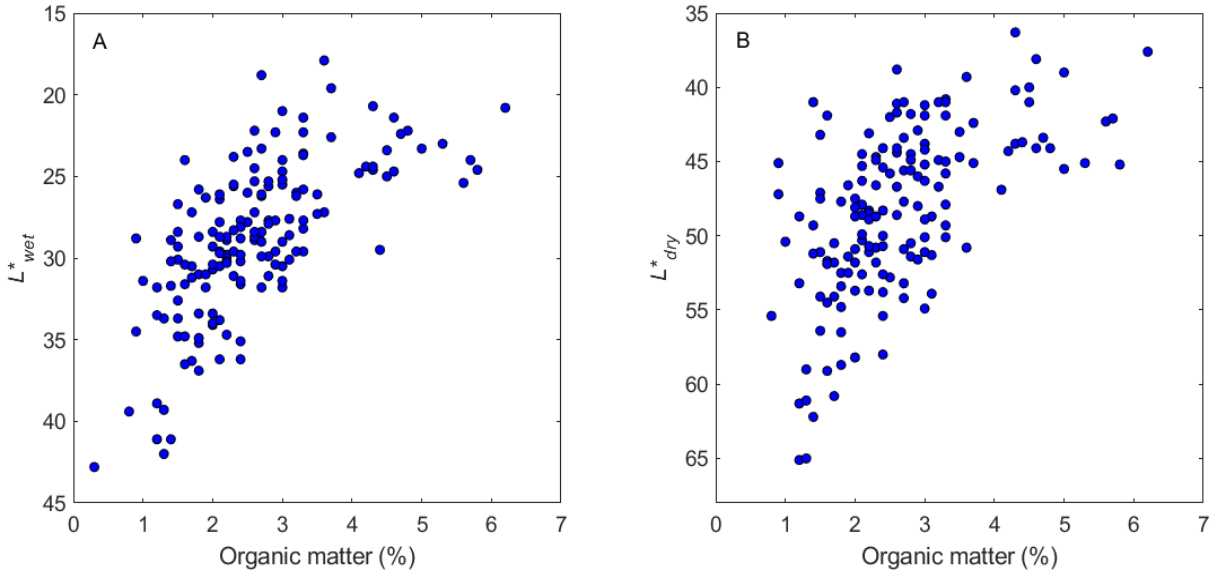

Figure 2.8 Relationship between soil organic matter and soil color expressed in the CIELAB color space in terms of light- and darkness (*L**) under A) wet conditions (L^*_{wet}) and B) Oven-dry conditions (L^*_{dry}). The lower the *L** value, the darker the soil color. Both figures show that soil color gets darker as organic matter content increases, regardless of the soil moisture status.

Table 2.6 Number of samples per soil moisture sensor depth (*N*) and depth-specific soil color expressed in the CIELAB color space. Values in bracket are standard deviation. Values for *L** represent lightness in color from black (0) to white (100), *a** represents a variation from green (−) to red (+), and *b** represents a variation from blue (−) to yellow (+).

Depth	*N*	L^*_{wet}	a^*_{wet}	b^*_{wet}	L^*_{dry}	a^*_{dry}	b^*_{dry}
cm							
5	40	27.3 (3.6)	5.6 (1.5)	9.2 (2.0)	47.7 (4.9)	6.7 (1.9)	12.8 (2.4)
10	40	27.3 (3.6)	5.4 (1.6)	9.0 (2.1)	46.6 (5.7)	6.6 (2.0)	12.8 (2.7)
20	40	28.1 (4.0)	5.7 (1.9)	9.3 (2.3)	46.9 (5.0)	6.7 (2.3)	13.0 (2.8)
50	40	32.0 (5.8)	6.8 (2.5)	12.0 (3.0)	51.9 (7.0)	7.4 (3.3)	15.0 (3.7)

In situ validation of soil moisture

The volumetric water content at the time of sampling was used to validate three common calibration models for the CS655 soil water reflectometers. The RMSE using the factory default calibration equation for the entire database was 0.084 cm^3 cm^{-3} (Figure 2.9A; Table 2.7). On the other hand, the validation of the three common models for the entire database using coefficients (*a*, *b*, and *c*) derived from laboratory sensor calibration in an independent study resulted in a similar accuracy with RMSE of 0.062 cm^3 cm^{-3} for Ledieu et al (1986), 0.060 cm^3 cm^{-3} for Evett et al., (2005), and 0.061 cm^3 cm^{-3} for Kargas and Soulis (2019) models (Figures 2.9B – 2.9D; Table 2.7). This implies that applying independent laboratory sensor calibration coefficients could improve the accuracy in soil moisture estimation by at least 29% compared to the factory-default model that is based on Topp et al. (1980). As expected, all the models had a similar RMSE using the optimized parameters from the in-situ soil samples, which interestingly, were similar to the accuracy of using the lab-calibration coefficients that were derived from the independent study (Table 2.7). Overall, the least discrepancy between laboratory-based and field-based calibration of the CS655 water reflectometer sensors in our soils suggests that an independent laboratory sensor calibration and field-based sensor calibration in site-specific soils are comparable. Thus, performing laboratory-based sensor calibrations could save mesonet managers from the laborious and daunting work associated with performing site-specific field sensor calibration across an entire network of stations.

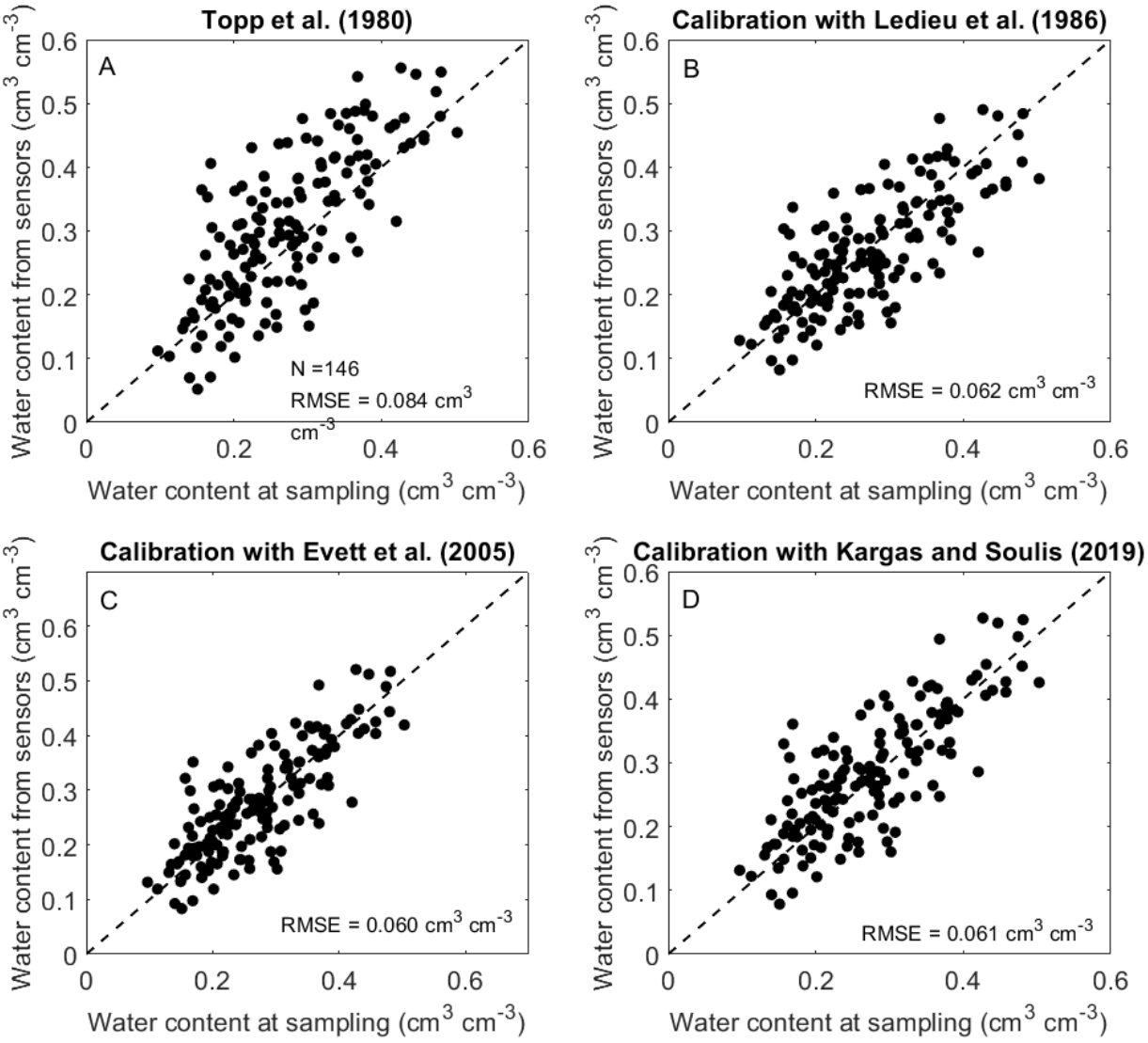

Figure 2.9 Observed volumetric soil water content (θ) based on the thermogravimetric method versus θ of the CS655 soil water reflectometers at the time of sampling obtained using A) the factory default calibration equation of Topp et al. (1980), and separate laboratory sensor calibration coefficients derived in an independent study based on the linear models by B) Ledieu et al. (1986), C) Evett et al. (2005), and D) Kargas and Soulis (2019). The dashed line represents the 1:1 line.

Table 2.7 In situ validation of the CS655 soil water reflectometer sensor using common models for estimating volumetric water content from the apparent dielectric permittivity using coefficients (a, b, c, and d) derived from an independent laboratory sensor calibration in a separate study. The optimized coefficients were obtained from the least-squares fitting of the models to the water contents of the in-situ soil samples at the time of sampling. *r* represents the coefficient of correlation, RMSE represents the root mean squared error, and MBE represents the mean bias error. Negative MBE represents underestimation and positive MBE represents overestimation.

Calibration model	*a*	*b*	*c*	*d*	*r*	RMSE	MBE
						$cm^3\ cm^{-3}$	$cm^3\ cm^{-3}$
Factory default							
Topp et al. 1980	-5.30×10^{-2}	2.92×10^{-2}	-5.50×10^{-4}	4.30×10^{-6}	0.76	0.084	0.03
Independent study							
Ledieu et al. 1986	-0.080	8.25×10^{-2}			0.77	0.062	-0.005
Evett et al. 2005	-0.101	9.94×10^{-2}	-7.67×10^{-2}		0.80	0.060	0.003
Kargas & Soulis 2019	-0.115	9.89×10^{-2}	-5.72×10^{-2}		0.79	0.061	0.009
Optimized coefficients							
Topp et al. 1980	0.122	8.58×10^{-3}	-3.30×10^{-6}	-7.40×10^{-7}	0.77	0.059	
Ledieu et al. 1986	7.80×10^{-3}	6.30×10^{-2}			0.77	0.058	
Evett et al. 2005	-9.70×10^{-3}	8.81×10^{-2}	-0.163		0.82	0.052	
Kargas & Soulis 2019	$-3.81\ 10^{-2}$	8.19×10^{-2}	-9.74×10^{-2}		0.81	0.054	

Based on the overall RMSE of the factory-default calibration equation of the CS655 water reflectometer in our soils, the overall uncertainty of the Kansas Mesonet soil moisture data is 0.084 $cm^3\ cm^{-3}$. The uncertainty of our soil moisture data was higher than the overall uncertainty of the soil moisture data for other networks with RMSE of 0.053 $cm^3\ cm^{-3}$ for both the Oklahoma Mesonet (Scott et al., 2013) and the Texas Soil Observation Network (TxSON) (Caldwell et al., 2018). The discrepancy between the uncertainty in our moisture data and the data of the other networks could be attributed to differences in the type of soil moisture sensor and differences in sample size used in the soil moisture validation. For instance, the Kansas Mesonet monitors soil moisture using a soil water reflectometer, whereas the Oklahoma Mesonet (McPherson et al., 2007) uses a heat dissipation sensor, which is based on soil matric potential. The TxSON on the other hand uses the same CS655 water reflectometer sensor and factory-

default equation as the Kansas Mesonet had a larger number and range of soils than the TxSON moisture validation (Caldwell et al., 2018), which is only 5% of the 320 total samples across 40 stations (at 5, 10, 20, and 50 cm depths) used in our moisture validation. The depth-specific RMSE using the default model in our soils increased with depth from 0.073 cm^3 cm^{-3} at 5cm depth to 0.11 cm^3 cm^{-3} at 50 cm depth, which is contrary to the trend of decreasing RMSE with depth from 0.061 cm^3 cm^{-3} at 5 cm to 0.033 cm^3 cm^{-3} at 75 cm depth reported for the Oklahoma Mesonet soil moisture data. Notwithstanding, the RMSE of the default equation at 5 cm depth (i.e. 0.073 cm^3 cm^{-3}) in our soils was equal to the RMSE reported in a laboratory calibration of the CS655 using the default equation and soil samples from the top 5 cm depth at five stations in the TxSON (Caldwell et al., 2018). To the best of our knowledge, the Kansas Mesonet and Oklahoma Mesonet are the only large-scale in situ networks that have been published in peer-reviewed journals networkwide in situ soil moisture validation, making the Kansas Mesonet soil moisture observations one of the most reliable soil moisture databases in the world for mesoscale environmental research applications.

Conclusions

We developed a comprehensive database of site-specific soil physical properties for the Kansas Mesonet, which is available at the KSU Soil Water Processes Lab upon request. Our soil database captured eight out of the 12 textural classes, which were dominated by fine soils with 93% of our samples having >20% clay content. Silty clay loam, silt loam, and silty clay soils were the dominant fine-textured soils in the Kansas Mesonet, whereas sandy loam and sandy clay loam were the only coarse soils found. The average bulk density of our soils ranged from 1.33 g cm^{-3} in silty clay loam to 1.67 1.33 g cm^{-3}. The median textural class saturated hydraulic conductivity in our soil varied from 0.52 to 47.1 cm d^{-1} and the average plant available water

capacity ranged from 0.13 cm^3 cm^{-3} in clay to 0.25 cm^3 cm^{-3} in silt loam. The database of soil physical properties allowed us to determine the uncertainty in the Kansas Mesonet soil moisture data and also allowed us to identify a better calibration model for the soil water reflectometers. The uncertainty in the soil moisture data was 0.084 cm^3 cm^{-3}, which could be improved by at least 29% compared to the factory-default equation for the moisture sensor when independent lab-calibrated sensor coefficients based on the models of Ledieu et al. (1986), Evett al. (2005), and Kargas and Soulis (2019) are used in the moisture equation for the sensors. These new models will improve estimates of rootzone soil water storage that can be used to better assess the inventory of soil water across the state of Kansas. This database opens new opportunities to use the Kansas Mesonet soil moisture and temperature observations for drought monitoring and drainage and groundwater recharge estimations, and also for other applications in civil engineering and urban planning.

References

Barkley, A., J. Tack, L.L. Nalley, J. Bergtold, R. Bowden, et al. 2014. Weather, disease, and wheat breeding effects on Kansas wheat varietal yields, 1985 to 2011. Agronomy Journal 106(1): 227–235. doi: 10.2134/agronj2013.0388.

Blanco-Canqui, H., R. Lal, W.M. Post, R.C. Izaurralde, and M.J. Shipitalo. 2006. Organic Carbon Influences on Soil Particle Density and Rheological Properties. Soil Science Society of America Journal 70(4): 1407–1414. doi: 10.2136/sssaj2005.0355.

Botula, Y.D., W.M. Cornelis, G. Baert, and E. van Ranst. 2012. Evaluation of pedotransfer functions for predicting water retention of soils in Lower Congo (D.R. Congo). Agricultural Water Management 111: 1–10. doi: 10.1016/j.agwat.2012.04.006.

Bristow, K.L., and R.D. White. 1994. Comparison of single and dual probes for measuring soil thermal properties with transient heating. Australian Journal of Soil Research 32(3): 447–464. doi: 10.1071/SR9940447.

Bronick, C.J., and R. Lal. 2005. Soil structure and management: A review. Geoderma 124(1–2): 3–22. doi: 10.1016/j.geoderma.2004.03.005.

Brookfield, A.E., M.C. Hill, M. Rodell, B.D. Loomis, R.L. Stotler, et al. 2018. In Situ and GRACE-Based Groundwater Observations: Similarities, Discrepancies, and Evaluation in the High Plains Aquifer in Kansas. Water Resources Research 54(10): 8034–8044. doi: 10.1029/2018WR023836.

Caldwell, T.G., T. Bongiovanni, M.H. Cosh, C. Halley, and M.H. Young. 2018. Field and Laboratory Evaluation of the CS655 Soil Water Content Sensor. Vadose Zone Journal 17(1): 170214. doi: 10.2136/vzj2017.12.0214.

Dane, J.H. and J.W. Hopmans, 2002. 3.3. 2 Laboratory. Methods of Soil Analysis: Part 4 Physical Methods, 5: 675-720.

Derakhshani, S.M., D.L. Schott, and G. Lodewijks. 2015. Micro-macro properties of quartz sand: Experimental investigation and DEM simulation. Powder Technology 269: 127–138. doi: 10.1016/j.powtec.2014.08.072.

Evett, S.R., J.A. Tolk, and T.A. Howell. 2005. Time Domain Reflectometry Laboratory Calibration in Travel Time, Bulk Electrical Conductivity, and Effective Frequency. Vadose Zone Journal 4(4): 1020–1029. doi: 10.2136/vzj2005.0046.

Farouki, O.T. 1981. Thermal properties of soils.

Flint, A.L. and L.E. Flint, 2002. 2.2 Particle Density. Methods of soil analysis: Part 4 physical methods, 5: 229 – 240.

Garbrecht, J.D., X.C. Zhang, and J.L. Steiner. 2014. Climate Change and Observed Climate Trends in the Fort Cobb Experimental Watershed. Journal of Environmental Quality 43(4): 1319–1327. doi: 10.2134/jeq2013.07.0286.

Gavlak, R., R. Horneck, and R.O. Miller. 2005. Particle size analysis: Hydrometer method.

Grossman, R.B. and T.G. Reinsch, 2002. 2.1 Bulk density and linear extensibility. Methods of soil analysis: Part 4 physical methods, 5: 201– 228.

van Genuchten, M.Th. 1980. A closed-form equation for predicting the hydraulic conductivity of unsaturated soils. Soil Science Society of America Journal 44: 892–898.

Gunal, H. and Ransom, M.D., 2005. Clay mineralogy, specific surface area and micromorphology of polygenetic soils from Eastern Kansas. Archives of Agronomy and Soil Science, 51(4): 459 – 468.

Johansen, O. 1975. Thermal conductivity of soils. doi: 10.1016/0148-9062(78)91007-0.

Kargas, G., and K.X. Soulis. 2019. Performance evaluation of a recently developed soil water content, dielectric permittivity, and bulk electrical conductivity electromagnetic sensor. Agricultural Water Management 213: 568–579. doi: 10.1016/j.agwat.2018.11.002.

Klute, A. 1965. Laboratory measurement of hydraulic conductivity of saturated soil. Methods of Soil Analysis, Part 1: Physical and Mineralogical Properties, Including Statistics of Measurement and Sampling: 210–221. doi: 10.2134/agronmonogr9.1.c13.

Layzell, A.L., R.D. Mandel, T.M. Rittenour, J.J. Smith, H.R. Harlow, et al. 2016. Stratigraphy, morphology, and geochemistry of late Quaternary buried soils on the high plains of southwesten Kansas, USA. Catena 144: 45–55.

Ledieu, J., P. de Ridder, P. de Clerck, and S. Dautrebande. 1986. A method of measuring soil moisture by time-domain reflectometry. Journal of Hydrology 88(3–4): 319–328. doi: 10.1016/0022-1694(86)90097-1.

van Lier, Q.D.J., 2017. Field capacity, a valid upper limit of crop available water? Agricultural Water Management 193: 214–220. doi: 10.1016/j.agwat.2017.08.017.

Liles, G.C., Beaudette, D.E., O'Geen, A.T. and Horwath, W.R., 2013. Developing predictive soil C models for soils using quantitative color measurements. Soil Science Society of America Journal, 77(6): 2173–2181.

Lipiec, J., B. Usowicz, and A. Ferrero. 2007. Impact of soil compaction and wetness on thermal properties of sloping vineyard soil. International Journal of Heat and Mass Transfer 50(19–20): 3837–3847. doi: 10.1016/j.ijheatmasstransfer.2007.02.008.

Lin, X., Harrington, J., Ciampitti, I., Gowda, P., Brown, D. and Kisekka, I., 2017. Kansas trends and changes in temperature, precipitation, drought, and frost-free days from the 1890s to 2015. Journal of Contemporary Water Research & Education, 162(1): 18 – 30.

Lollato, R.P., G.P. Bavia, V. Perin, M. Knapp, E.A. Santos, et al. 2020. Climate-risk assessment for winter wheat using long-term weather data. Agronomy Journal 112(3): 2132–2151. doi: 10.1002/agj2.20168.

Lollato, R.P., J.T. Edwards, and T.E. Ochsner. 2017. Meteorological limits to winter wheat productivity in the U.S. southern Great Plains. Field Crops Research 203: 212–226. doi: 10.1016/j.fcr.2016.12.014.

Lu, S., T. Ren, Y. Gong, and R. Horton. 2007. An Improved Model for Predicting Soil Thermal Conductivity from Water Content at Room Temperature. Soil Science Society of America Journal 71(1): 8–14. doi: 10.2136/sssaj2006.0041.

McBride, R.A., R.L. Slessor, and P.J. Joosse. 2012. Estimating the Particle Density of Clay-rich Soils with Diverse Mineralogy. Soil Science Society of America Journal 76(2): 569–574. doi: 10.2136/sssaj2011.0177n.

McLaren, K., 1976. XIII—The development of the CIE 1976 (L* a* b*) uniform colour space and colour-difference formula. Journal of the Society of Dyers and Colourists, 92(9): 338-341.

McPherson, R.A., C.A. Fiebrich, K.C. Crawford, R.L. Elliott, J.R. Kilby, et al. 2007. Statewide monitoring of the mesoscale environment: A technical update on the Oklahoma Mesonet. Journal of Atmospheric and Oceanic Technology 24(3): 301–321. doi: 10.1175/JTECH1976.1.

Miller, R.L., C.L. Ziegler, and M.I. Biggerstaff. 2020. Seven-doppler radar and in situ analysis of the 25-26 June 2015 Kansas MCS during PECAN. Monthly Weather Review 148(1): 211–240. doi: 10.1175/MWR-D-19-0151.1.

Nachabe, M.H. 1998. Refining the definition of field capacity in the literature. Journal of irrigation and drainage engineering 124(4): 230–232.

Ochsner, T.E., R. Horton, and T. Ren. 2001. A New Perspective on Soil Thermal Properties. Soil Science Society of America Journal 65(6): 1641–1647. doi: 10.2136/sssaj2001.1641.

Pan, W., R.P. Boyles, J.G. White, and J.L. Heitman. 2012. Characterizing soil physical properties for soil moisture monitoring with the North Carolina environment and climate observing network. Journal of Atmospheric and Oceanic Technology 29(7): 933–943. doi: 10.1175/JTECH-D-11-00104.1.

Parker, N., W.M. Cornelis, K. Frimpong, E. Oppong Danso, E. Bessah, et al. 2021. Short-term effects of rice straw biochar on hydraulic properties and aggregate stability of an Acrisol. Soil Research: 1–31.

Patrignani, A., M. Knapp, C. Redmond, and E. Santos. 2020a. Technical overview of the kansas mesonet. Journal of Atmospheric and Oceanic Technology 37(12): 2167–2183. doi: 10.1175/JTECH-D-19-0214.1.

Patrignani, A., N. Mohankumar, C. Redmond, E.A. Santos, and M. Knapp. 2020b. Optimizing the spatial configuration of mesoscale environmental monitoring networks using a geometric approach. Journal of Atmospheric and Oceanic Technology 37(5): 943–956. doi: 10.1175/JTECH-D-19-0167.1.

Pfeiffer, L., and C.Y.C. Lin. 2014. Does efficient irrigation technology lead to reduced groundwater extraction? Empirical evidence. Journal of Environmental Economics and Management 67(2): 189–208. doi: 10.1016/j.jeem.2013.12.002.

Rawls, W.J., C.L. Brakensiek, and K.E. Saxton. 1982. Estimation of soil water properties. Transactions - American Society of Agricultural Engineers 25(5): 1316–1328. doi: 10.13031/2013.33720.

Reynolds, W.D. and D.E. Elrick, 2002. 3.4. 3.3 Constant head well permeameter (vadose zone). Methods of Soil Analysis: Part 4 Physical Methods, 5: 844-858.

Reynolds, W.D., B.T. Bowman, R.R. Brunke, C.F. Drury, and C.S. Tan. 2000. Comparison of Tension Infiltrometer, Pressure Infiltrometer, and Soil Core Estimates of Saturated Hydraulic Conductivity. Soil Science Society of America Journal 64(2): 478–484. doi: 10.2136/sssaj2000.642478x.

Reynolds, W.D., C.F. Drury, C.S. Tan, C.A. Fox, and X.M. Yang. 2009. Use of indicators and pore volume-function characteristics to quantify soil physical quality. Geoderma 152(3–4): 252–263. doi: 10.1016/j.geoderma.2009.06.009.

Saxton, K.E., and W.J. Rawls. 2006. Soil Water Characteristic Estimates by Texture and Organic Matter for Hydrologic Solutions. Soil Science Society of America Journal 70(5): 1569–1578. doi: 10.2136/sssaj2005.0117.

Schaap, M.G., F.J. Leij, and M.T. Van Genuchten. 2001. Rosetta: A computer program for estimating soil hydraulic parameters with hierarchical pedotransfer functions. Journal of Hydrology 251(3–4): 163–176. doi: 10.1016/S0022-1694(01)00466-8.

Schelle, H., L. Heise, K. Jänicke, and W. Durner. 2013. Water retention characteristics of soils over the whole moisture range: A comparison of laboratory methods. European Journal of Soil Science 64(6): 814–821. doi: 10.1111/ejss.12108.

Scott, B.L., T.E. Ochsner, B.G. Illston, J.B. Basara, and A.J. Sutherland. 2013. New soil property database improves oklahoma mesonet soil moisture estimates. Journal of Atmospheric and Oceanic Technology 30(11): 2585–2595. doi: 10.1175/JTECH-D-13-00084.1.

Sparks, D.L., Page, A.L., Helmke, P.A., Loeppert, R.H., Soltanpour, P.N., Tabatabai, M.A., Johnston, C.T. and Sumner, M.E., 1996. Methods of Soil Analysis Part 3—Chemical Methods; SSSA Book Ser. 5.3. Soil Science Society of America and American Society of Agronomy: Madison, WI, USA.

Spielvogel, S., Knicker, H. and Kögel-Knabner, I., 2004. Soil organic matter composition and soil lightness. Journal of Plant Nutrition and Soil Science, 167(5): 545 – 555.

Steward, D.R., X. Yang, S.Y. Lauwo, S.A. Staggenborg, G.L. MacPherson, et al. 2011. From precipitation to groundwater baseflow in a native prairie ecosystem: A regional study of the Konza LTER in the Flint Hills of Kansas, USA. Hydrology and Earth System Sciences 15(10): 3181–3194. doi: 10.5194/hess-15-3181-2011.

Tack, J., A. Barkley, and L. Lanier Nalley. 2015. Estimating Yield Gaps with Limited Data: An Application to United States Wheat. American Journal of Agricultural Economics 97(5): 1464–1477. doi: 10.1093/ajae/aau157.

Tian, Z., T. Ren, R. Horton, and J.L. Heitman. 2020. Estimating soil bulk density with combined commercial soil water content and thermal property sensors. Soil and Tillage Research 196(May 2019): 104445. doi: 10.1016/j.still.2019.104445.

Topp, G.C., J.L. Davis, and A.P. Annan. 1980. Electromagnetic determination of soil water content: Measurements in coaxial transmission lines. 16(3): 574–582.

Tsoodle, L.J., B.B. Golden, and A.M. Featherstone. 2006. Factors Influencing Kansas Agricultural Farm Land Values.

de Vries, D.A. 1963. Thermal properties of soils: 210–235. In W.R. van Wijk (ed.) Physics of plant environment. North-Holland Publ. Co., Amsterdam, the Netherlands.

Wilson, T.B., C.B. Baker, T.P. Meyers, J. Kochendorfer, M. Hall, et al. 2016. Site-Specific Soil Properties of the US Climate Reference Network Soil Moisture. Vadose Zone Journal 15(11): 1–14. doi: 10.2136/vzj2016.05.0047.

Zhang, M., J. Bi, W. Chen, X. Zhang, and J. Lu. 2018. Evaluation of calculation models for the thermal conductivity of soils. International Communications in Heat and Mass Transfer 94(March): 14–23. doi: 10.1016/j.icheatmasstransfer.2018.02.005.

Zhang, Y., and M.G. Schaap. 2019. Estimation of saturated hydraulic conductivity with pedotransfer functions: A review. Journal of Hydrology 575(May): 1011–1030. doi: 10.1016/j.jhydrol.2019.05.058.

Chapter 3 - Reconstructing Precipitation Events Using Co-located Soil Moisture Information

This work has been accepted for publication in the *Journal of Hydrometeorology*

Nathaniel Parker and Andres Patrignani

Abstract

Complete and accurate precipitation records are important for developing reliable flood warning systems, streamflow forecasts, rainfall-runoff estimates, and numerical land surface predictions. Existing methods for flagging missing precipitation events and filling gaps in the precipitation record typically rely on precipitation from neighboring stations. In this study, we investigated an alternative method for back-calculating precipitation events using changes in rootzone soil water storage. We hypothesized that using a different variable (i.e., soil moisture) from the same monitoring station will be more accurate in estimating hourly precipitation than using the same variable (i.e., precipitation) from the nearest neighboring station. Precipitation events were estimated from soil moisture as the sum of hourly changes in profile soil water storage. Hourly precipitation and soil moisture observations were obtained for a mesoscale network in the central U.S. Great Plains from May 2017 to December 2020. The proposed method based on soil moisture had a minimum detectable limit of 7.6 mm (95^{th} percentile of undetected precipitation events) due to canopy and soil interception. The method was outperformed by the nearest neighbor (NN) interpolation method when neighboring stations were at distances of <10 km. However, the proposed method outperformed the NN method in 22 out of 27 stations when the nearest stations were at distances >10 km. Using changes in soil water storage resulted effective in flagging and reconstructing actual missing precipitation events

caused by pluviometer malfunction, highlighting new opportunities for using readily available in situ soil moisture information for operational quality control in mesoscale environmental monitoring networks.

Introduction

Precipitation is an atmospheric essential climate variable and its accurate quantification is crucial for agricultural, hydrological, and ecological research (Bojinski, et al. 2014). In the U.S., precipitation has been measured using manually-operated pluviometers since 1890 by the U.S. National Weather Service (NWS) Cooperative Observer Program (COOP) (Fiebrich 2009) and since 1997 by the Community Collaborative Rain, Hail, and Snow (CoCoRaHS) citizen science network (Reges et al. 2016). With the advent of electronic dataloggers and the increasing need to record precipitation totals and precipitation intensity at higher temporal resolution (e.g., minute, hourly), automated pluviometers based on tipping-bucket, weighing-bucket, and siphon mechanisms have become standard instrumentation in automated weather networks (McPherson et al. 2007; Patrignani et al. 2020a; Shulski et al. 2018; Sun et al. 2018). However, human errors (in the case of manual pluviometers), and occasional instrument malfunctioning or failure due to normal wear and obstruction of the rain collector in both manual and automated pluviometers can go unnoticed, thus introducing gaps in the historical precipitation record (Shafer et al. 2000; Michaelides et al. 2009). These gaps in the historical precipitation record can ultimately propagate and affect the prediction accuracy of the soil water balance in land surface models, streamflow predictions, and runoff estimates from rainfall-runoff models (Chen et al. 2018; Tan and Yang 2020).

Detecting missing precipitation events due to malfunctioning pluviometers often requires a combination of manual and automated quality control procedures. Manual checks typically

include auxiliary information collected during site visits (e.g. evidence of clogged pluviometer or faulty bearings in tipping bucket mechanism) and corroboration with rainfall observations in nearby stations and multi-sensor gridded precipitation products by trained operators (Shafer et al. 2000; Patrignani et al. 2020a). Automated checks for gross errors in precipitation observations typically include i) range tests, which are aimed at flagging observations that fall outside a pre-established range based on physically plausible values and climate extremes; and ii) step tests, which are aimed at identifying differences between successive observations to identify suspicious changes above an allowable threshold value (Fiebrich and Crawford 2001; Shafer et al. 2000). In the absence of co-located rain gauges, missing precipitation events are typically filled by spatial interpolation of precipitation information from nearby stations (i.e. gap filling using the same variable from different locations). Common spatial interpolation methods for filling missing precipitation records include nearest neighbor (Bárdossy and Pegram 2014), Thiessen polygon (Mair and Fares 2011), and inverse distance weight (di Piazza et al. 2011). These interpolation methods are simple to implement and are available in most software packages (Kashani and Dinpashoh 2012), but do not account for the spatial autocorrelation of precipitation among neighboring stations (Mair and Fares 2011). More sophisticated spatial interpolation methods based on geostatistical principles such as ordinary kriging (Bárdossy and Pegram 2014), kriging with external drift (Verworn and Haberlandt 2011), and geographically weighted regression (di Piazza et al. 2011) can solve this problem by accounting for the spatial structure of precipitation events. But, the inherently high spatial variability and the different timing of precipitation events among neighboring stations implies that even sophisticated spatial interpolation methods can result in inaccurate estimation of missing precipitation events, particularly at sub-daily scales (i.e. minute and hourly observations) (Ciach and Krajewski 2006;

Teegavarapu and Pathak 2008; Cristiano et al. 2017). As an alternative, neural networks trained using time series of precipitation events for the same station have shown promising results for replacing missing precipitation events, surpassing the accuracy of geostatistical interpolation methods (Teegavarapu and Chandramouli 2005; Kashani and Dinpashoh 2012). However, artificial neural networks typically rely on continuous precipitation time series without missing records, which is the very problem they are trying to solve.

Other alternatives for filling missing precipitation events include the use of ground radars, multi-sensor gridded products, and remote sensors onboard orbiting satellites. For instance, the hourly and daily Next-Generation Weather Radar (NEXRAD) gridded precipitation products provide quality-controlled, multi-sensor (radar and rain gauge) precipitation data available at 4-km spatial resolution for the contiguous U.S. (Heiss et al. 1990; Young et al. 2000; Krajewski and Smith 2002). Multi-sensor gridded products provide areal average useful for hydrological and agricultural applications; however, gridded products may not always represent precipitation amounts at the point level (Figure B1 in Appendix B), and gridded products often result in large datasets that are not practical for real-time precipitation quality control onboard of station dataloggers.

An alternative approach for flagging and filling missing precipitation events that can be implemented in dataloggers and post-processing routines that has the potential to resolve uncertainties related to horizontal spatial interpolation methods and the timing of precipitation events in neighboring stations is the use of soil moisture observations collected at the same station (i.e. gap filling using a different variable from the same location). The strong link between precipitation and soil moisture has been widely used to estimate surface and rootzone soil moisture from precipitation observations (Pan et al. 2003; Dorigo et al. 2013; Coopersmith et

al. 2015), but recent studies have suggested the possibility of doing just the opposite, to reconstruct precipitation events from changes in soil water storage (Crow et al. 2009; Brocca et al. 2013, 2015; Pellarin et al. 2020; Parker and Patrignani 2020; Filippucci et al. 2020). The concept relies on using the soil as a natural rain gauge by relating temporal changes in the soil water storage to precipitation. While this method relies on stations equipped with co-located pluviometers and soil moisture sensors, there is a growing number of statewide and nationwide mesoscale networks that monitor rootzone soil moisture. For instance, the North American Soil Moisture Database is a new high-quality observational soil moisture database that consists of 1,800 stations across North America (Quiring et al., 2016), and similar initiatives have been developed for other parts of the world (Dorigo et al., 2011). This new wave of mesoscale networks that include soil moisture as a standard measurement opens new opportunities for leveraging readily available in situ soil moisture observations for quality control (QC) and quality assurance (QA) of other essential variables like precipitation. This is particularly relevant considering that the typical distance between neighboring stations in statewide mesoscale networks is >25 km and between 70 to 200 km in nationwide networks (Ochsner et al., 2013; Brotzge et al., 2020; Patrignani et al., 2020b). Thus, the objectives of this study were to test the accuracy of using changes in rootzone soil water storage as i) a qualitative quality assurance method for detecting the occurrence of false-negative precipitation events due to malfunctioning pluviometers and ii) as a quantitative method for filling gaps in precipitation records. We propose this approach as an alternative method for precipitation observations with the potential to complement existing QA and QC methods. The scope of this study is aimed at conceptualizing and testing the proposed method using the soil as a natural rain gauge in its simplest form, solely using sensor observations and without accounting for additional soil hydraulic properties or

sophisticated modeling procedures so that researchers and network managers alike can easily implement the method as part of routine operations. In other words, we evaluate whether changes in soil moisture storage at the same station can be used to flag and reconstruct missing precipitation events using a mesoscale in situ network in the U.S. Great Plains as a case study scenario.

Materials and Methods

Concept and assumptions

The link between the change in soil water storage and precipitation is explicit in the equation describing the soil water balance, which for a rainfed system neglecting capillary rise can be represented as:

$$\Delta S = P - E - T - RO - D - I \qquad [1]$$

where ΔS is the change in soil water storage (mm), P is precipitation (mm), E is evaporation from the soil surface (mm), T is plant transpiration (mm), RO is surface runoff (mm), D is deep drainage (mm), and I is canopy and litter interception (mm). For the change in soil water storage to equate precipitation, $\Delta S \cong P$, several conditions need to be met, at least during the period of the rainfall event. For this reason, in this study, we used a soil water balance at an hourly time scale. During the occurrence of a precipitation event, the air near the land surface typically approaches the saturation vapor pressure (i.e. relative humidity ~100 %), dramatically reducing the vapor pressure deficit and the atmospheric water demand (Campbell and Norman 1998). Under these conditions and for this study, evaporative and transpirational losses were assumed negligible during the precipitation event (i.e. E and $T \approx 0$). Considering the typically low rainfall intensity in the U.S. Central Plains (i.e. <5 mm h^{-1} average peak rainfall intensity in the region) (Lee et al. 2017) and that stations of the Kansas Mesonet (see the section on

precipitation and soil moisture dataset below) are mostly located on landscapes with less than 1% slopes covered with natural vegetation, the runoff was also assumed to be negligible (i.e. $RO \approx 0$). If we further assume that most precipitation events in this region have a duration of only a few hours (typically <3 hours, Lee et al., 2017), then it results unlikely that precipitation that infiltrates the soil profile will move beyond the depth of the deepest soil moisture sensor at the stations of the Kansas Mesonet (i.e. 50 cm depth). Therefore, the drainage rate during the duration of precipitation events was also assumed negligible (i.e. $D \approx 0$). This assumption implies that we ignored any preferential flow through macropores and soil cracks. A brief discussion is presented in the section on testing of model assumptions below to discuss the magnitude of the drainage term by adding a simple hydraulic conductivity model. The soil moisture sensors of the Kansas Mesonet are installed under natural vegetation, so unlike the previous components of the soil water balance, the interception component cannot be assumed negligible (i.e. $I \neq 0$). Small precipitation events that are often intercepted by vegetation canopy and litter evaporate without reaching the soil surface. Even then, the precipitation water that reaches the soil surface still needs to enter the sensing volume of the topmost (i.e. 5 cm depth) soil moisture sensor to be detected. Thus, we know a priori that the proposed approach has a detectable limit below which cannot be used to predict the occurrence of precipitation events. Accounting for the interception component, equation (1) simplifies to:

$$P = \Delta S + I \qquad [2]$$

In this study, the interception component in equation (2) was determined from a histogram of precipitation events that did not result in a measurable change in soil water storage (i.e. undetected precipitation events). We selected the 95^{th} percentile of the precipitation amount of undetected events by the array of soil moisture sensors as an arbitrary, but a reasonable

approximation of canopy and litter interception. As mentioned earlier, the interception term in our study also accounts for a small fraction of soil water storage present near the soil surface that is beyond the sensing volume of the topmost sensor at 5 cm depth. In this context, the magnitude of the interception term represents the minimum detectable precipitation event using the proposed method. Undoubtedly, we made some important simplifying assumptions that would not hold under most field circumstances, but we hypothesize that these assumptions hold during typical precipitation events in the central U.S. with the aim of generating a first-order approximation of precipitation events based on changes in rootzone (i.e. top 50 cm) soil water storage.

Precipitation and soil moisture dataset

Available hourly observations of precipitation and soil moisture were obtained from the Kansas Mesonet from the deployment of soil moisture sensors in 2017 to 31 December 2020. The Kansas Mesonet is an environmental monitoring network established in 1986 by the Kansas State Research and Extension that consists of 62 stations distributed across the state of Kansas (Patrignani et al. 2020a). The stations are located in long-term sites characterized by landscapes with <1% slope and permanent natural vegetation dominated by warm-season grasses. Stations of the Kansas Mesonet are located across precipitation gradient that ranges from 200 mm per year in the western portion of the state to 780 mm in the eastern portion of the state. Liquid precipitation is measured at all stations using a tipping bucket rain gauge (Model TE525, Texas Electronics Inc. Dallas, TX) with a resolution of 0.25 mm. We used hourly precipitation and soil moisture information from 30 stations of the Kansas Mesonet equipped with soil moisture records longer than one year and an additional 17 stations without soil moisture sensors were included to obtain precipitation for the nearest neighbor interpolation (Figure 3.1). The use of

hourly data was essential to meet the assumptions of the soil water balance components stated earlier. For this study, the minimum inter-event time (MIT) that defines individual precipitation events was assumed to be one hour (Dunkerley 2015; Medina-Cobo et al. 2016).

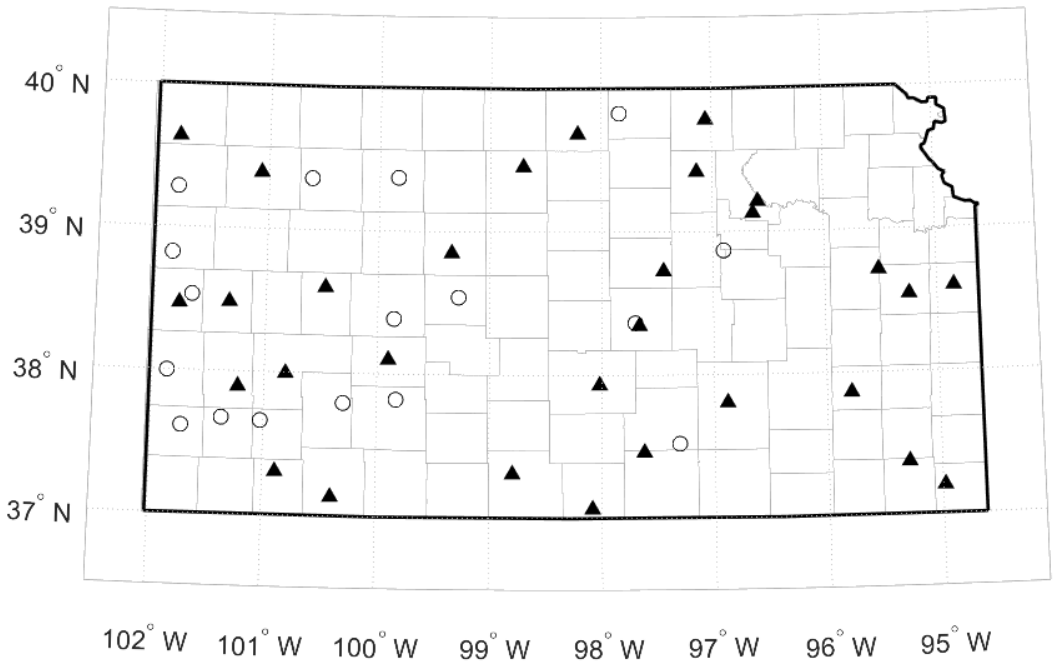

Figure 3.1 Distribution of the 47 stations of the Kansas Mesonet considered in this study. Filled triangles represent stations with precipitation and soil moisture records (N=30) and open circles represent stations with precipitation and without soil moisture records (N=17) that were considered for the nearest neighbor approach.

In stations of the Kansas Mesonet, volumetric water content is monitored at 5, 10, 20, and 50 cm depths using soil water reflectometers (Model CS655, Campbell Scientific Inc., Logan, UT) since 2016. The soil moisture sensors were calibrated using soil samples collected from all the stations monitoring soil moisture between June and November 2019. The calibration equation was obtained by relating the volumetric water content (θ) of the soil samples determined with the thermo-gravimetric method as a function of the apparent dielectric permittivity (K_a, unitless) and bulk electrical conductivity (EC_b, in dS m^{-1}) (Evett et al. 2005)

reported by the soil moisture sensor at the time of soil sampling. The calibration equation used in this study is:

$$\theta = -0.025 + 0.091\sqrt{K_a} - 0.176\sqrt{EC_b} \qquad [3]$$

The RMSE of the calibration equation in our soils was 0.05 cm^3 cm^{-3}, which is 44% less than the RMSE of the sensor manufacturer's equation based on the third-order polynomial proposed by Topp et al. (1980) (RMSE = 0.09 cm^3 cm^{-3}).

Computation of changes in soil water storage

After computing the volumetric water content of each soil moisture sensor, the total soil water storage (S) in a soil profile was approximated using the trapezoidal rule of integration, which is a common approach in the literature for integrating vertical measurements of soil moisture to compute profile soil water storage (e.g. Nachabe et al. 2004; Gao et al. 2019):

$$S_t = \theta_{1,t} Z_{1,t} + \sum_{i=2}^{n} \frac{\theta_{i-1,t} + \theta_{i,t}}{2} \left(Z_{i,t} - Z_{i-1,t}\right) \qquad [4]$$

where *t* is time in hours, Z_i (mm) is the depth of the *i-th* sensor, θ_i is the volumetric water content of the *i-th* sensor, and *n* is the total number of sensors in the soil profile. For the 0-5 cm soil layer, we assumed that the sensor placed at 5 cm depth represents the soil moisture of the surface layer (i.e. 0-5 cm). Then, the predicted precipitation from soil moisture was computed based on the sum of hourly changes in the soil water storage for each observed precipitation event. The approach for reconstructing precipitation events from changes in soil water storage is illustrated in Figure 3.2A using a 5-hour precipitation event from 14 May 2018 23:00 to 15 May 2018 03:00 Central Standard Time (CST) recorded at the Parsons station. Figure 3.2A illustrates the use of the soil profile as a natural rain gauge, in which the soil water storage at each sensor depth changes as the rainfall event progresses. Then, the sum of hourly changes in rootzone soil water

storage can be used to reconstruct detailed cumulative precipitation dynamics (Figure 3.2B). In this particular example, the observed total precipitation was 46.5 mm and the estimated total precipitation based on changes in soil water storage was 48.7 mm (Figure 3.2B). In previous stages of this manuscript, we also considered reconstructing precipitation events using the difference in soil water storage between an hour before and an hour after the precipitation event. However, precipitation estimates were the same as using the sum of hourly changes in soil water storage. As a result, we favored the simplest approach based on the sum of hourly changes in soil water storage, which does not require knowledge of the start and end of a precipitation event, and thus can be easily implemented as a near-real-time precipitation quality control procedure onboard of common dataloggers (e.g. Supplemental code in Appendix B).

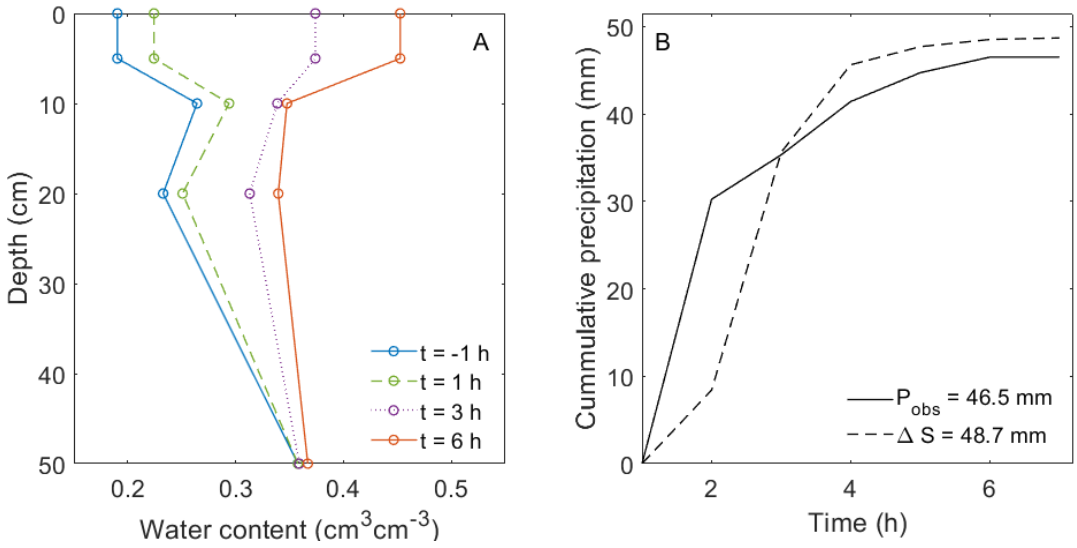

Figure 3.2 Example illustrating changes in profile soil moisture during A) 5-hour precipitation event at the Parsons station of the Kansas Mesonet from 14 May 2018 23:00 to 15 May 2018 03:00 Central Standard Time (CST), and B) the corresponding cumulative precipitation measured by the station pluviometer (P_{obs}) and the cumulative precipitation reconstructed using changes in soil water storage (ΔS). Times (t) are expressed in hours relative to the start of the precipitation event. Soil water content at time t = -1 h represents the water content of the soil profile at an hour before the start of the precipitation event and t = 6 h represents the soil water content at an hour after the end of the precipitation event.

For each precipitation event, we also obtained additional metrics such as antecedent soil water storage (mm), antecedent soil water deficit (mm), and antecedent relative saturation. The antecedent soil water storage was estimated as the soil water storage an hour before a precipitation event. The antecedent soil water deficit was computed as the difference between the saturation point and the antecedent soil water storage. The saturation point was approximated as the maximum value of the soil water storage time series for each station. The antecedent relative saturation was computed as the ratio of the antecedent soil water storage to the saturation point. Before evaluating the accuracy of the proposed soil moisture-based precipitation approach, we removed precipitation events smaller than the minimum detectable threshold of 7.6 mm (see the section on testing of model assumptions below). We also removed precipitation events during the winter season with soil temperature values ≤ 1 ^{o}C because of the change in the apparent dielectric permittivity of partially frozen soils that affects the estimation of volumetric water content (Figure B2 in Appendix B) (Zhang et al. 2003; Seyfried and Grant 2007).

The accuracy of the proposed approach for reconstructing precipitation events from changes in rootzone soil water storage was evaluated both qualitatively and quantitatively. The qualitative evaluation involved the determination of true positive precipitation events correctly detected with changes in soil moisture storage and false-negative precipitation events that were not detected with the proposed approach. For this analysis, the occurrence of a precipitation event based on soil moisture was only considered when the changes in soil water storage were greater than 1 mm to avoid including small soil moisture fluctuations due to sensor noise and thermal gradients. The quantitative evaluation of the proposed approach was done using root mean squared error (RMSE), mean absolute error (MAE), and mean bias error (MBE). We selected RMSE because it is a commonly used error metric and allowed us to compare our

findings with other studies in the literature. The MAE was also included in our analysis as a robust error metric that is less sensitive to outliers compared to RMSE (Willmott and Matsuura 2005). The MBE measures the tendency of a model to underestimate or overestimate observations and expresses the mean difference between predicted and observed variables (Harrison and Bales 2014). A negative MBE value represents underestimation and a positive MBE represents overestimation. All data analysis was performed using Matlab R2020b (Mathworks, Inc., Natick, MA).

Comparison with nearest-neighbor interpolation approach

To assess the accuracy of the proposed method relative to common methods for filling missing precipitation events, we compared the quantitative accuracy of our soil moisture-based approach to the nearest neighbor interpolation approach. We evaluated the nearest neighbor approach using precipitation events greater than the minimum detectable threshold of the soil moisture approach obtained from all 47 stations considered in this study. The nearest neighbor interpolation method works by replacing missing precipitation events at a target station with precipitation records from the nearest station in terms of geographical distance. Similar to the soil moisture approach, the accuracy of the nearest neighbor approach was evaluated using RMSE, MAE, and MBE.

Results and Discussion

Testing of model assumptions

Evaporation and transpiration assumptions

One of the assumptions of the proposed method for reconstructing precipitation events based on changes in soil water storage is that soil evaporation and plant transpiration are

negligible during precipitation events. Since stations of the Kansas Mesonet also record air temperature and relative humidity at hourly intervals, we used these variables to compute the atmospheric vapor pressure deficit during the precipitation events. The median relative humidity (RH) recorded during all precipitation events was 95% (Figure 3.3A) and the median resulting vapor pressure deficit was 0.1 kPa (Figure 3.3B). Vapor pressure deficit is a primary driver of soil evaporation (Or et al. 2013) and plant transpiration (Sinclair et al. 2017), thus, the nearly zero vapor pressure deficit recorded during precipitation events provides some evidence for the assumption of negligible evaporation and transpiration. It is worth mentioning that while this assumption seems valid for hourly precipitation events, the assumption of negligible evaporation and transpiration will likely not hold at daily time steps, which could lead to precipitation underestimation when using the proposed soil moisture-based approach to reconstruct rainfall due to pre- and post-storm evapotranspiration resulting from hours of the day without precipitation. For instance, on 19 June 2020 at the Hays station of the Kansas Mesonet, the vapor pressure deficit increased from 0.1 to 1.0 kPa following a four-hour precipitation event (Figure 3.3C). This assumption seems to work well in the U.S. Great Plains, but this assumption will need to be tested before implementation in other parts of the world.

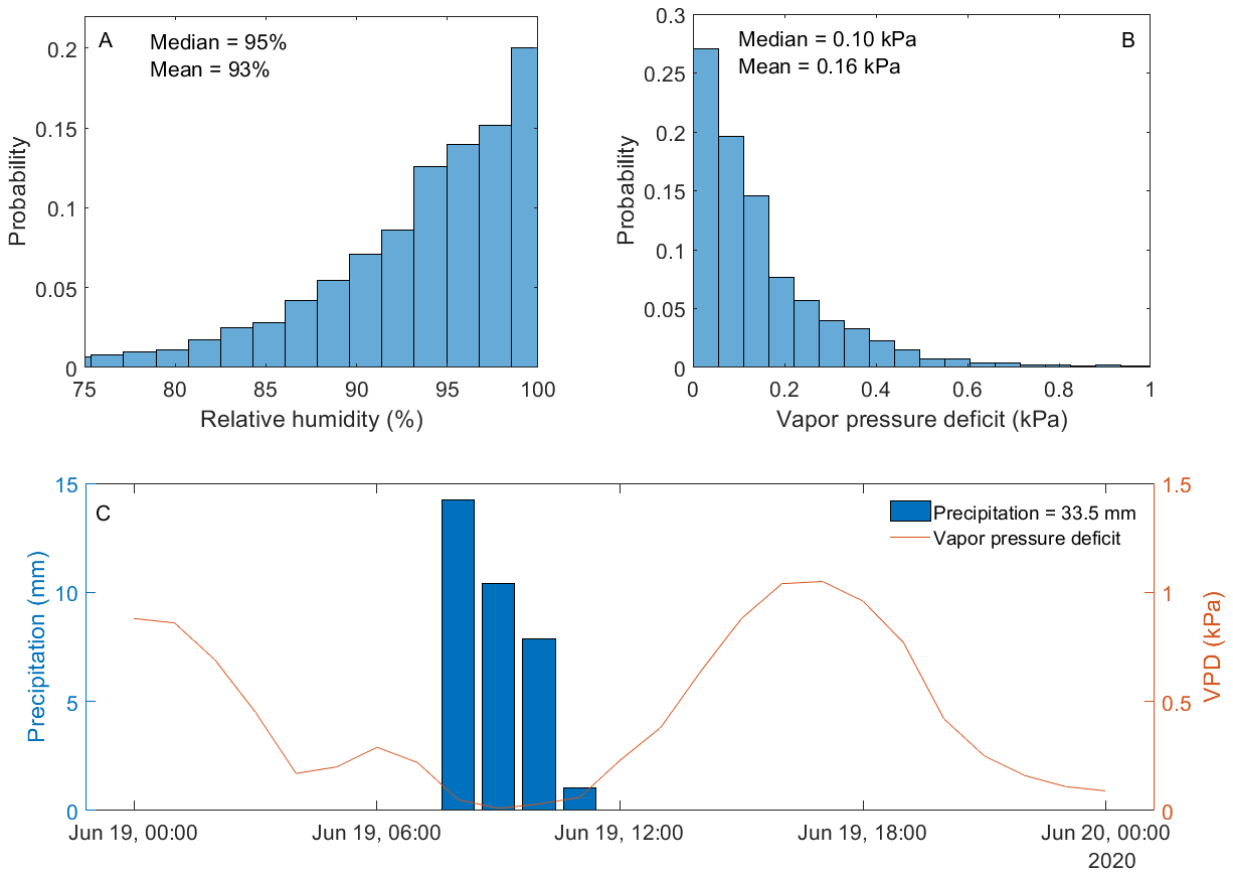

Figure 3.3 Distribution of A) relative humidity and B) vapor pressure deficit precipitation event for 2497 hourly precipitation events across 30 stations of the Kansas Mesonet from 15 May 2017 to 31 December 2020. C) Example of the lower vapor pressure deficit (VPD) during a precipitation event recorded at the Hays station of the Kansas Mesonet on 19 June 2020. Times are reported in Central Standard Time (CST).

Interception assumption

The interception threshold determined based on the 95th percentile of 9,031 precipitation events in all the stations monitoring soil moisture that did not result in a measurable increase in soil water storage was 7.6 mm. This value is higher than the canopy interception threshold of 4 mm determined for prairie grass in the region (Zou et al. 2015), which is not surprising since the interception threshold derived in this study comprises canopy interception and a small amount of infiltrated water that likely did not reach the sensing volume of the topmost (i.e. 5 cm) moisture

sensor. During these small precipitation events, all soil moisture sensors typically exhibited negative changes in volumetric soil water content. Our findings imply that a precipitation event totaling >7.6 mm is required for the proposed approach based on changes in soil water storage to work in this region. As a result, the remaining analyses in this study were performed using a total of 2,497 precipitation events >7.6 mm.

Drainage assumption

To test the assumption of negligible drainage we approximated the magnitude of the drainage term for a typical rainfall event using the Campbell (1974) soil hydraulic conductivity model using a unit gradient assumption (i.e., gravity-driven flow). In this case, the hourly drainage rate at 50 cm depth was assumed to be equal to the hydraulic conductivity for that hour. Due to the lack of site-specific soil hydraulic properties for the Kansas Mesonet, we used soil hydraulic properties for the Campbell model for U.S. soils (Rawls et al. 1982; Rawls et al. 1992) corresponding to the predominant soil textural class at the 50 cm sensor depth across the Kansas Mesonet (i.e. silty clay loam, K_{sat}= 1.5 mm h^{-1}, b = 6.6). Overall, the median duration of the 2,497 precipitation events analyzed in this study was 4 hours, which resulted in an estimated median drainage of 0.28 mm for the entire rainfall event, suggesting that assuming negligible drainage beyond the 50 cm sensor depth during typical precipitation events results in small errors that could be considered negligible for the purposes of this study. To quantify the impact of longer precipitation events on the proposed approach, a more detailed discussion is provided in the quantitative analysis section below.

Distribution of precipitation events

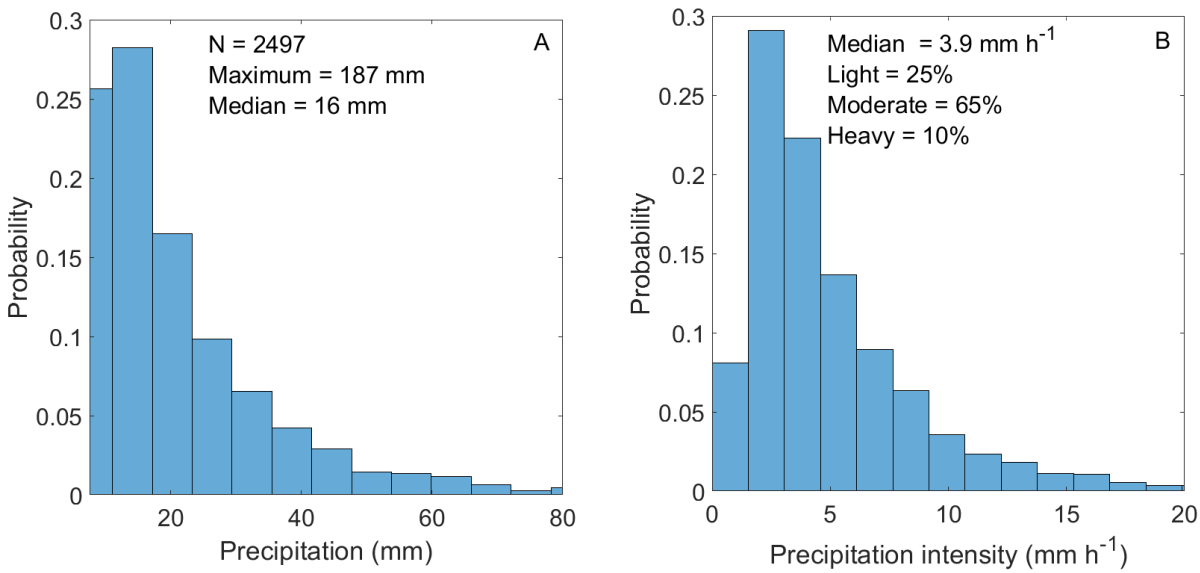

Figure 3.4 A) histogram of precipitation amount, and B) histogram of precipitation intensity for the 2497 precipitation events in the resulting dataset across 30 stations of the Kansas Mesonet from 15 May 2017 to 31 December 2020. Rainfall intensity was classified as light (rainfall intensity <2.5 mm h^{-1}), moderate (rainfall intensity ≥2.5 to <10 mm h^{-1}), and heavy (rainfall intensity >10 mm h^{-1}) according to the classification by the World Meteorological Organization. The x-axes of the figures were truncated for visual clarity.

Our study spanned an approximate area of 231,000 km^2 across a gradient of 400 to 1200 mm in annual rainfall. Based on the minimum detectable precipitation threshold, our dataset resulted in 2497 precipitation events with a median precipitation amount of 16 mm and a median precipitation duration of 4 hours (Figure 3.4A). The maximum precipitation amount was 187 mm, which was recorded at the Ottawa 2SE station from 31 July 2019 at 22:00 CST to 1 August 2019 at 07:00 CST. Similarly, the maximum sum of changes in soil water storage was 100 mm, a value also recorded at the Ottawa 2SE station at the time of the maximum precipitation event. The median precipitation intensity of the dataset was 3.9 mm h^{-1} and the maximum recorded precipitation intensity was 45.7 mm h^{-1} (Figure 3.4B), which was recorded at Miami station on 29 January 2020 from 09:00 CST to 12:00 CST. Based on the precipitation intensity

classification system of the World Meteorological Organization (2017), 25% of the precipitation events were classified as light events (<2.5 mm h^{-1}), 65% as moderate (≥2.5 to <10 mm h^{-1}), and 10% as heavy precipitation events (≥10 mm h^{-1}). Our findings show that precipitation events in this region of the U.S Great Plains are largely dominated by light and moderate-intensity precipitation events, which accounted for 90% of the total precipitation events during the study period.

Qualitative analysis

Overall, using changes in rootzone soil water storage correctly flagged 2,044 out of the 2,497 precipitation events >7.6 mm, while the remaining 453 precipitation events were not detected by the soil (Table 3.1). This represents 82% accuracy in detecting precipitation events greater than the interception threshold. The remaining 453 (18%) undetected precipitation events typically occurred when the antecedent soil moisture was at or near saturation conditions, with an average antecedent relative saturation of the 453 undetected events of 0.82. The failure of soils at or near saturation conditions in responding to precipitation events was also documented in previous studies that estimated precipitation using in situ soil moisture (Brocca et al. 2013, 2015) and satellite-based soil moisture products (Crow et al. 2011; Brocca et al. 2014, 2019; Pellarin et al. 2020) and is further discussed in the section on the quantitative analysis below.

Table 3.1 Qualitative evaluation of precipitation detection by soil moisture using 2497 hourly observations that exceeded 7.6 mm from 30 stations of the Kansas Mesonet.

Soil moisture response	Number of precipitation events	Percentage of total precipitation events
Detected	2044	82
Not detected	453	18

Interestingly, the proposed approach based on changes in soil water storage was able to identify actual missing precipitation events in the Kansas Mesonet precipitation record that remained unknown until this study. For example, a missing precipitation event that went unnoticed at the Gypsum station on 22 April 2019 from 00:00 to 03:00 CST was correctly identified using the proposed approach based on changes in soil water storage (Figure 3.5A). The sum of hourly changes in soil water storage for the same period totaled 24.3 mm whereas the rain gauge recorded no precipitation occurrence. Verification with a multi-sensor gridded precipitation product with 4-km spatial resolution generated by the U.S. National Weather Service (NWS, https://water.weather.gov/precip) for the same day revealed a precipitation event of 19.1 mm, suggesting that a missing precipitation event occurred at the Gypsum station. Further inspection of the visit sheets filled by the field technician of the Kansas Mesonet revealed that the rain gauge at Gypsum station was clogged during a posterior station visit (Figure B3 in Appendix B). Similarly, a malfunctioning rain gauge failed to capture multiple precipitation events during July 2017 at the Lake City station. During the same period, the estimated precipitation based on changes in the soil water storage totaled 50.2 mm (Figure 3.5B). Verification with the gridded precipitation product generated by the NWS for the corresponding days revealed multiple precipitation events totaling 50.8 mm. Again, crosschecking with a visit sheet filled by the field technician revealed that the rain gauge at the Lake City station was clogged on a posterior station visit (Figure B4 in Appendix B). The ability to flag missing precipitation events using the proposed approach coupled with the high (82%) accuracy of the proposed approach in flagging precipitation events shows a promising application of co-located soil moisture observations for precipitation quality control in mesoscale networks. The proposed approach could complement existing methods for precipitation quality control and quality

assurance such as the use of precipitation records from neighboring stations (Einfalt and Michaelides 2008) and multi-sensor gridded precipitation products (Shafer et al. 2000; Patrignani et al. 2020a).

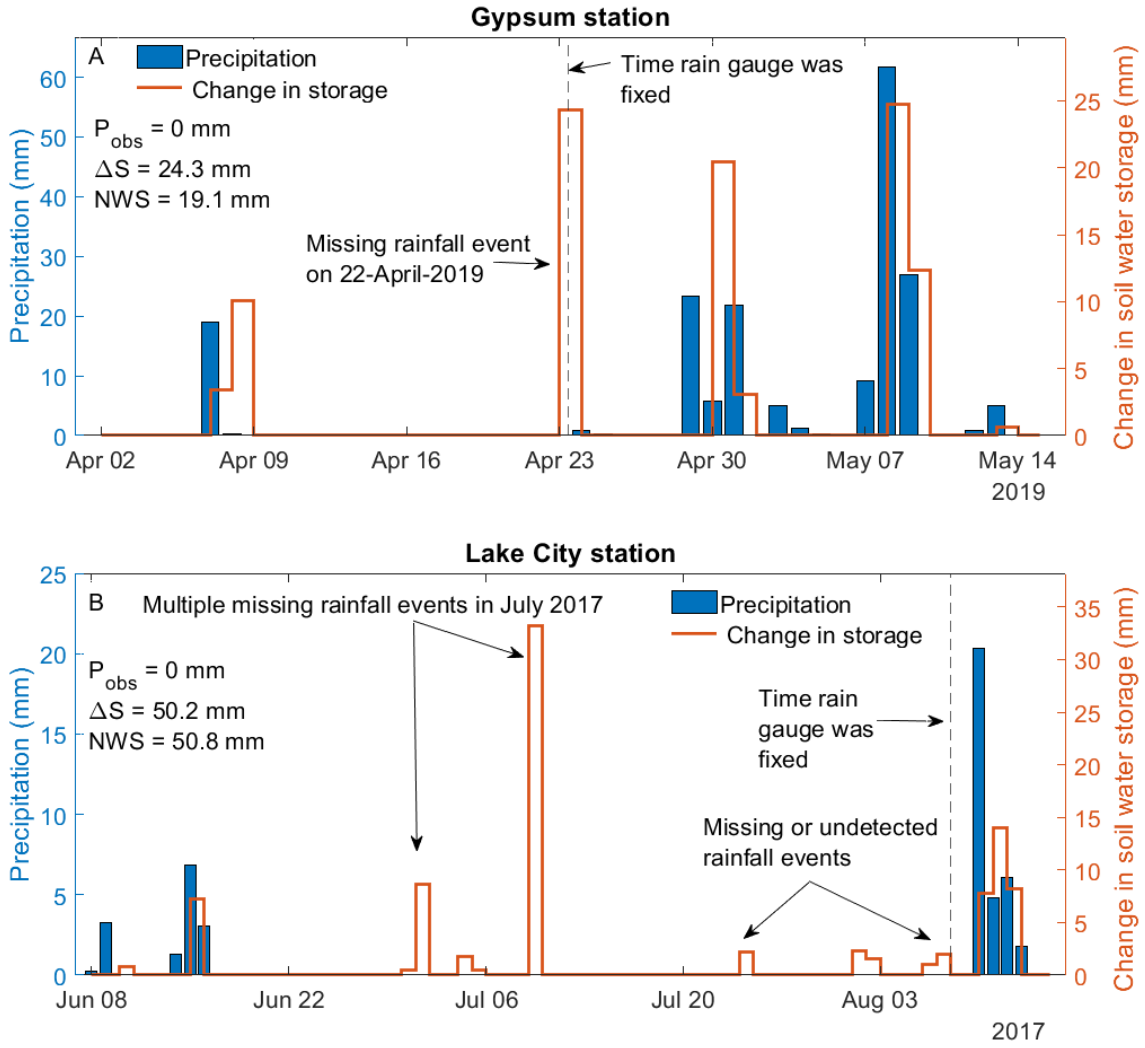

Figure 3.5 Examples of precipitation events that were effectively captured by the proposed approach based on changes in soil water storage, but that were missed due to a malfunctioning pluviometer at A) the Gypsum station on 22 April 2019 00:00 to 03:00 CST and at B) the Lake City station for July. Both figures comprise hourly results that have been aggregated into daily intervals for visual clarity. We also retrieved the precipitation total for the same dates obtained from the U.S. National Weather Service (NWS) 4-km multi-sensor gridded product that in both cases provided an independent precipitation observation. P_{obs} is the observed precipitation at the station and ΔS is the observed change in soil profile water storage at the station. Rain gauges in both stations were fixed during a time without rainfall.

Quantitative analysis

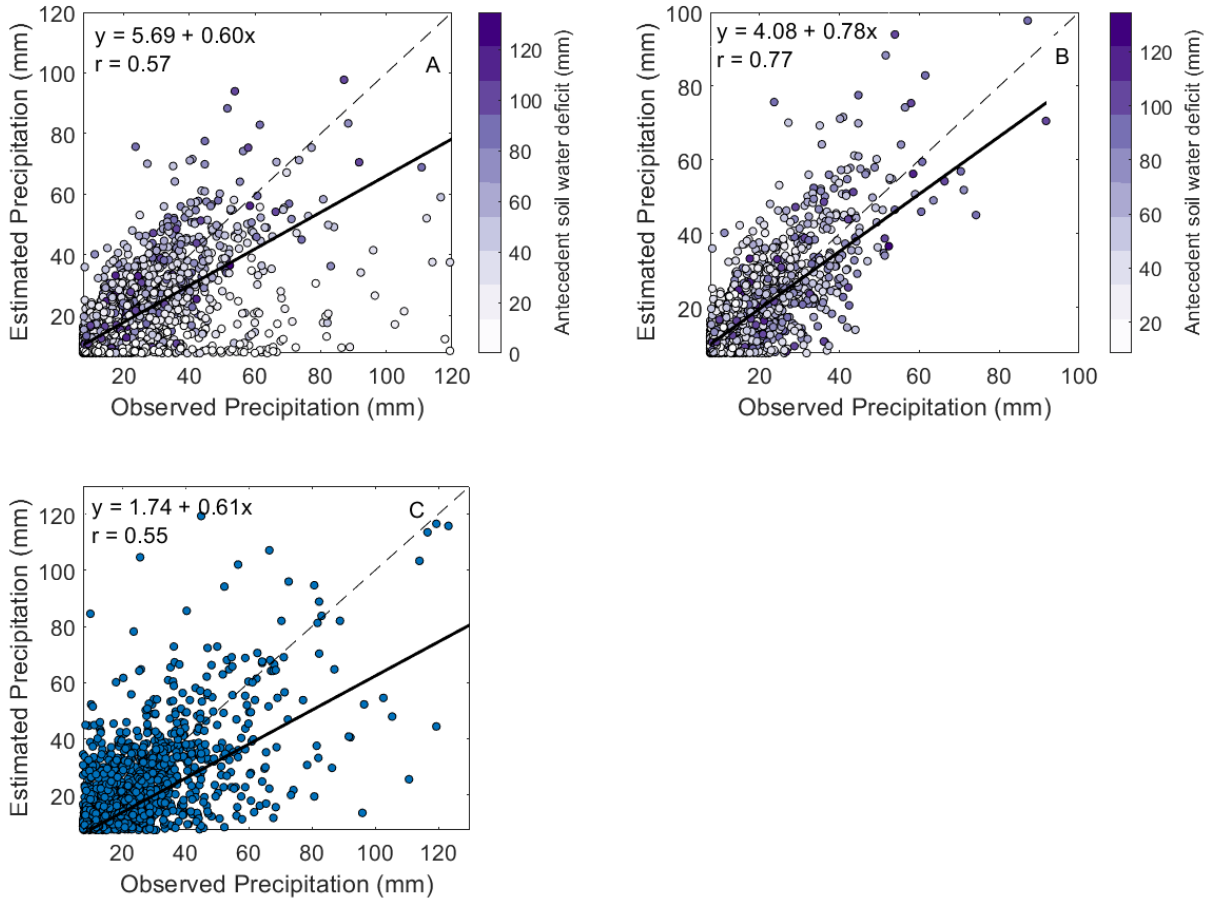

Figure 3.6 Comparison of rain gauge observation to predicted precipitation using A) change in soil water storage for all precipitation events (N = 2497), B) change in soil water storage for precipitation events lower than the antecedent soil water deficit (N = 1716), and C) nearest neighbor interpolation for precipitation events exceeding 7.6 mm from 15 May 2017 to 31 December 2020. The soil moisture approach used precipitation events across 30 stations monitoring soil moisture while the nearest neighbor approach used 2497 precipitation events across all 47 stations of the Kansas Mesonet, including stations with and without soil moisture sensors. Dash lines represent the 1:1 line and solid lines represent fitted linear regressions (in both cases the linear model had $p<0.001$).

Accuracy of precipitation estimation using in situ soil moisture

The quantitative accuracy of the proposed approach for estimating precipitation based on the sum of hourly changes in soil water storage resulted in $r = 0.57$, an RMSE of 14.1 mm, and MAE of 8.0 mm, with a slight tendency to underestimate the total observed precipitation with an

MBE of -3.0 mm (Figure 3.6A). The RMSE of the proposed in situ soil moisture-based approach is similar to the range in RMSE of 11.8 to 16.4 mm reported in a previous study for 5-day accumulated global precipitation derived by coupling satellite-based global soil moisture products with the SM2RAIN algorithm (Brocca et al. 2014). Considering all stations and precipitation events >7.6 mm (i.e. interception threshold), the proposed approach based on soil moisture performed similarly to the nearest neighbor interpolation technique, which resulted in r = 0.55 an RMSE of 16.6 mm and MAE of 10.6 mm (Figure 3.6C). In addition, the nearest neighbor interpolation approach showed a higher precipitation underestimation than the soil moisture-based approach with an MBE of -5.8 mm (Figure 3.6C). The comparatively higher precipitation underestimation by the nearest neighbor interpolation than the soil moisture-based approach could be attributed to the inherently high spatial and temporal variability of precipitation events as a consequence of the distance between stations (Ciach and Krajewski 2006; Sadler et al. 2017; Patrignani et al. 2020b), especially at sub-daily intervals. When we only considered precipitation events totaling less than the antecedent soil water deficit before the precipitation event, the accuracy of our approach improved by about 30%, with an RMSE of 7.7 mm and MAE of 5.5 mm (Figure 3.6B). This improvement was not surprising since the soil profile had sufficient pore space to store infiltrating water, indicating that the proposed approach works best for precipitation events totaling less than the antecedent soil water deficit. Thus, the proposed approach has a minimum and a maximum precipitation detection threshold that can be obtained from the time series of soil moisture and precipitation itself.

A major limitation of the proposed approach occurs when the soil moisture is at or near saturation conditions that limit the soil's ability to store infiltrating water, leading to precipitation underestimation. For instance, in the near-saturation scenario in Ottawa 2SE station (Figure 3.7),

the inability of the soil profile to capture subsequent precipitation events after reaching near-saturation conditions on 7 October 2018 resulted in a total change in soil water storage of 72 mm, which amounts to only 29% of the observed total precipitation of 249 mm during the period. At near-saturation soil moisture conditions, the soil has negligible air-filled porosity to store additional precipitation and also the infiltrating water can drain beyond the deepest sensor depth without necessarily changing the storage of the soil profile, and if the rainfall rate exceeds the infiltrability of the soil, then part of the rainfall may also result in ponding or runoff (Brocca et al. 2014; Crow et al. 2011). The proposed soil moisture-based approach without a drainage term may have limited applicability in regions where soils are frequently at or near saturation conditions.

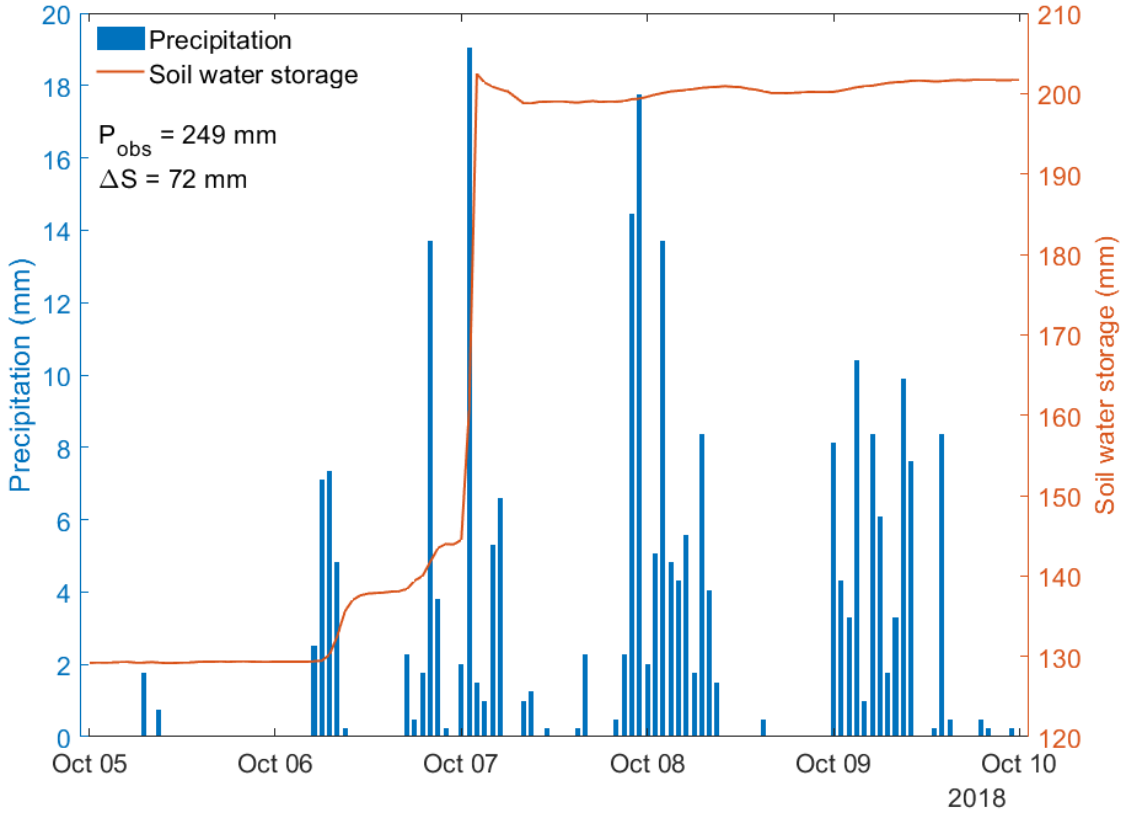

Figure 3.7 Example of precipitation underestimation by the proposed approach based on changes in soil water storage caused by near-saturation conditions due to several consecutive precipitation events at the Ottawa 2SE station. Pobs is the observed precipitation **a**nd ΔS is the change in soil profile water storage.

Drainage beyond the deepest moisture sensor, especially under near saturation conditions, can be circumvented by adding a drainage term to the proposed equation based on hourly changes in soil water storage. In this study, the addition of a drainage term based on the Campbell model to the proposed approach resulted in RMSE = 13.0 mm and MAE = 7.7 mm, an error that is marginally lower (for a substantially more complicated method) than solely using the sum of hourly differences in soil water storage (Figure B5 in Appendix B). A previous study on different sites in Western Europe using a single soil moisture sensor near the soil surface (i.e. 5 to 30 cm) and characterized by coarse-textured soils (e.g. sand and sandy loam; Brocca et al., 2013), showed that drainage accounted for up to 30% of the precipitation estimates (Brocca et al. 2015). The low drainage rates in our study are likely attributed to the deeper array of sensors and the predominantly fine-textured soils across Kansas that typically have hydraulic conductivities (K_{sat} ~1.5 mm h^{-1}) that are an order of magnitude lower than coarse-textured soils (e.g. K_{sat} for sand ~25.9 mm h^{-1}, Rawls et al. 1982).

We also observed that in precipitation events with intensities >10 mm h^{-1} underestimation could have been caused by high antecedent soil moisture conditions coupled with ponding and possible runoff. The case where high-intensity precipitation events are underestimated in high antecedent soil moisture conditions was also observed by Brocca et al. (2015). Out of the 2497 precipitation events in our dataset, 781 events (31%) occurred when the antecedent soil water deficit (i.e. available air-filled porosity) before the start of the precipitation event was smaller than the total amount of the precipitation event.

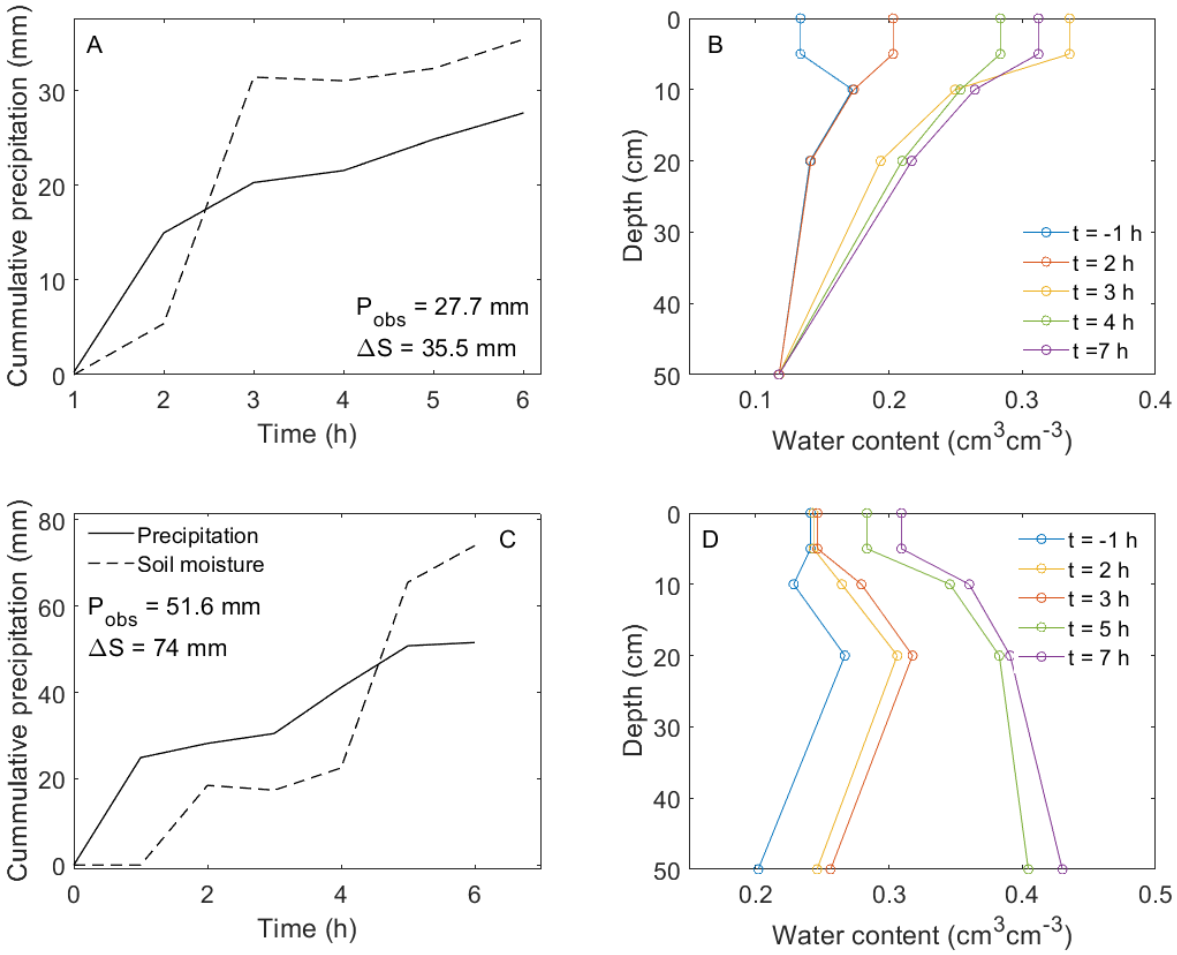

Figure 3.8 Time series of observed (Pobs) and predicted cumulative precipitation from changes in soil water storage (ΔS) (A and C) and the corresponding profile soil water content dynamics (B and D) for overestimated precipitation events. The top row illustrates an example for a sandy loam at the Lake City station from 5 July 2019 22:00 to 6 July 2019 03:00 CST and the bottom row illustrates an example for a silty clay loam soil at the Ashland Bottoms station from 29 June 2017 04:00 to 29 June 2017 09:00 CST. Soil water content at time t = -1 h represents the water content of the soil profile at an hour before the start of the precipitation event and t = 7 h represents the soil water content at an hour after the end of the precipitation event.

On some occasions, we also found that the proposed approach overestimated the observed precipitation amount. For instance, after a six-hour precipitation event totaling 27.7 mm in a sandy loam soil with an antecedent water deficit of 39.1 mm at the Lake City station, the resulting changes in soil water storage totaled 35.5 mm, which is 28% above the observed precipitation (Figure 3.8A). Similarly, a 51.6 mm precipitation event in a silty clay loam with an

antecedent water deficit of 81.7 mm resulted in an estimated precipitation amount of 74 mm at the Ashland Bottoms station (Figure 3.8C), which is 43% above the observed precipitation. One possible reason for the precipitation overestimation could be attributed to the method for computing soil water storage using the trapezoidal rule, especially in the layer between the 20 and 50 cm sensor depths, where small errors in volumetric water content could greatly affect the computed water storage in the 300 mm-thick layer. Another explanation for the overestimation might be due to additional water contribution from surface runoff, subsurface lateral flow, and water table rise (for stations located near rivers). However, because most stations of the Kansas Mesonet were deployed in vegetated landscapes with <1% slope and deep water tables, conditions prone to surface and sub-surface runoff and water table rise likely to occur at a few specific stations (e.g. Cherokee and Woodson stations, Table 3.2).

Comparison with nearest-neighbor interpolation

The comparison of the nearest neighbor interpolation and the soil moisture-based approach at each station that monitors soil moisture showed that the nearest neighbor approach consistently outperforms the proposed soil moisture-based approach when the distance to the nearest station is ≤10 km (Table 3.2). At distances ≤10 km, the nearest neighbor approach resulted in an average correlation of 0.84 (SD = 0.01) and an average MAE of 5.8 mm (SD = 0.27 mm), while the soil moisture-based approach resulted in an average correlation of 0.53 (SD = 0.01) and average MAE = 8.5 mm (SD = 0.13 mm) (Table 3.2). At distances between 10 and 15 km the two methods had comparable performance and were probably within the error of the method itself (Figure B6 in Appendix B). On the other hand, as the distance to the nearest neighboring station increased beyond ~10 to 15 km, the soil moisture-based approach outperformed the nearest neighbor approach in 22 out of 27 cases, exhibiting an average

correlation of 0.64 (SD = 0.03) and MAE of 7.5 mm (SD = 0.37 mm) compared to the mean correlation of 0.47 (SD = 0.03) and MAE of 11.4 mm (SD = 0.36) for the nearest neighbor approach (Table 3.2). This suggests that for stations with the nearest neighbor station located >10 to 15 km, using the proposed soil moisture-based approach could be more accurate than using the nearest neighbor interpolation approach for filling the gap in missing precipitation at hourly intervals. This result is especially relevant in sparse networks where the distance to the nearest station can be several orders of magnitude larger than the range in spatial autocorrelation of precipitation events. For instance, a study in central Oklahoma using a dense network of 25 rain gauges over a 9 km^2 area revealed that the distance at which precipitation events are no longer correlated is 4 km (Ciach and Krajewski 2006). In contrast, the median distance between nearest neighbor stations in the Oklahoma Mesonet (McPherson et al. 2007) is about 30 km, indicating that even in one of the densest statewide mesoscale networks in the U.S. there is an opportunity to further explore the use of co-located soil moisture information for QA and QC procedures and for filling missing precipitation records at hourly time scales in mesoscale environmental monitoring networks. The potential could be even greater for nationwide networks such as the Soil Climate Analysis Network (Schaefer et al. 2007) with a median distance between neighbors of 69 km and for the U.S. Climate Reference Network (Diamond et al. 2013) with a median distance of 197 km. The applicability of the proposed approach could be particularly helpful in sparse networks outside the U.S. in which high-resolution multi-sensor precipitation products are unavailable.

Table 3.2 Comparison of precipitation estimation error between the proposed soil moisture approach (SM) and the nearest neighbor interpolation approach (NN) for all precipitation events greater than 7.6 mm at each of the 30 stations of the Kansas Mesonet that monitors rootzone soil moisture. The predicted precipitation from soil moisture was computed as the sum of hourly changes in soil water storage + interception value of 7.6 mm.

Station	Nearest station	Distance	Events	R_{NN}	R_{SM}	MAE NN	MAE SM
		km				mm	mm
McPherson 1S	McPherson	4	100	0.88	0.45	4.2	7.8
Ashland Bottoms	Manhattan	10	111	0.85	0.55	6.2	9.2
Manhattan	Ashland Bottoms	10	118	0.80	0.58	7.1	8.5
Tribune	Tribune 6NE	12	53	0.50	0.67	6.5	4.7
Lakin	Grant	27	63	0.51	0.86	10.6	4.4
Viola	Haysville	28	105	0.65	0.78	10.9	7.6
Leoti	Tribune 6NE	30	47	0.32	0.35	10.5	7.2
Ottawa 2SE	Overbrook	30	100	0.60	0.66	11.1	10.9
Overbrook	Ottawa 2SE	30	92	0.59	0.62	11.4	8.6
Hodgeman	Spearville	32	48	0.54	0.83	8.3	5.0
Cherokee†	Parsons	33	87	0.65	0.27	12.3	10.2
Parsons	Cherokee	33	117	0.59	0.51	12.9	11.6
Hays	La Crosse	35	77	0.25	0.74	14.3	8.2
Miami	Ottawa 2SE	35	108	0.35	0.30	13.5	11.8
Jewell	Scandia	36	75	0.48	0.69	9.2	7.8
Garden City	Lakin	38	55	0.35	0.53	11.8	6.4
Cheyenne	Sherman	39	11	0.09	0.55	15.4	7.8
Colby	Sheridan	40	58	0.47	0.78	10.5	6.3
Clay	Washington	41	90	0.33	0.63	11.3	8.0
Washington	Clay	41	86	0.45	0.61	9.5	6.3
Satanta	Haskell	41	60	0.22	0.69	13.2	6.1
Gypsum	McPherson	46	97	0.28	0.81	11.9	6.4
Meade	Satanta	47	61	0.58	0.82	11.5	4.6
Osborne	Jewell	49	72	0.69	0.84	8.8	5.3
Butler	Haysville	49	72	0.68	0.59	11.4	7.9
Hutchinson 10SW	McPherson 1S	56	48	0.66	0.68	10.4	8.4
Lane‡	Ness City	59	55	0.00	0.67	14.9	6.2
Harper	Viola	60	92	0.57	0.81	12.0	6.4
Lake City	Harper	68	79	0.69	0.71	11.1	7.9
Woodson†	Parsons	70	78	0.60	0.23	11.6	9.5

† Stations had a high water table from June 2019 to June 2020 and soil was at near-saturation conditions, leading to poor correlation with their common nearby station in Parsons, KS.

‡ Station had the nearest neighbor correlation of -0.004434, which rounds up to 0.00 in 2 decimal places.

To illustrate the limitations of using nearest neighbors to fill precipitation gaps at sub-daily time scales we analyzed two precipitation events of similar amount and duration, but with

neighboring stations at different distances. For the case of close neighboring stations, during a 5-hour precipitation event of 24.9 mm at Ashland Bottoms station on 18 May 2017 17:00 CST, the nearest neighbor station (i.e. Manhattan station, about 10 km away) recorded a precipitation event of 19.8 mm, which started at about an hour earlier than the soil moisture response at the Ashland Bottoms station (Figure 3.9A). The resulting sum of hourly changes in soil water storage at the Ashland Bottoms stations was 20.5 mm, indicating that when stations have close neighbors, the nearest neighbor approach shows comparable precipitation amount and timing to the soil moisture approach. For the case of a station with far neighbors, during a 5-hour precipitation event of 33.3 mm at Woodson station on 17 April 2019 15:00 CST, the nearest neighbor station (i.e. Parsons station, about 70 km away) recorded precipitation of 11.2 mm (Figure 3.9B) and the timing of the precipitation event was delayed by 2 hours. Similarly, the precipitation event at the Ottawa 2SE station (89 km away, second nearest station) started an hour earlier while the precipitation at the Butler station (97 km away, third nearest station) started two hours earlier than the precipitation at the Woodson station (Figure 3.9B). The soil moisture sensors at the Woodson station responded immediately to the precipitation event and the resulting sum of hourly changes in soil water storage was 30 mm. In other words, none of the nearest stations, which are located ≥70 km from the Woodson station was able to accurately capture both the amount and timing of the precipitation event compared to the soil moisture-based approach. Future studies should consider testing the performance of soil moisture-derived precipitation against more sophisticated spatial interpolation methods and gridded precipitation products from multi-sensors, radars, and remote sensing satellites.

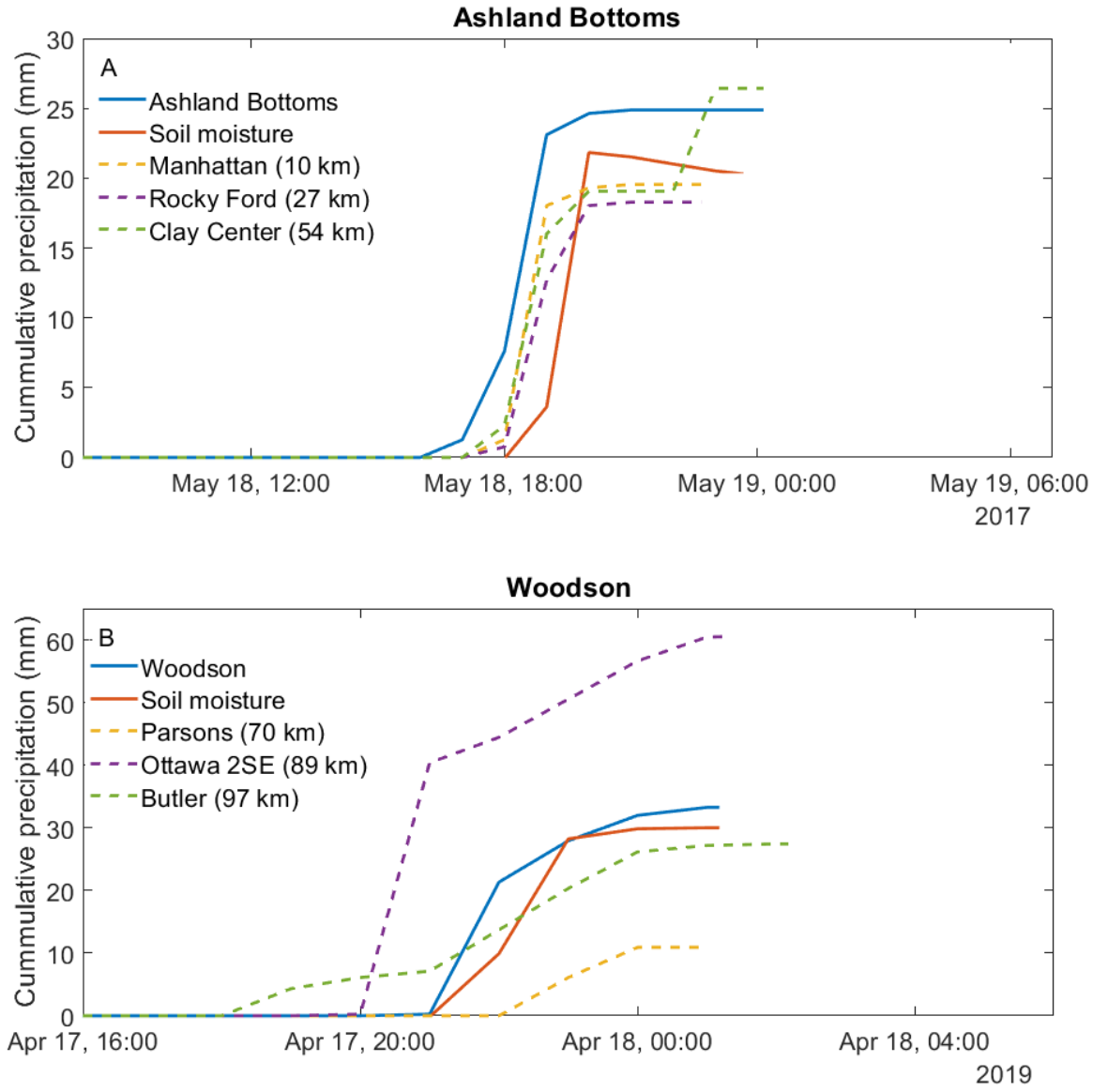

Figure 3.9 Timing of precipitation events within the same storm for a station of the Kansas Mesonet with close nearest neighboring stations (A, Ashland Bottoms) and a station with distant nearest neighboring stations (B, Woodson). The figure highlights that changes in soil water storage may constitute a better alternative to estimate both the amount and timing of precipitation events in stations with distant nearest neighbors compared to using information from nearest neighboring stations. Times are reported in Central Standard Time (CST).

Our approach could be particularly useful in hydrological and mesoscale environmental monitoring networks equipped with co-located pluviometers and soil moisture sensors. In North America, mesoscale networks that include soil moisture as a standard measurement have been expanding as a consequence of state and federal initiatives (Quiring et al., 2016). This includes

new statewide networks like the West Texas Mesonet (Schroeder et al., 2005), the Alabama Mesonet (Kimball et al., 2010), New York State Mesonet (Brotzge et al., 2020), the Kentucky Mesonet (Mahmood et al., 2019), the Manitoba Agriculture Mesonet (Ojo and Manaigre, 2021); and federal networks like the U.S. Climate Reference Network (Diamond et al. 2013), the Soil Climate Analysis Network (Schaefer et al. 2007), and the National Ecological Observatory Network (Keller et al., 2008) that monitor precipitation and soil moisture at most stations. Outside North America, there is also a growing number of in situ networks that monitor soil moisture like the Czech Hydrometeorological Institute Network (Mozny et al., 2013), the Wales Soil Moisture Network (Petropoulous and McCalmont, 2017), the COSMOS-UK network across the United Kingdom (Evans et al., 2016) and the CosmOz soil moisture monitoring network across Australia (Hawdon et al., 2014). As the number of mesoscale networks that include soil moisture observations increases, there is an increasing potential to use the proposed approach for both quality control and quality assurance of precipitation observations, and as a more general method to guide the reconstruction of precipitation from soil moisture observations.

Conclusions

We investigated a simple approach for reconstructing precipitation events at hourly time steps based on the sum of hourly changes in rootzone soil water storage. The proposed method was tested using 30 stations of the Kansas Mesonet equipped with co-located pluviometers and an array of permanent soil moisture sensors distributed along the rootzone. The use of changes in soil water storage proved effective as a qualitative method for flagging precipitation events (accuracy = 82%) and as a quantitative method (MAE = 8.0 mm, RMSE = 14.1 mm) for reconstructing precipitation events >7.6 mm. At the individual stations, the soil moisture approach proved more accurate than the nearest neighbor approach at stations with the nearest

station distance >15 km. Our findings highlight a promising application of in situ soil moisture information as a practical and complementary method for operational quality control and quality assurance of precipitation and as a method to fill gaps in the historical precipitation record without the need for horizontal spatial assumptions in mesoscale networks.

Acknowledgments

The authors wish to thank Christopher Redmond, Mary Knapp, and Randall Mai from the Kansas Mesonet for providing access to the visit sheets and precipitation and soil moisture datasets for this study. This work was supported by the U.S.D.A. National Institute of Food and Agriculture Hatch Multistate projects award #1021229 and #1021608, by the U.S. Geological Survey award #G16AP00054, and by the Kansas State University Agricultural Experiment Station contribution number 22-058-J.

References

Bárdossy, A., and G. Pegram, 2014: Infilling missing precipitation records - A comparison of a new copula-based method with other techniques. *J. Hydrol.*, **519**, 1162–1170, https://doi.org/10.1016/j.jhydrol.2014.08.025

Bojinski, Stephan ; Verstraete, Michel ; Peterson, Thomas C ; Richter, Carolin ; Simmons, Adrian ; Zemp, M., 2014: The concept of Essential Climate Variables in support of climate research, applications, and policy. *Bull. Am. Meteorol. Soc.*, **95**, 1431–1443, https://doi.org/10.1175/BAMS-D-14-00017.1.

Brocca, L., T. Moramarco, F. Melone, and W. Wagner, 2013: A new method for rainfall estimation through soil moisture observations. *Geophys. Res. Lett.*, **40**, 853–858, https://doi.org/10.1002/grl.50173.

Brocca, L., and Coauthors, 2014: Soil as a natural rain gauge: Estimating global rainfall from satellite soil moisture data. *J. Geophys. Res. Atmos. rainfall from Satell. soil moisture data*, **119**, 5128–5141, https://doi.org/10.1002/2014JD021489.

Brocca, L., and Coauthors, 2015: Rainfall estimation from in situ soil moisture observations at several sites in Europe: An evaluation of the SM2RAIN algorithm. *J. Hydrol. Hydromechanics*, **63**, 201–209, https://doi.org/10.1515/johh-2015-0016.

Brocca, L., and Coauthors, 2019: SM2RAIN-ASCAT (2007-2018): Global daily satellite rainfall data from ASCAT soil moisture observations. *Earth Syst. Sci. Data*, **11**, 1583–1601, https://doi.org/10.5194/essd-11-1583-2019.

Brotzge, J.A., J. Wang, C.D. Thorncroft, E. Joseph, N. Bain, N. Bassill, N. Farruggio, J.M. Freedman, K. Hemker Jr, D. Johnston, and E. Kane, 2020: A technical overview of the New York State Mesonet standard network. *Journal of Atmospheric and Oceanic Technology, 37(10)*, 1827–1845.

Campbell, G. S., 1974: A simple method for determining unsaturated conductivity from moisture retention data. *Soil Sci.*, **117**, 311–314, https://doi.org/10.1097/00010694-197406000-00001.

Campbell, G. S., and J. M. Norman, 1998: *An Introduction to Environmental Biophysics*. Second edi. Springer Science+Business Media, lnc, 1–281 pp.

Chen, L., J. Xu, G. Wang, H. Liu, L. Zhai, S. Li, and C. Sun, 2018: Influence of rainfall data scarcity on non-point source pollution prediction : Implications for physically based models. *J. Hydrol.*, **562**, 1–16, https://doi.org/10.1016/j.jhydrol.2018.04.044.

Ciach, G. J., and W. F. Krajewski, 2006: Analysis and modeling of spatial correlation structure in small-scale rainfall in Central Oklahoma. *Adv. Water Resour.*, **29**, 1450–1463, https://doi.org/10.1016/j.advwatres.2005.11.003.

Coopersmith, E. J., J. E. Bell, and M. H. Cosh, 2015: Extending the soil moisture data record of the U.S. Climate Reference Network (USCRN) and Soil Climate Analysis Network (SCAN). *Adv. Water Resour.*, **79**, 80–90, https://doi.org/10.1016/j.advwatres.2015.02.006.

Cristiano, E., M. ten Veldhuis, and N. van de Giesen, 2017: Spatial and temporal variability of rainfall and their effects on hydrological response in urban areas – a review. *Hydrol. Earth Syst. Sci.*, **21**, 3859–3878, https://doi.org/10.5194/hess-21-3859-2017.

Crow, W. T., G. J. Huffman, R. Bindlish, and T. J. Jackson, 2009: Improving satellite-based rainfall accumulation estimates using spaceborne surface soil moisture retrievals. *J. Hydrometeorol.*, **10**, 199–212, https://doi.org/10.1175/2008JHM986.1.

Crow, W. T., M. J. Van Den Berg, G. J. Huffman, and T. Pellarin, 2011: Correcting rainfall using satellite-based surface soil moisture retrievals: The Soil Moisture Analysis Rainfall Tool (SMART). *Water Resour. Res.*, https://doi.org/10.1029/2011WR010576.

Diamond, H. J., and Coauthors, 2013: U.S. climate reference network after one decade of operations status and assessment. *Bull. Am. Meteorol. Soc.*, **94**, 485–498, https://doi.org/10.1175/BAMS-D-12-00170.1.

Dorigo, W. A., and Coauthors, 2013: Global Automated Quality Control of In Situ Soil Moisture Data from the International Soil Moisture Network. *Vadose Zo. J.*, **12**, vzj2012.0097, https://doi.org/10.2136/vzj2012.0097.

Dorigo, W.A., and Coauthors, 2011: The International Soil Moisture Network: a data hosting facility for global in situ soil moisture measurements. *Hydrology and Earth System Sciences,* **15**, 1675–1698.

Dunkerley, D., 2015: Intra-event intermittency of rainfall: an analysis of the metrics of rain and no-rain periods. *Hydrol. Process.*, **29**, 3294–3305, https://doi.org/10.1002/hyp.10454.

Einfalt, T., and Silas Michaelides, 2008: *Quality control of precipitation data. In Precipitation: Advances in Measurement, Estimation, and Prediction*. Springer-Verlag, 101–126 pp.

Evans, J.G., H.C. Ward, J.R. Blake, E.J. Hewitt, R. Morrison, M. Fry, L.A. Ball, L.C. Doughty, J.W. Libre, O.E. Hitt, and D. Rylett, 2016: Soil water content in southern England derived from a cosmic-ray soil moisture observing system–COSMOS-UK. *Hydrological Processes*, **30,** 4987–4999.

Evett, S. R., J. A. Tolk, and T. A. Howell, 2005: Time Domain Reflectometry Laboratory Calibration in Travel Time, Bulk Electrical Conductivity, and Effective Frequency. *Vadose Zo. J.*, **4**, 1020–1029, https://doi.org/10.2136/vzj2005.0046.

Fiebrich, C. A., 2009: History of surface weather observations in the United States. *Earth-Science Rev.*, **93**, 77–84, https://doi.org/10.1016/j.earscirev.2009.01.001.

Fiebrich, C. A., and K. C. Crawford, 2001: The impact of unique meteorological phenomena detected by the Oklahoma Mesonet and ARS Micronet on automated quality control. *Bull.*

Am. Meteorol. Soc., **82**, 2173–2187, https://doi.org/10.1175/1520-0477(2001)082<2173:TIOUMP>2.3.CO;2.

Filippucci, P., and Coauthors, 2020: Soil moisture as a potential variable for tracking and quantifying irrigation: A case study with proximal gamma-ray spectroscopy data. *Adv. Water Resour.*, **136**, 103502, https://doi.org/10.1016/j.advwatres.2019.103502.

Gao, X., X. Zhao, L. Brocca, D. Pan, and P. Wu, 2019: Testing of observation operators designed to estimate profile soil moisture from surface measurements. *Hydrol. Process.*, **33**, 575–584, https://doi.org/10.1002/hyp.13344.

Harrison, B., and R. Bales, 2014: Percent bias assessment of water-supply outlooks in the Colorado river basin. 91–100.

Hawdon, A., D. McJannet, and J. Wallace, 2014: Calibration and correction procedures for cosmic-ray neutron soil moisture probes located across Australia. *Water Resources Research*, **50**, 5029–5043.

Heiss, W., D. McGrew, and D. Sirmans, 1990: Nexrad - Next generation weather radar (WSR-88D). *Microw. J.*, **33**, 79.

Kashani, H. M., and Y. Dinpashoh, 2012: Evaluation of efficiency of different estimation methods for missing climatological data. *Stoch. Environ. Res. Risk Assess.*, **26**, 59–71, https://doi.org/10.1007/s00477-011-0536-y.

Keller, M., D.S. Schimel, W.W. Hargrove, and F.M. Hoffman, 2008: A continental strategy for the National Ecological Observatory Network. *The Ecological Society of America*: 282–284.

Kimball, S.K., M.S. Mulekar, S. Cummings, and J. Stamates, 2010: The University of South Alabama Mesonet and coastal observing system: A technical and statistical overview. *Journal of Atmospheric and Oceanic Technology*, **27**, 1417–1439.

Krajewski, W. F., and J. A. Smith, 2002: Radar hydrology: rainfall estimation. *Adv. Water Resour.*, **25**, 1387–1394, https://doi.org/10.1016/j.jhydrol.2010.05.041.

Lee, H., D. E. Waliser, R. Ferraro, T. Iguchi, C. D. Peters-Lidard, B. Tian, P. C. Loikith, and D. B. Wright, 2017: Evaluating hourly rainfall characteristics over the U.S. great Plains in dynamically downscaled climate model simulations using NASA-unified WRF. *J. Geophys. Res.*, **122**, 7371–7384, https://doi.org/10.1002/2017JD026564.

Mahmood, R., M. Schargorodski, S. Foster, and A. Quilligan, 2019: A technical overview of the Kentucky Mesonet. *Journal of Atmospheric and Oceanic Technology*, **36**, 1753-1771.

Mair, A., and A. Fares, 2011: Comparison of Rainfall Interpolation Methods in a Mountainous Region of a Tropical Island. *J. Hydrol. Eng.*, **16**, 371–383, https://doi.org/10.1061/(ASCE)HE.1943-5584.0000330.

McPherson, R. A., and Coauthors, 2007: Statewide monitoring of the mesoscale environment: A technical update on the Oklahoma Mesonet. *J. Atmos. Ocean. Technol.*, **24**, 301–321, https://doi.org/10.1175/JTECH1976.1.

Medina-Cobo, M. T., A. P. García-Marín, J. Estévez, and J. L. Ayuso-Muñoz, 2016: The identification of an appropriate Minimum Inter-event Time (MIT) based on multifractal characterization of rainfall data series. *Hydrol. Process.*, **30**, 3507–3517, https://doi.org/10.1002/hyp.10875.

Michaelides, S., V. Levizzani, E. Anagnostou, P. Bauer, T. Kasparis, and J. E. Lane, 2009: Precipitation: Measurement, remote sensing, climatology and modeling. *Atmos. Res.*, **94**, 512–533, https://doi.org/10.1016/j.atmosres.2009.08.017.

Možný, M., M. Trnka, P. Hlavinka, D. Bareš, D. Semerádová, V. Potop, and Z. Žalud, 2013: Use of a soil moisture network in the Czech Republic. In Proceedings international scientific conference Environmental changes and adaptation strategies, Skalica **9**.-11.9. 2013, 3 s.

Nachabe, M., C. Masek, and J. Obeysekera, 2004: Observations and Modeling of Profile Soil Water Storage above a Shallow Water Table. *Soil Sci. Soc. Am. J.*, **68**, 719–724, https://doi.org/10.2136/sssaj2004.7190.

Ochsner, E., M.H. Cosh, R. Cuenca,Y. Hagimoto, Y.H. Kerr, E.G. Njoku, and M. Zreda, 2013: State of the art in large-scale soil moisture monitoring. *Soil Science Society of America Journal*, 1–32.

Ojo, E.R. and L. Manaigre, 2021: The Manitoba Agriculture Mesonet: Technical Overview. *Bulletin of the American Meteorological Society*, 1–39.

Or, D., P. Lehmann, E. Shahraeeni, and N. Shokri, 2013: Advances in Soil Evaporation Physics-A Review. *Vadose Zo. J.*, **12**, vzj2012.0163, https://doi.org/10.2136/vzj2012.0163.

Pan, F., C. D. Peters-Lidard, and M. J. Sale, 2003: An analytical method for predicting surface soil moisture from rainfall observations. *Water Resour. Res.*, **39**, https://doi.org/10.1029/2003WR002142.

Parker, N., and A. Patrignani, 2020: A Pilot experiment to replace missing rainfall events using soil moisture information from the Kansas Mesonet. Kansas Agricultural Experiment Station Research Reports, 16–19.

Patrignani, A., M. Knapp, C. Redmond, and E. Santos, 2020a: Technical Overview of the Kansas Mesonet. *J. Atmos. Ocean. Technol.*, **37**, 2167–2183, https://doi.org/10.1175/JTECH-D-19-0214.1.

Patrignani, A., N. Mohankumar, C. Redmond, E. A. Santos, and M. Knapp, 2020b: Optimizing the spatial configuration of mesoscale environmental monitoring networks using a geometric approach. *J. Atmos. Ocean. Technol.*, **37**, 943–956, https://doi.org/10.1175/JTECH-D-19-0167.1.

Pellarin, T., and Coauthors, 2020: The precipitation inferred from soil moisture (PrISM) near real-time rainfall product: Evaluation and comparison. *Remote Sens.*, **12**, https://doi.org/10.3390/rs12030481.

Petropoulos, G.P. and J.P. McCalmont, 2017: An operational in situ soil moisture & soil temperature monitoring network for West Wales, UK: The WSMN network. Sensors, **17**, 1481.

di Piazza, A., F. Lo Conti, L. V. Noto, F. Viola, and G. La Loggia, 2011a: Comparative analysis of different techniques for spatial interpolation of rainfall data to create a serially complete monthly time series of precipitation for Sicily, Italy. *Int. J. Appl. Earth Obs. Geoinf.*, **13**, 396–408, https://doi.org/10.1016/j.jag.2011.01.005.

Quiring, S.M., T.W. Ford, J.K. Wang, A. Khong, E. Harris, T. Lindgren, D.W. Goldberg, and Z. Li, 2016: The North American soil moisture database: Development and applications. *Bulletin of the American Meteorological Society*, **97,** 1441–1459, https://doi.org/10.1175/BAMS-D-13-00263.1.

Rawls, W. J., C. L. Brakensiek, and K. E. Saxton, 1982: Estimation of soil water properties. *Trans. - Am. Soc. Agric. Eng.*, **25**, 1316–1328, https://doi.org/10.13031/2013.33720.

Rawls, W.J., L.R. Ahuja, and D.L. Brakensiek, 1992: Estimating soil hydraulic properties from soils data. In Indirect Methods for Estimating the Hydraulic Properties of Unsaturated Soils. *M.T. van Genuchten, F.J. Leij, and L.J. Lund, Editors*. *Univ. of California, Riverside: Riverside, California*. 329 – 340.

Reges, H. W., N. Doesken, J. Turner, N. Newman, A. Bergantino, and Z. Schwalbe, 2016: CoCoRaHS: The evolution and accomplishments of a volunteer rain gauge network. *Bull. Am. Meteorol. Soc.*, **97**, 1831–1846, https://doi.org/10.1175/BAMS-D-14-00213.1.

Sadler, J. M., J. L. Goodall, and M. M. Morsy, 2017: Effect of rain gauge proximity on rainfall estimation for problematic urban coastal watersheds in Virginia Beach, Virginia. *J. Hydrol. Eng.*, **22**, https://doi.org/10.1061/(ASCE)HE.1943-5584.0001563.

Schaefer, G. L., M. H. Cosh, and T. J. Jackson, 2007: The USDA Natural Resources Conservation Service Soil Climate Analysis Network (SCAN). *J. Atmos. Ocean. Technol.*, **24**, 2073–2077, https://doi.org/10.1175/2007JTECHA930.1.

Schroeder, J.L., W.S. Burgett, K.B. Haynie, I. Sonmez, G.D. Skwira, A.L. Doggett, and J.W. Lipe, 2005: The West Texas mesonet: a technical overview. Journal of Atmospheric and Oceanic Technology, **22**, 211–222.

Seyfried, M. S., and L. E. Grant, 2007: Temperature Effects on Soil Dielectric Properties Measured at 50 MHz. *Vadose Zo. J.*, **6**, 759–765, https://doi.org/10.2136/vzj2006.0188.

Shafer, M. A., C. A. Fiebrich, D. S. Arndt, S. E. Fredrickson, and T. W. Hughes, 2000: Quality assurance procedures in the Oklahoma Mesonetwork. *J. Atmos. Ocean. Technol.*, **17**, 474–494, https://doi.org/10.1175/1520-0426(2000)017<0474:QAPITO>2.0.CO;2.

Shulski, M., S. Cooper, G. Roebke, and Al Dutcher, 2018: The Nebraska Mesonet: Technical overview of an automated state weather network. *J. Atmos. Ocean. Technol.*, **35**, 2189–2200, https://doi.org/10.1175/JTECH-D-17-0181.1.

Sinclair, T. R., J. Devi, A. Shekoofa, S. Choudhary, W. Sadok, V. Vadez, M. Riar, and T. Rufty, 2017: Limited-transpiration response to high vapor pressure deficit in crop species. *Plant Sci.*, **260**, 109–118, https://doi.org/10.1016/j.plantsci.2017.04.007.

Sun, Q., C. Miao, Q. Duan, H. Ashouri, S. Sorooshian, and K. L. Hsu, 2018: A Review of Global Precipitation Data Sets: Data Sources, Estimation, and Intercomparisons. *Rev. Geophys.*, **56**, 79–107, https://doi.org/10.1002/2017RG000574.

Tan, M. L., and X. Yang, 2020: Effect of rainfall station density, distribution and missing values on SWAT outputs in tropical region. *J. Hydrol.*, **584**, 124660, https://doi.org/10.1016/j.jhydrol.2020.124660.

Teegavarapu, R. S. V., and V. Chandramouli, 2005: Improved weighting methods, deterministic and stochastic data-driven models for estimation of missing precipitation records. *J. Hydrol.*, **312**, 191–206, https://doi.org/10.1016/j.jhydrol.2005.02.015.

Teegavarapu, R. S. V., and C. Pathak, 2008: Infilling of rain gage records using radar (NEXRAD) data: Influence of spatial and temporal variability of rainfall processes. *World Environ. Water Resour. Congr. 2008 Ahupua'a - Proc. World Environ. Water Resour. Congr. 2008*, **316**, 1–9, https://doi.org/10.1061/40976(316)406.

Topp, G. C., J. L. Davis, and A. P. Annan, 1980: Electromagnetic determination of soil water content: Measurements in coaxial transmission lines. **16**, 574–582.

Verworn, A., and U. Haberlandt, 2011: Spatial interpolation of hourly rainfall-effect of additional information, variogram inference and storm properties. *Hydrol. Earth Syst. Sci.*, **15**, 569–584, https://doi.org/10.5194/hess-15-569-2011.

Willmott, C. J., and K. Matsuura, 2005: Advantages of the mean absolute error (MAE) over the root mean square error (RMSE) in assessing average model performance. *Clim. Res.*, **30**, 79–82, https://doi.org/10.3354/cr030079.

World Meteorological Organization, 2017: *Guide to Meteorological Instruments and Methods of observation*. I.8-1 to I.9-1 pp.

Young, C. B., A. A. Bradley, W. F. Krajewski, A. Kruger, and M. L. Morrissey, 2000: Evaluating NEXRAD multisensor precipitation estimates for operational hydrologic forecasting. *J. Hydrometeorol.*, **1**, 241–254, https://doi.org/10.1175/1525-7541(2000)001<0241:ENMPEF>2.0.CO;2.

Zhang, L., J. Shi, Z. Zhang, and K. Zhao, 2003: The estimation of dielectric constant of frozen soil-water mixture at microwave bands. *Int. Geosci. Remote Sens. Symp.*, **4**, 2903–2905, https://doi.org/10.1109/igarss.2003.1294626.

Zou, C. B., G. L. Caterina, R. E. Will, E. Stebler, and D. Turton, 2015: Canopy interception for a tallgrass prairie under juniper encroachment. *PLoS One*, **10**, 1–19, https://doi.org/10.1371/journal.pone.0141422.

Chapter 4 - Revisiting Laboratory Methods for Measuring Soil Water Retention Curves

This work will be submitted to the *Soil Science Society of America Journal*

Nathaniel Parker, Gerard J. Kluitenberg, and Andres Patrignani

Abstract

Soil water retention curves describe the relationship between soil water content and soil matric potential that is key to understanding soil water processes such as soil water storage, soil water availability, and soil water flow. Traditional laboratory methods for measuring water retention typically consist of suction table, pressure cells, and pressure plates. However, the advancement of technology has resulted in the commercial availability of newer methods based on precision mini-tensiometers and water potential meters. This study investigated the discrepancy between water retention curves (SWRC) measured solely based on traditional methods and SWRC measured solely based on modern methods using 24 soils samples that span five textural classes. The SWRC measured using both traditional and modern methods were similar in all the soils at matric potentials close to saturation (i.e. 0 – 10 kPa), which resulted in similar saturation and field capacity water contents. At the dry-end of the retention curve, the traditional method resulted in higher water contents than the modern method in the fine soils, which resulted on average 120% higher residual water content and 25% higher permanent wilting point water content in the clay and silty clay soils, whereas no discrepancy was observed in the sandy loam soils. The higher water contents for the traditional method in the fine soils resulted in 35% less plant available capacity in the clay and 47% less PAWC in the silty clay soils compared to the modern method.

Introduction

The soil water retention curve describes the energy-state of soil water from saturation to oven-dryness conditions, thus providing key soil hydraulic information for agricultural and hydrological research on the state and fate of soil water. For instance, soil water retention curves are often used as model inputs for simulating evapotranspiration and water redistribution (Skaggs, 1978; Garg and Gupta, 2015; Feki et al., 2018), estimating potential groundwater recharge rates (Solone et al., 2012; Wyatt et al., 2017), and modeling solute transport in the vadose zone (Vogel et al., 2000; Gärdenäs et al., 2005). Soil water retention curves are typically determined empirically by equilibrating water in soil samples with a body of water at a known potential. A pair of measurements of volumetric water content and soil matric potential represents a point in the soil water retention curve. Because the energy state of soil water spans multiple orders of magnitude, different principles, and thus different methods and instruments, are often required to complete the measurements from soil saturation to oven-dryness conditions (Bittelli and Flury, 2009; Parker et al., 2021).

Traditional laboratory methods for determining soil water retention curves usually include the use of suction tables (range from 0 to -100 kPa) (Stackman et al., 1969), pressure cells (range from 0 to -100 kPa), and pressure plate apparatus (range from -100 to -1,500 kPa) (Richards and Fireman, 1943; Richards, 1948, 1965). The suction table (also known as sand/kaolin box) enables accurate measurements of soil matric potential in the wet end of the retention curve, typically from 0 to -10 kPa (sandbox) or 0 to -100 kPa (kaolin box), and is often used together with the pressure plate apparatus (Romano and Santini, 2002; Solone et al., 2012). Pressure cells and pressure plate apparatus comprise a porous ceramic plate on which soil samples are placed in an enclosed pressure chamber. A known positive pressure from compressed air is applied on the

soil samples in the chamber to drain out water from the samples through the ceramic plate until equilibrium is reached (i.e. when water no longer flows out of the vessel), then the corresponding volumetric water content is determined using the thermogravimetric method.

More modern methods for measuring soil water retention curves include the evaporation method that relies on mini-precision tensiometers and the chilled mirror method using a water potential meter (Campbell et al., 2007). A key advantage of the evaporation method is that it provides a more detailed and continuous water retention curve from 0 to -90 kPa (Schindler et al., 2010). The modern dewpoint method based on the water potential meter operates by measuring the relative humidity of the air around a soil sample in a sealed chamber using a chilling mirror technique and then converting the relative humidity to total water potential using the Kelvin equation (Campbell et al., 2007). The combination of the evaporation and dew point methods allows measurement of soil water retention from saturation to -300 MPa, which is a much wider range than the traditional methods.

Although the modern methods provide a more detailed and wider range of water retention measurements, the traditional methods are still predominantly used partly due to legacy instrumentation in soil physics laboratories and the ability to process large batches of soil samples in a single run than the modern techniques. Some previous studies have shown that the pressure plate apparatus may be prone to substantial errors at low (i.e. a more negative) matric potentials (Richards and Ogata, 1961; Campbell, 1988; Bittelli and Flury, 2009; Solone et al., 2012). For instance, a study comparing the matric potential of pressure plate-equilibrated silt loam soils at -1,500 kPa with that obtained using a dew point potential meter resulted in up to 81% higher (less negative) matric potential values than the targeted -1,500 kPa (Bittelli and Flury, 2009). Similarly, another group of researchers investigating possible errors of pressure

plate apparatus for measuring water retention curves found that in fine-textured soils the pressure plate apparatus overestimated the volumetric water content by up to about 40% compared to values obtained using a dewpoint water potential meter (Solone et al., 2012). The associated errors with the pressure plate apparatus at low matric potentials are typically attributed to loss of hydraulic contact between soil and the ceramic plate due to soil shrinkage (Campbell, 1988), water reabsorption by soil after releasing the pressure on the plate (Richards and Ogata, 1961), and failure to reach equilibrium within a reasonable period of a few weeks to a few months due to the inherently low hydraulic conductivity of soils at low matric potentials (Campbell, 1988; Gee et al., 2002). Since pressure plate apparatus has been the most widely used method in the scientific literature, existing knowledge in the form of pedotransfer functions has been strongly influenced also based on soil samples analyzed using this approach (Arya and Paris, 1981; Schaap et al., 2001; Saxton and Rawls, 2006; Vereecken et al., 2010). Previous studies investigating the discrepancy between traditional and modern methods for measuring soil water retention have primarily focused on the dry-end of the retention curves (Cresswell et al., 2008; Bittelli and Flury, 2009; Solone et al., 2012; Gubiani et al., 2013). Therefore, there is a need to investigate the magnitude of the discrepancy between soil water retention curves determined using traditional and modern methods over the entire range from saturation to oven-dryness. There is also a need to better quantify the implications of using different retention curves on estimations of plant available water (Gubiani et al., 2013; Schelle et al., 2013; Rahardjo et al., 2019). The objective of this study was to quantify the magnitude of the differences in soil water retention curves determined using traditional methods and modern methods. Are these two approaches interchangeable for soil physics research? What are the implications of using either method? Throughout this study, the term “traditional methods” is reserved for the combination of

suction table, pressure cells, and pressure plates; while the term “modern methods” is reserved for the combination of the evaporation approach using precision mini-tensiometers and a dew point water potential meter.

Materials and methods

Soil sampling

For this experiment, undisturbed soil samples from 5 different soil textural classes were collected from three fields with perennial grassland and cropland on 8 June 2020. At each location, we collected at least five undisturbed soil samples with a volume of 100 cm^3 each (i.e. height of 5.1 cm and 5 cm i.d.) from the top 80 cm profile using a core sampler (model C, Eijkelkamp Agrisearch Equipment). Before the sampling process, we scraped the top 2-cm soil to remove any dense root system that could affect the sampling process. Soils samples were immediately covered with plastic lids to prevent water loss and then placed in a carrying case to avoid disturbance during transportation to the laboratory. Soil samples were stored in a refrigerator at 6 ºC until samples were analyzed.

Laboratory soil water retention measurements

Soil saturation and Saturated hydraulic conductivity

The soils were saturated in a 5 mM $CaCl_2$ solution in a desiccator with ¾ of the height immersed in the solution. Before the saturation process, we secured the face of the sample ring to be placed in the $CaCl_2$ solution with a cheesecloth and a rubber ring to prevent soil loss. We left the samples to saturate in the $CaCl_2$ solution for at least 5 days. After the 5 days, samples that did not attain saturation were put under vacuum suction for at least 2 more days to facilitate the saturation. Saturated hydraulic conductivity (K_{sat}) of the soils was measured using the constant

head method (Reynolds and Elrick, 2002) in a close-path permeameter (Eijkelkamp Agrisearch Equipment). For the samples with very low permeability, we used the falling head method (Reynolds and Elrick, 2002). Both the constant head and falling head K_{sat} measurements were carried out following the procedure in the operational manual of the permeameter at a temperature of 21±2 ºC.

Soil water retention curve

Soil water retention curves were determined for the soil samples using traditional and modern laboratory methods. The traditional method combined suction table (model 08.01, Eijkelkamp Agrisearch Equipment), pressure cells (Tempe cells, Soil Moisture Equipment Corp.), and pressure plate (model 1500F2, Soil Moisture Equipment Corp). The modern method combined the evaporation method based on mini-tensiometers (Hyprop II, Meter Group, Inc.) and dewpoint water potential meter (WP4C, Meter Group, Inc.). To minimize the effect of sample variability on the experiment and allow a fair comparison of the methods, the same samples were passed through both the traditional and modern water retention measurements. This is a distinct feature of our experiment that has not been implemented in previous studies comparing traditional and modern methods.

We measured the water retention by first equilibrating the undisturbed soil samples at tensions of -0.1, -2, and -5 kPa using the suction table and then equilibrated the samples at tensions of -10, -33, and -70 kPa using pressure cells. The measurements in both the suction table and pressure cells were conducted following the procedures in Dane and Hopmans (2002). In both the suction table and the pressure cell measurements, we established hydraulic equilibrium after two consecutive days with <0.2% change in the soil mass. In addition, a check soil sample was included with the suction table measurements to verify the consistency of the

method. After the water retention measurement at -70 kPa in the pressure cell, the undisturbed samples were re-saturated in a 5 mM $CaCl_2$ solution for at least 2 days and then again measured the saturated soil mass before starting the measurements using the evaporation method. The evaporation-based water retention measurements were done at pressures ranging from 0 to ~ -80 kPa following the instructions in the Hyprop user manual. We deemed the evaporation measurements completed immediately after the air-entry potential of one mini-tensiometer cup is reached (Kirste et al., 2019). We then measured the equilibrium mass of the soil samples and then proceeded with the dewpoint water potential meter experiment.

After dismounting the soil samples from the evaporation experiment, ten subsamples of 10 g were collected along the hydraulic gradient of each soil sample and placed in stainless steel cups to measure the water potential using a dewpoint water potential meter. Before using the water potential meter, we first calibrated the instrument using a manufacturer-certified KCl solution of 0.5 mol Kg^{-1} concentration (Meter Group, Inc.). After reaching equilibrium in the water potential meter we recorded the water potential and then the samples were oven-dried at 105^{o}C for 48 hours to determine the gravimetric water content. The volumetric water content at the point of equilibrium with the water potential meter was estimated using the bulk density of the soil. To ensure the best results, all measurements with the water potential meter were done in "precise mode" following the user instructions in the user's manual. After the dewpoint experiment, the soils were manually ground using pestle and mortar (model 60325, CoorsTek Inc.), passed through a 2 mm sieve (ASTM E-11, Humboldt Manufacturing Co.), and then stored in small paper envelopes inside a plastic container at room temperature.

Since for soil samples the water potential is the additive result of soil matric and osmotic potential, knowledge of the osmotic potential is required to infer the soil matric potential. Thus,

we also determined the osmotic potential of each sample based on the bulk electrical conductivity of the saturated paste extract. The saturated paste extract was prepared by mixing 5 ±0.01 g of ground and sieved soil with 5 ±0.01 g of deionized water in a 10-ml tube (i.e. 1:1 soil to water ratio by mass), The mixture was then agitated on a linear mechanical shaker for 3 hours, and then the mixture was separated by centrifuging the mixture at 2500 rpm for one hour (model, FS3500, Cole Parmer, Inc.). We then extracted the clear solution into a 10-ml PYREX Griffin beaker and measured the electrical conductivity of the solution using an EC meter (model PC100, Cole Parmer, Inc.). The electrical conductivity reading (EC in dS m^{-1}) approximates the osmotic potential of the saturated paste extract (ψ_{os} in kPa) by the equation (Campbell and Gee, 1986):

$$\psi_{OS} = -36\,EC \qquad [1]$$

ψ_{os} is then converted to the osmotic potential of the soil (ψ_o) using equation 2, which is given by:

$$\psi_o = \psi_{os}\,(\theta_s/\theta) \qquad [2]$$

Where was θ_s is the saturation water content of the soil and θ_s is measured volumetric water content of the soil sample. The osmotic potential of the soil samples was then subtracted from the values of soil water potential to obtain the matric potential of the soil.

The final step was to determine the soil water content at -500, -1000, and -1500 kPa using the pressure plate apparatus (model 1500F2, Soil Moisture Equipment Corp.). We performed each of the pressure plate measurements using approximately 15 g of the sieved soil contained within a ring of 5 cm in diameter and 1 cm height following the procedure in Dane and Hopmans (2002). Three replicates per soil sample were run for the pressure plate experiment. After setting the ceramic plates in the pressure chamber, we covered the entire samples in the pressure plate with moist paper towels to prevent the compressed air from drying the soils during equilibration

in the pressure plate. The samples remained in the pressure plate for at least 15 days or until 5 consecutive days with no measurable water outflow from the vessel. A check soil was added to each pressure plate. At end of the measurements, the soil samples were oven-dried at 105ºC for 48 hours to determine the gravimetric water content of the samples. For the samples equilibrated in the pressure plate at -1,500 kPa, we also verified the matric potential in the water potential meter to determine the deviation from the targeted -1500 kPa matric potential.

For each soil sample, we fitted the van Genuchten soil water retention model van Genuchten (1980) using ordinary least-squares in Matlab R2020b (Mathworks, Natick, MA). The van Genuchten model is given as:

$$\frac{\theta - \theta_r}{\theta_s - \theta_r} = [1 + (-\alpha\psi_m)^n]^{-m} \qquad [3]$$

where θ ($cm^3\ cm^{-3}$) is volumetric water content, θ_s ($cm^3\ cm^{-3}$) is saturated water content, θ_r ($cm^3\ cm^{-3}$) is residual water content, ψ_m (kPa) is matric potential, α (kPa^{-1}) is a fitted parameter relating to the inverse of air-entry pressure, n (dimensionless) is a measure of pore size distribution, and m = 1–1/n (Schaap et al., 2001).

2.2.3 Particle size analysis

The fraction of sand, silt, and clay content of all the 24 samples was determined using the hydrometer method (Gavlak et al., 2005). The analysis was performed using 40 ±0.05 g of oven-dry and ground soil that passed through a 2 mm sieve. Soil samples were mixed with 100 ml of a 0.08 M of sodium hexametaphosphate as the dispersing agent. Then, samples were agitated using a linear shaker for 16 hours. The next morning, samples were transferred to 1-liter cylinders and the remaining volume of the cylinder was topped with de-ionized water at room temperature. Samples were manually agitated using a perforated plunger and the suspension density was

measured at the 40 s mark using a Buoyoucos hydrometer (ASTM 152-H, Humboldt Manufacturing Co.). This first reading of the suspension density was repeated twice. A second reading of the suspension density was carried at around seven hours from the end of the agitation based on the laboratory temperature (~ 22 ^{o}C). We also measured the gravimetric water content of the samples using 15 g of soil from each sample to account for any trace of soil moisture in the samples. As with previous procedures, one soil sample of known particle sizes was added to every batch of particle size analysis.

Results and Discussion

General soil physical properties

The 24 soil samples in our dataset spanned five textural classes, which comprise clay loam, silty clay loam, silty clay, clay, and sandy loam soils. The highest sand content was 61%, which was recorded in the sandy loam soils of samples 22ABR and 23ABR, whereas the lowest sand fraction of 11% was recorded in the silty clay loam soils of 10AB and 11AB (Table 4.1). On the other hand, the highest percent clay of 44% was recorded in the clay soil of sample 09W, whereas the lowest clay content of 5% was recorded in the sandy loam soils (samples 15R - 19R; 20ABR -21ABR). The organic matter of our soils varied from 0.9 to 2.8% with higher organic matter content overall in the fine-textured soils. Bulk density of the soils varied from 1.34 g cm^{-3} in 23ABR to 1.73 g cm^{-3} in 08W (Table 4.1). Opposite to the bulk density, porosity varied from 0.35 cm^3 cm^{-3} in 08W to 0.50 in 23ABR cm^3 cm^{-3}. Interestingly, the clay and silty clay soils (samples 07W to 08W) had the highest values for bulk density and the lowest porosity values in our soils, which was likely due to compaction by the weight of the overlying soil layers due to the deeper depths (54 – 82 cm) from which the clay and silty clay samples were collected.

Indeed, in comparison to the textural class bulk density threshold for root-restricting conditions of the USDA (USDA-NRCS, 1996), the bulk density values of the clay, and silty clay soils suggest the existence of root-restricting conditions. The saturated hydraulic conductivity of the samples spanned three orders of magnitude, varying from 0.22 in the clay loam soil of sample 02W to 180.54 cm d^{-1} in sample 23ABR sandy loam. As expected, the sandy loam soils had higher saturated hydraulic conductivity than the fine-textured soils due to the inherently higher macroporosity of sandy soils than fine soils (Campbell and Norman, 1998).

Table 4.1 Sample location and measured textural class, percent sand, percent clay, percent silt, organic matter (OM), bulk density (ρb), total porosity (Ø), saturated hydraulic conductivity (Ks), osmotic potential (ψos), and verified matric potential of samples equilibrated at -1500 kPa in the dewpoint water potential meter (ψ_{verify}). Abbreviated textural classes are clay loam (C L), silty clay loam (Si C L), silty clay (Si C), clay (C), and sandy loam (S L).

Sample code	Soil depth	Texture	Sand	Clay	Silt	OM	ρ_b	Ø	Ks	ψ_{os}	ψ_{verify}
	cm		—————— % ——————				g cm^{-3}	cm^3 cm^{-3}	cm d^{-1}	— kPa—	
01W	3 – 8	C L	31	33	36	2.6	1.49	0.44	0.57	-25.6	-824
02W	2 – 7	C L	29	33	38	2.7	1.50	0.43	0.22	-26.6	-713
03W	3 – 8	C L	31	32	37	2.5	1.41	0.47	0.28	-25.3	-915
04W	2 – 7	C L	31	32	37	2.7	1.41	0.47	0.26	-25.5	-815
05W	2 – 7	C L	29	33	38	2.5	1.43	0.46	1.58	-24.3	-966
06W	63 – 68	Si C L	18	40	42	1.2	1.46	0.45	5.57	-21.5	-379
07W	54 – 59	Si C	19	41	40	1.0	1.66	0.37	0.31	-19.3	-291
08W	69 – 74	Si C	18	41	41	0.9	1.73	0.35	0.29	-20.1	-390
09W	77 – 82	C	17	44	39	0.9	1.64	0.38	0.43	-19.5	-381
10AB	3 – 8	Si C L	11	36	53	2.7	1.50	0.43	3.09	-34.3	-376
11AB	3 – 8	Si C L	11	34	55	2.8	1.55	0.42	0.41	-30.3	-490
12AB	3 – 8	Si C L	13	33	54	2.7	1.53	0.42	0.64	-30.3	-540
13AB	2 – 7	Si C L	13	32	55	2.7	1.55	0.42	3.89	-31.3	-529
14AB	2 – 7	Si C L	13	34	53	2.6	1.49	0.44	28.0	-34.2	-546
15R	3 – 8	S L	52	5	43	1.6	1.52	0.43	14.9	-16.4	-1584
16R	4 – 9	S L	50	5	45	1.4	1.55	0.41	22.9	-13.1	-1777
17R	3 – 8	S L	49	5	46	1.4	1.54	0.42	8.79	-20.4	-1920
18R	3 – 8	S L	52	5	43	1.3	1.55	0.41	10.7	-13.3	-1747
19R	3 – 8	S L	50	5	45	1.4	1.55	0.42	7.13	-15.1	-1975
20ABR	3 – 8	S L	60	5	35	0.9	1.54	0.42	23.3	-10.1	-800
21ABR	4 – 9	S L	60	5	35	1.1	1.52	0.43	64.7	-11.0	-779
22ABR	5 – 10	S L	61	6	33	0.9	1.47	0.45	57.6	-9.43	-721
23ABR	4 – 9	S L	61	6	33	1.0	1.34	0.50	181	-9.29	-831
24ABR	4 – 9	S L	59	6	35	1.0	1.58	0.40	22.2	-9.97	-920

Numbers in the sample code represent the ring number and letters in the sample code represent the name of the sampling location. W is Washington, AB is Ashland Bottoms, and ABR is Ashland Bottoms River.

Osmotic potential and verified matric potential of pressure plate-equilibrated samples at -1500 kPa

The osmotic potential of our soils by saturated paste extract that was measured using an electrical conductivity meter varied from -9.3 kPa to -34.3 kPa in silty clay loam (Table 4.1), which are similar to the osmotic potential of soils in previous studies determined by saturated paste extract using dew point potential meter (Bittelli and Flury, 2009; Solone et al., 2012). In comparison with the accuracy of the dew point potential meter, all our osmotic potential values fell within the error margin of the water potential meter (±50 kPa error at 0 to -5000 kPa) and thus, confirms the assumption of negligible osmotic potential used in the previous studies that measured close to zero osmotic potential using the water potential meter (Bittelli and Flury, 2009; Solone et al., 2012; Schelle et al., 2013). However, we did not assume the negligible osmotic potential for our soils in this study.

Several studies have reported a lack of soil equilibration in water retention measured at -1500 kPa using the pressure plate (Campbell and Gee, 1986; Gee et al., 2002; Cresswell et al., 2008; Bittelli and Flury, 2009; Parker and Patrignani, 2021), so we also verified using the water potential meter the matric potential of the soils samples that were equilibrated at -1500 kPa using pressure plate. The verified matric potentials of 19 out of the 24 samples analyzed using the water potential meter resulted in matric potential values higher (less negative) than the -1500 kPa applied to the pressure plate with matric potentials > -1000 kPa (Table 4.1). These 19 soils that were wetter than the targeted -1500 kPa comprise all the fine-textured soils and 5 sandy loam soils of samples 20AB to 24AB, which is consistent with the observations in the previous studies that samples equilibrated in the pressure plate at -1500 kPa do not reach the targeted matric potential at equilibrium, especially in fine-textured soils (Campbell and Gee, 1986; Gee et al.,

2002; Cresswell et al., 2008; Bittelli and Flury, 2009; van Lier et al., 2019; Parker and Patrignani, 2021). On the other hand, the verified matric potentials for the remaining 5 out of the 24 samples, which are all sandy loam soils of samples 15R to 19R, resulted in lower (i.e. more negative) matric potential than the targeted -1500 kPa with values ranging from -1584 to -1975 kPa (Table 4.1), suggesting that the period of two weeks for equilibration time may be slightly too long, causing the soils to dry by the compressed air. It is worth mentioning that while it was also possible for the compressed air in the pressure plate to have dried the sandy soil samples, we did not observe during our experiment that the compressed air was responsible for the lower matric potential in the five sandy soils since the moist paper towels used to cover the samples during the pressure plate experiment still appeared moist after opening the pressure plate upon equilibration.

Traditional versus modern techniques

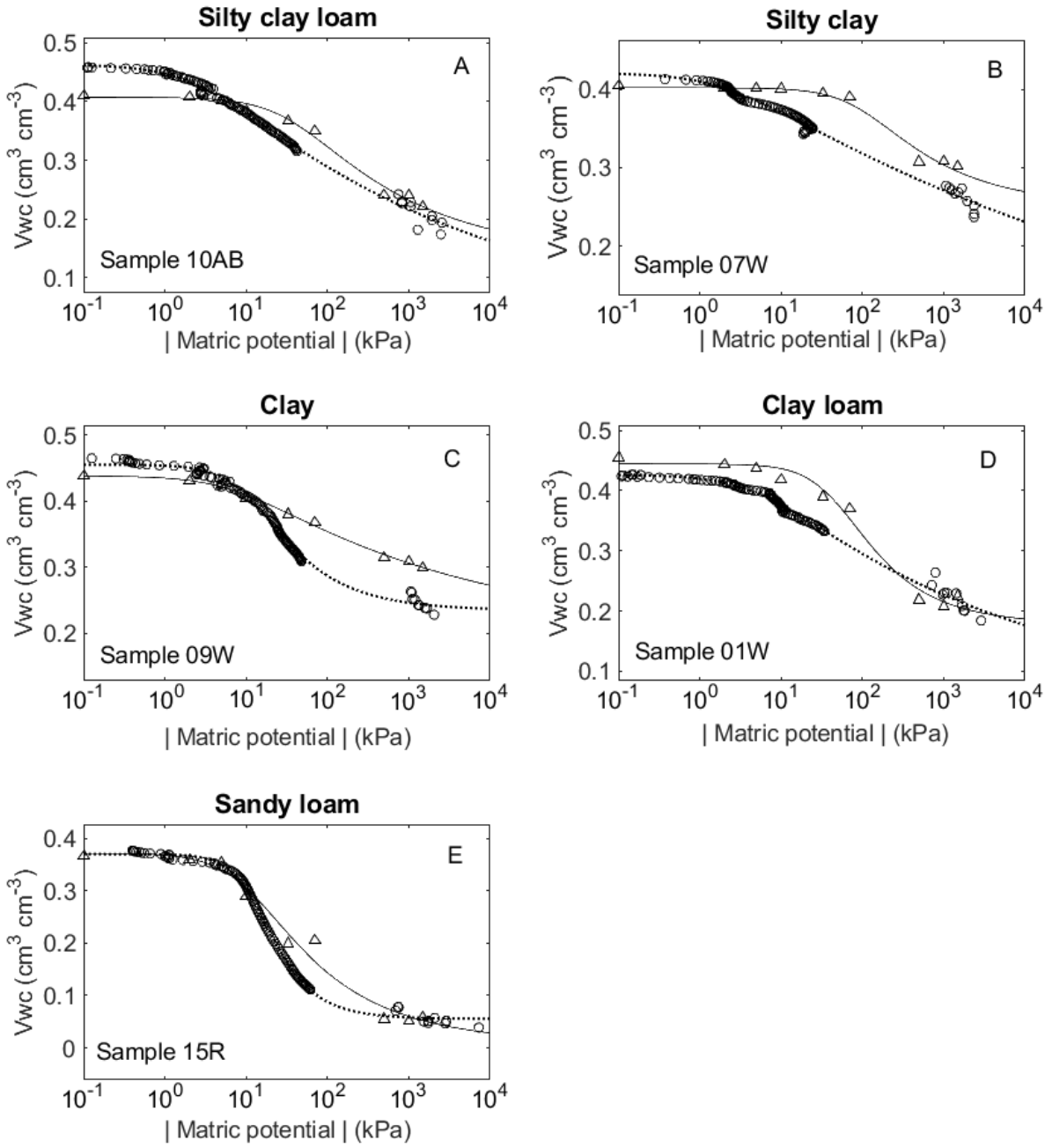

Figure 4.1 Representative of measured (symbols) and fitted (lines) soil water retention curves determined using the combination of suction table, pressure cell, and pressure plate (traditional) and a combination of mini-tensiometers and dewpoint potential meter (modern) laboratory techniques in A) 10AB silty clay loam, B) 07W silty clay, C) 09W clay, D) 01W clay loam, and E) 15R sandy loam. Triangular symbols and solid lines represent the traditional techniques, while circles and dotted lines represent the modern techniques.

Five representative water retention curves for the soils measured by combining suction table, pressure cells, and pressure plate (traditional methods) and by combining mini-tensiometers and water potential meter (modern methods) are shown in Figure 4.1. Both water retention curves measured using modern and traditional laboratory techniques resulted in similar water contents in all the soils at matric potentials close to saturation (from 0 to ~ -10 kPa). The modern method resulted in marginally higher water content than the traditional method in the silty clay loam soil at near saturation with a difference of 0.05 cm^3 cm^{-3}, which might be because the silty clay loam soil did not reach full saturation at the beginning of the traditional water retention experiment. The similarity between the water retention measurements at matric potentials near saturation indicates a good agreement between the suction table and pressure cells and the mini-tensiometer techniques in measuring soil water retention at matric potentials > -10 kPa. At matric potentials between -10 kPa and -500 kPa, there were marked differences between the retention curves for the two methods with the traditional method having higher water contents than the modern method in all the soils. The largest discrepancy was recorded in the clay and silty clay soils, whereas sandy loam and silty clay loam soils resulted in the least discrepancy, which is consistent with observations made in soils of the same texture in previous studies that compared the pressure plate to the point potential meter (Solone et al., 2012) and inverse parameter estimation from evaporation experiment (van Lier et al., 2019). Interestingly, despite the pressure plate-equilibrated soils having greater (less negative) matric potential than the targeted -1500 kPa when verified with the water potential meter, the water retention curves for both traditional and modern methods converged at matric potentials from -500 to -1500 kPa in the sandy loam, silty clay loam, and clay loam soils. The convergence of both curves from -500 and -1500 kPa implies that discrepancy between the verified matric potential and the

targeted matric potential of -1500 kPa in the pressure plate might not necessarily translate into a large discrepancy in water content at -1500 kPa as was also reported in the study by Cresswell et al. (2008).

Soil hydraulic parameters

Table 4.2 Fitted hydraulic parameters of the van Genuchten (1980) model derived from the water retention measurements for the soil samples using traditional (suction table, pressure cell, and pressure plate) and modern (mini-tensiometers and dew point potential meter) laboratory techniques. θ_s, is saturation water content, θ_r is residual water content, and α relates to the inverse of air-entry pressure, and n is a measure of pore size distribution. θ_s, and θ_r, are also results from the fitting exercise. Abbreviated textural classes are clay loam (C L), silty clay loam (Si C L), silty clay (Si C), clay (C), and sandy loam (S L).

			Traditional techniques				Modern techniques			
Sample code	Soil depth	Texture	θ_s	θ_r	α	n	θ_s	θ_r	α	n
	cm		—$cm^3\ cm^{-3}$—		kPa^{-1}	—	—$cm^3\ cm^{-3}$—		kPa^{-1}	—
01W	3 – 8	C L	0.44	0.18	0.02	1.64	0.43	0.05	0.19	1.14
02W	2 – 7	C L	0.44	0.20	0.02	2.02	0.42	0.01	0.29	1.12
03W	3 – 8	C L	0.45	0.01	0.07	1.20	0.43	0.01	0.34	1.14
04W	2 – 7	C L	0.46	0.01	0.11	1.18	0.44	0.01	0.32	1.14
05W	2 – 7	C L	0.47	0.01	0.10	1.18	0.45	0.01	0.34	1.13
06W	63 – 68	Si C L	0.60	0.25	0.01	2.26	0.59	0.02	0.05	1.27
07W	54 – 59	Si C	0.40	0.25	0.01	1.45	0.42	0.01	0.52	1.07
08W	69 – 74	Si C	0.38	0.25	0.01	1.34	0.42	0.22	0.07	1.71
09W	77 – 82	C	0.44	0.19	0.15	1.16	0.46	0.23	0.09	1.66
10AB	3 – 8	Si C L	0.41	0.13	0.03	1.31	0.46	0.01	0.39	1.13
11AB	3 – 8	Si C L	0.39	0.22	0.02	1.85	0.45	0.01	0.24	1.15
12AB	3 – 8	Si C L	0.37	0.19	0.03	1.43	0.42	0.01	0.29	1.13
13AB	2 – 7	Si C L	0.39	0.19	0.02	1.58	0.43	0.01	0.21	1.14
14AB	2 – 7	Si C L	0.43	0.21	0.01	2.09	0.48	0.01	0.11	1.19
15R	3 – 8	S L	0.37	0.01	0.10	1.43	0.37	0.06	0.08	2.11
16R	4 – 9	S L	0.36	0.01	0.05	1.47	0.37	0.05	0.07	2.08
17R	3 – 8	S L	0.38	0.01	0.05	1.51	0.40	0.06	0.08	2.16
18R	3 – 8	S L	0.38	0.01	0.07	1.46	0.38	0.05	0.08	2.11
19R	3 – 8	S L	0.38	0.01	0.04	1.53	0.40	0.06	0.08	2.08
20ABR	3 – 8	S L	0.40	0.03	0.17	1.46	0.35	0.06	0.10	2.27
21ABR	4 – 9	S L	0.34	0.06	0.15	3.25	0.28	0.04	0.13	2.62
22ABR	5 – 10	S L	0.42	0.04	0.18	1.72	0.36	0.05	0.13	2.03
23ABR	4 – 9	S L	0.45	0.01	0.27	1.37	0.39	0.05	0.13	1.91
24ABR	4 – 9	S L	0.33	0.06	0.15	2.31	0.27	0.03	0.11	2.96

Numbers in the sample code represent the ring number and letters in the sample code represent the name of the sampling location. W is Washington, AB is Ashland Bottoms, and ABR is Ashland Bottoms River.

The fitted soil hydraulic parameters of the van Genuchten (1980) model derived from water retention curves developed using traditional and modern laboratory techniques are presented in Table 4.2. The resulting saturated water content (θ_s) from the soil water retention curves were similar in all the soils with average θ_s of 0.41 cm^3 cm^{-3} for both the traditional and modern techniques, which agrees with the water retention curves presented in Figure 4.1. Unlike θ_s, the residual water content (θ_r) showed significant differences between both methods at 5% significance level with an average θ_r of 0.11 cm^3 cm^{-3} for the traditional method and 0.05 cm^3 cm^{-3} for the modern method, which implies 120% more θ_r on average for the traditional method than the modern method (Table 4.2). The largest discrepancy in θ_r between both methods was observed in the fine-textured soils with silty clay loam recording the highest mean difference of 0.19 cm^3 cm^{-3}, whereas the sandy loam soils recorded similar values of θ_r between both methods. The significantly higher θ_r for the traditional method than the modern method, especially in the fine-textured soils, is consistent with the results in previous studies (Bittelli and Flury, 2009; Solone et al., 2012; van Lier et al., 2019). The α parameter, which is the inverse of air-entry potential was significantly lower in the retention curves for the traditional method with an average α of 0.08 kPa^{-1} than for the modern method with an average α of 0.19 kPa^{-1}, which implies 58% less α for the traditional method compared to the modern method (Table 4.2). Similar to θ_r, the discrepancy in α between the methods was more pronounced in the fine soils than the sandy loam soils. Our result for α is contrary to the results of previous studies (Bittelli and Flury, 2009; Solone et al., 2012), which could be due to differences in the type of instrument used for the water retention measurements at the wet-end, since both studies by Bittelli and Flury (2009) and Solone et al. (2012) solely combined suction table and pressure plate (i.e. traditional method) for their wet-end water retention measurements, whereas we used mini-tensiometers in

this study. The water retention curves also showed marked differences in parameter *n*, which describe the slope of the water retention curve, between the traditional and modern methods in some of our soils. The traditional method resulted in a steeper slope (i.e. higher *n* values) than the modern method in the silty clay loam soils with a mean difference of 0.59. On the contrary, the modern method resulted in steeper slopes than the traditional method in the sandy loam (mean difference in $n = 0.48$) and clay soils (mean difference in $n = 0.5$) (Table 4.2).

Plant available water capacity

Overall, the water retention measurements from the traditional and modern techniques resulted in similar θ_{-10} in all the 24 soils analyzed with a mean difference of 0.01 $cm^3\ cm^{-3}$ (Table 4.3). The traditional method resulted in a marginally higher θ_{-10} in the clay loam soils (samples 01W to 05W) with an average θ_{-10} of 0.04 $cm^3\ cm^{-3}$, but the difference was not significant at 5% significance level. The similarity in θ_{-10} between both methods in all the soils was expected since the water retention curves for both methods were similar at matric potentials from 0 to -10 kPa as discussed in the traditional vs. modern techniques section. The observed similarity in θ_{-10} between the suction table and evaporation method in our soils agrees with the result of Schelle et al. (2013). Unlike θ_{-10}, the traditional method resulted in significantly higher θ_{-1500} than the modern method in fine-textured soils. The highest discrepancy of 0.06 $cm^3\ cm^{-3}$ occurred in the clay soil (sample 09W), followed by the silty clay soils with an average of 0.055 $cm^3\ cm^{-3}$, and the silty clay loam soil with 0.032 $cm^3\ cm^{-3}$ (Table 4.3). The result suggests that measuring θ_{-1500} using the pressure plate could result in up to 25% higher water content compared to using the water potential meter in fine-textured soil. On the other hand, a similar θ_{-1500} was observed between both methods in all the sandy loam and clay loam soils. Our result for θ_{-1500} is consistent with the reports in previous studies that using the pressure plate leads to higher water contents at

matric potentials close to -1500 kPa in fine-textured soils, but with a minimal impact in coarse soils (Bittelli and Flury, 2009; Solone et al., 2012; Schelle et al., 2013; van Lier et al., 2019). The previous studies attributed the higher water contents of pressure plate-equilibrated samples at potentials ≤-1,500 kPa to loss of hydraulic contact between soil samples and the ceramic plate due to soil shrinkage (Campbell, 1988), water reabsorption by soil after releasing the pressure in the pressure plate (Richards and Ogata, 1961), and lack of equilibration due to the extremely low hydraulic conductivity of soils at the dry end of the retention curve (Campbell, 1988; Gee et al., 2002). During our pressure plate experiments, a slight push of the soil samples upon reaching equilibrium to check for loss of hydraulic contact showed that the soils were firmly seated on the ceramic plates, indicating no loss of hydraulic contact occurred in our experiment. Thus, the higher water contents of our fine soils in the pressure plate at -1,500 kPa was likely due to water reabsorption from the ceramic plates after releasing the pressure and (or) lack of equilibration of the soils at matric potentials ≤ -1500 kPa, as evidenced by the higher matric potential of the pressure plate samples when verified with the dew point potential meter (as shown in Table 4.1). The estimated plant available water capacity (PAWC) using θ_{-10} and θ_{-1500} that were measured using the traditional and modern methods was similar in almost all the soils, except in the clay soil of sample 09W and the silty clay soil of sample 08W, in which the traditional method resulted in 0.06 $cm^3\ cm^{-3}$ (i.e. 35%) less PAWC for sample 09W and 0.08 $cm^3\ cm^{-3}$ (i.e. 47%) less PAWC for sample 08W compared to the modern method (Table 4.3). The similarity in PAWC in most of our soils suggests that the marginal differences in θ_{-10}, despite not being statistically significant at a 5% significant level using analysis of variance, were adequate to reduce the effects of the discrepancy in θ_{-1500} between both the traditional and modern methods on PAWC. On the other hand, the lower estimated PAWC resulting from the traditional method

than the PAWC from the modern method in the clay and the silty clay soils is consistent with the result of the previous study in which the higher θ_{-1500} in the pressure plate resulted in lower PAWC than the modern method in fine soils (Bittelli and Flury, 2009).

Table 4.3 Water contents at field capacity (θ-10), permanent wilting point (θ-1500), and plant available water capacity (PAWC), and difference in plant available water capacity (ΔPAWC) estimated from the water retention measurements for the soil samples using traditional (suction table, pressure cells, and pressure plate) and modern (mini-tensiometers and dew point potential meter) laboratory techniques. θ_s, is saturation water content, θ_r is residual water content, and α relates to the inverse of air-entry pressure, and n is a measure of pore size distribution. θ_s, and θ_r, are also results from the fitting exercise. Abbreviated textural classes are clay loam (C L), silty clay loam (Si C L), silty clay (Si C), clay (C), and sandy loam (S L).

Sample code	Soil depth	Texture	Traditional techniques			Modern techniques			
			θ_{-10}	θ_{-1500}	PAWC	θ_{-10}	θ_{-1500}	PAWC	ΔPAWC
	cm		—— $cm^3\ cm^{-3}$ ——			— $cm^3\ cm^{-3}$ —			
01W	3 – 8	C L	0.42	0.23	0.19	0.38	0.22	0.16	0.03
02W	2 – 7	C L	0.42	0.22	0.20	0.36	0.21	0.15	0.05
03W	3 – 8	C L	0.40	0.20	0.20	0.35	0.19	0.16	0.04
04W	2 – 7	C L	0.40	0.21	0.19	0.37	0.19	0.18	0.01
05W	2 – 7	C L	0.41	0.22	0.19	0.38	0.21	0.17	0.02
06W	63 – 68	Si C L	0.57	0.26	0.31	0.55	0.20	0.35	-0.04
07W	54 – 59	Si C	0.40	0.30	0.10	0.37	0.26	0.11	-0.01
08W	69 – 74	Si C	0.38	0.29	0.09	0.39	0.22	0.17	-0.08
09W	77 – 82	C	0.41	0.30	0.11	0.41	0.24	0.17	-0.06
10AB	3 – 8	Si C L	0.38	0.22	0.16	0.38	0.21	0.17	-0.01
11AB	3 – 8	Si C L	0.38	0.23	0.15	0.38	0.19	0.19	-0.04
12AB	3 – 8	Si C L	0.35	0.22	0.13	0.35	0.19	0.16	-0.03
13AB	2 – 7	Si C L	0.37	0.22	0.15	0.37	0.20	0.17	-0.02
14AB	2 – 7	Si C L	0.42	0.22	0.20	0.43	0.19	0.24	-0.04
15R	3 – 8	S L	0.29	0.06	0.23	0.30	0.06	0.24	-0.01
16R	4 – 9	S L	0.30	0.06	0.24	0.30	0.05	0.25	-0.01
17R	3 – 8	S L	0.33	0.06	0.27	0.33	0.06	0.27	0.00
18R	3 – 8	S L	0.30	0.06	0.24	0.30	0.05	0.25	-0.01
19R	3 – 8	S L	0.31	0.06	0.25	0.33	0.06	0.27	-0.02
20ABR	3 – 8	S L	0.25	0.05	0.20	0.26	0.06	0.20	0.00
21ABR	4 – 9	S L	0.14	0.05	0.09	0.16	0.04	0.12	-0.03
22ABR	5 – 10	S L	0.24	0.05	0.19	0.24	0.05	0.19	0.00
23ABR	4 – 9	S L	0.27	0.04	0.23	0.26	0.05	0.21	0.02
24ABR	4 – 9	S L	0.16	0.04	0.12	0.16	0.03	0.13	-0.01

Numbers in the sample code represent the ring number and letters in the sample code represent the name of the sampling location. W is Washington, AB is Ashland Bottoms, and ABR is Ashland Bottoms River.

Conclusions

In this study, we investigated the discrepancies between soil water retention measurements in laboratory conditions using traditional and modern methods. The traditional method consisted of a combination of suction table, pressure cells, and pressure plate, while the modern methods consisted of the combination of mini-tensiometers and a water potential meter. Overall, traditional and modern methods performed similarly at the wet end of the soil water retention curve (mean difference = 0.004 cm^3 cm^{-3}) and at the dry end in sandy loam soils (mean difference = 0.021 cm^3 cm^{-3}). However, the traditional pressure plate extractor overestimated the soil water content of the fine-textured soils, except in clay loam soil, at the dry-end of the retention curve compared to the modern water potential meter. This discrepancy in fine-textured soils, translated in up to 120% higher residual water content and 25% higher water content at permanent wilting point than the modern method. In turn, the traditional method could result in up to 47% lower plant available capacity estimates than the modern method in fine soils. In agreement with prior studies, our findings suggest that the choice of a laboratory water retention measurement technique has important effects on the dry-end of the retention curve in fine-textured soils, whereas coarse-textured soils seem to be unaffected by the choice of water retention measurement method. Future studies should investigate the concomitant effects of the fitted soil hydraulic parameters derived from the water retention curve using different methods on the water flow simulations in hydrological models.

References

Arya, M.L., and F.J. Paris. 1981. A Physicoempirical Model to Predict the Soil Moisture Characteristic from Particle-Size Distribution and Bulk Density Data. Soil Science Society of America Journal 45(9): 1023–1030.

Bittelli, M., and M. Flury. 2009. Errors in water retention curves determined with pressure plates. Soil Science Society of America Journal 73(5): 1453–1460. doi: 10.2136/sssaj2008.0082.

Campbell, G.S. 1988. Soil water potential measurement: An overview. Irrigation Science 9(4): 265–273. doi: 10.1007/BF00296702.

Campbell, G.S., and G.W. Gee. 1986. Water potential: Miscellaneous methods. Methods of Soil Analysis, Part 1: Physical and Mineralogical Methods 9(9): 619–633. doi: 10.2136/sssabookser5.1.2ed.c25.

Campbell, G.S., and J.M. Norman. 1998. An Introduction to Environmental Biophysics. Second edi. Springer Science+Business Media, lnc, New York.

Campbell, G.S., D.M. Smith, and B.L. Teare. 2007. Application of a Dew Point Method to Obtain the Soil Water Characteristic. Experimental Unsaturated Soil Mechanics: 71–77. doi: 10.1007/3-540-69873-6_7.

Cresswell, H.P., T.W. Green, and N.J. McKenzie. 2008. The Adequacy of Pressure Plate Apparatus for Determining Soil Water Retention. Soil Science Society of America Journal 72(1): 41–49. doi: 10.2136/sssaj2006.0182.

Dane, J.H. and J.W. Hopmans, 2002. 3.3. 2 Laboratory. Methods of Soil Analysis: Part 4 Physical Methods, 5: 675-720.

Feki, M., G. Ravazzani, A. Ceppi, and M. Mancini. 2018. Influence of soil hydraulic variability on soil moisture simulations and irrigation scheduling in a maize field. Agricultural Water Management 202: 183–194. doi: 10.1016/j.agwat.2018.02.024.

Gärdenäs, A.I., J.W. Hopmans, B.R. Hanson, and J. Šimůnek. 2005. Two-dimensional modeling of nitrate leaching for various fertigation scenarios under micro-irrigation. Agricultural Water Management 74(3): 219–242. doi: 10.1016/j.agwat.2004.11.011.

Garg, N.K., and M. Gupta. 2015. Assessment of improved soil hydraulic parameters for soil water content simulation and irrigation scheduling. Irrigation Science 33(4): 247–264. doi: 10.1007/s00271-015-0463-7.

Gavlak, R., R. Horneck, and R.O. Miller. 2005. Particle size analysis: Hydrometer method.

Gee, G.W., A.L. Ward, Z.F. Zhang, G.S. Campbell, and J. Mathison. 2002. The Influence of Hydraulic Nonequilibrium on Pressure Plate Data. Vadose Zone Journal 1(1): 172–178. doi: 10.2113/1.1.172.

van Genuchten, M.Th. 1980. A closed-form equation for predicting the hydraulic conductivity of unsaturated soils. Soil Science Society of America Journal 44: 892–898. https://hwbdocuments.env.nm.gov/Los Alamos National Labs/TA 54/11569.pdf.

Gubiani, P.I., J.M. Reichert, C. Campbell, D.J. Reinert, and N.S. Gelain. 2013. Assessing Errors and Accuracy in Dew-Point Potentiometer and Pressure Plate Extractor Meaurements. Soil Science Society of America Journal 77(1): 19–24. doi: 10.2136/sssaj2012.0024.

Kirste, B., S.C. Iden, and W. Durner. 2019. Determination of the Soil Water Retention Curve around the Wilting Point: Optimized Protocol for the Dewpoint Method. Soil Science Society of America Journal 83(2): 288–299. doi: 10.2136/sssaj2018.08.0286.

van Lier, Q. D. J., E.A.R. Pinheiro, and L. Inforsato. 2019. Hydrostatic equilibrium between soil samples and pressure plates used in soil water retention determination: Consequences of a questionable assumption. Revista Brasileira de Ciencia do Solo 43: 1–14. doi: 10.1590/18069657rbcs20190014.

Parker, N., W.M. Cornelis, K. Frimpong, E. Oppong Danso, E. Bessah, et al. 2021. Short-term effects of rice straw biochar on hydraulic properties and aggregate stability of an Acrisol. Soil Research: 1–31.

Parker, N., and A. Patrignani. 2021. Evaluating Traditional and Modern Laboratory Techniques for Determining Permanent Wilting Point. Kansas Agricultural Experiment Station Research Reports 7(5). doi: 10.4148/2378-5977.8080.

Rahardjo, H., A. Satyanaga, H. Mohamed, S.C. Yee Ip, and R.S. Shah. 2019. Comparison of Soil–Water Characteristic Curves from Conventional Testing and Combination of Small-Scale Centrifuge and Dew Point Methods. Geotechnical and Geological Engineering 37(2): 659–672. doi: 10.1007/s10706-018-0636-2.

Reynolds, W.D. and D.E. Elrick, 2002. 3.4. 3.3 Constant head well permeameter (vadose zone). Methods of Soil Analysis: Part 4 Physical Methods, 5: 844-858.

Richards, L.A. and Fireman, M., 1943. Pressure-plate apparatus for measuring moisture sorption and transmission by soils. Soil Science, 56(6):395-404..

Richards, L.A. 1948. Porous plate apparatus for measuring moisture retention and transmission by soil. Soil Science 66(2): 105–110. doi: 10.1097/00010694-194808000-00003.

Richards, L.A. 1965. Physical condition of water in soil. Methods of Soil Analysis, Part 1: Physical and Mineralogical Properties, Including Statistics of Measurement and Sampling: 128–152. doi: 10.2134/agronmonogr9.1.c8.

Richards, L.A., and G. Ogata. 1961. Psychrometric Measurements of Soil Samples Equilibrated on Pressure Membranes1. Soil Science Society of America Journal 25(6): 456. doi: 10.2136/sssaj1961.03615995002500060012x.

Romano, N., and A. Santini. 2002. Water Retention and Storage: Field. Methods of Soil Analysis (January 2014): 739–758.

Saxton, K.E., and W.J. Rawls. 2006. Soil Water Characteristic Estimates by Texture and Organic Matter for Hydrologic Solutions. Soil Science Society of America Journal 70(5): 1569–1578. doi: 10.2136/sssaj2005.0117.

Schaap, M.G., F.J. Leij, and M.T. van Genuchten. 2001. Rosetta: A computer program for estimating soil hydraulic parameters with hierarchical pedotransfer functions. Journal of Hydrology 251(3–4): 163–176. doi: 10.1016/S0022-1694(01)00466-8.

Schelle, H., L. Heise, K. Jänicke, and W. Durner. 2013. Water retention characteristics of soils over the whole moisture range: A comparison of laboratory methods. European Journal of Soil Science 64(6): 814–821. doi: 10.1111/ejss.12108.

Schindler, U., W. Durner, G. von Unold, and L. Müller. 2010. Evaporation Method for Measuring Unsaturated Hydraulic Properties of Soils: Extending the Measurement Range. Soil Science Society of America Journal 74(4): 1071–1083. doi: 10.2136/sssaj2008.0358.

Skaggs, R.W. 1978. A water management model for shallow water table soils.

Solone, R., M. Bittelli, F. Tomei, and F. Morari. 2012. Errors in water retention curves determined with pressure plates: Effects on the soil water balance. Journal of Hydrology 470–471: 65–74. doi: 10.1016/j.jhydrol.2012.08.017.

Stackman, W.P., Valk, G.A., van der Harst, G.G., 1969. Determination of soil moisture retention curves: I. Sand box apparatus. In: Range pF 0 to 2.7. Wageningen, ICW, 119.

USDA-NRCS. 1996. Soil Quality Resource Concerns: Compaction USDA Natural Resources Conservation Service.

Vereecken, H., M. Weynants, M. Javaux, Y. Pachepsky, M.G. Schaap, et al. 2010. Using Pedotransfer Functions to Estimate the van Genuchten-Mualem Soil Hydraulic Properties: A Review. Vadose Zone Journal 9(4): 795–820. doi: 10.2136/vzj2010.0045.

Vogel, T., H.H. Gerke, R. Zhang, M.T. van Genuchten, and G.E. Brown. 2000. Modeling flow and transport in a two-dimensional dual-permeability system with spatially variable hydraulic properties.

Wyatt, B.M., T.E. Ochsner, C.A. Fiebrich, C.R. Neel, and D.S. Wallace. 2017. Useful Drainage Estimates Obtained from a Large-Scale Soil Moisture Monitoring Network by Applying the Unit-Gradient Assumption. Vadose Zone Journal 16(6): vzj2017.01.0016. doi: 10.2136/vzj2017.01.0016.

Chapter 5 - General Conclusions

The Kansas Mesonet is an automated network of about 62 environmental monitoring stations spread across the State of Kansas to monitor real-time essential weather and soil variables in the region. While the weather data are often used for agricultural outreach programs and research activities, lack of information on the physical properties of the soils at each mesonet station has limited the usefulness of the soil moisture and soil temperature data in advancing the understanding of soil water and soil thermal processes at the mesoscale level. Thus, developing a soil physical property database for the Kansas Mesonet is of great importance in promoting the usefulness of the soil moisture and soil temperature observations. In this dissertation, we tackled three central challenges to improve mesoscale soil moisture monitoring using the Kansas Mesonet: i) we developed a new database of soil physical property for each station of the Kansas Mesonet that monitors soil moisture, ii) reconstructed precipitation events using changes in rootzone soil water storage for precipitation quality control and quality assurance in mesoscale networks, and ii) investigated the compatibility between soil water retention curves measured using old laboratory methods based on suction table, pressure cells, and pressure plate and water retention curves measured using newer methods based on mini-tensiometers and dewpoint water potential meter.

In the first study, we developed a site and sensor depth-specific soil physical property database for 40 out of the 62 stations monitoring root-zone soil moisture in the Kansas Mesonet. The resulting database comprises 14 depth-specific soil hydraulic properties and three soil thermal properties for all the 40 stations studied. Our soil database captured eight out of the 12 soil textural classes, which were mainly fine soils that occupied 93% of the 320 samples analyzed. Silty clay loam, silt loam, and silty clay soils were the most represented fine soils in

our database. Sandy loam and sandy clay loam were the least represented soils and also the only coarse-textured soils in our database. The average range of soil bulk density of our database was from 1.33 g cm^{-3} to 1.67 1.33 g cm^{-3}. The median saturated hydraulic conductivity for our soil textural classes varied from 0.52 to 47.1 cm d^{-1}, while the average range of plant available water capacity was from 0.13 cm^3 cm^{-3} in clay to 0.25 cm^3 cm^{-3} in silt loam. Our soil physical property database enabled us to discover improved calibration models for the Kansas Mesonet soil moisture sensors, which reduced the uncertainty in the soil moisture observations by 29% after using calibration models that incorporate both electrical conductivity and dielectric permittivity. These new models will improve estimates of root zone soil water storage that can be used to better assess the inventory of soil water across the state of Kansas. This database has great potential to expand the usage of the Kansas Mesonet soil moisture and temperature observations for diverse applications at the mesoscale level, including drought monitoring, groundwater recharge estimations, and urban planning.

The second study proposed a new approach for reconstructing hourly precipitation events in mesoscale stations using co-located changes in rootzone soil water storage. Precipitation was calculated as the sum of the hourly change in soil water storage and the approach was validated using 2497 precipitation events across 30 stations of the Kansas Mesonet equipped with co-located rain gauges and soil moisture sensors. The use of changes in soil water storage proved effective as a qualitative method for flagging precipitation events with an accuracy of 82% and as a quantitative method with an MAE of 8.0 mm for reconstructing precipitation events >7.6 mm. On a station-by-station basis, the soil moisture approach resulted more accurate than the nearest neighbor interpolation method at stations with >10 km distance from their closest surrounding station. Our results offer a great opportunity to use the concurrent changes in soil

moisture during precipitation events as an alternative approach for operational quality control and quality assurance of precipitation events in mesoscale networks.

The third study investigated whether traditional and modern methods are interchangeable for measuring soil water retention curves in laboratory conditions. The traditional method consists of a suction table, pressure cells, and pressure plate, whereas the modern method consists of mini-tensiometers and water potential meter. The study revealed that overall, the traditional suction table and pressure cells, and the modern mini-tensiometer produce similar results at the wet end of the retention curve. The traditional pressure plate and modern water potential meter method also produce similar results at the dry-end of the water retention curve in sandy loam soils. In fine-textured soils, however, the traditional pressure place could result in up to 120% higher residual water content and 25% higher water content at permanent wilting point than the modern method, which in effect could result in up to 47% less plant available water capacity using the traditional method. Overall, the findings from our study indicate that the choice of water retention measurement technique, regardless of whether it is a modern or traditional method, could have pronounced impacts at the dry-end of the retention curve in clayey soils, but does not affect sandy soils.

Appendix A - Supplemental Materials for Chapter 2

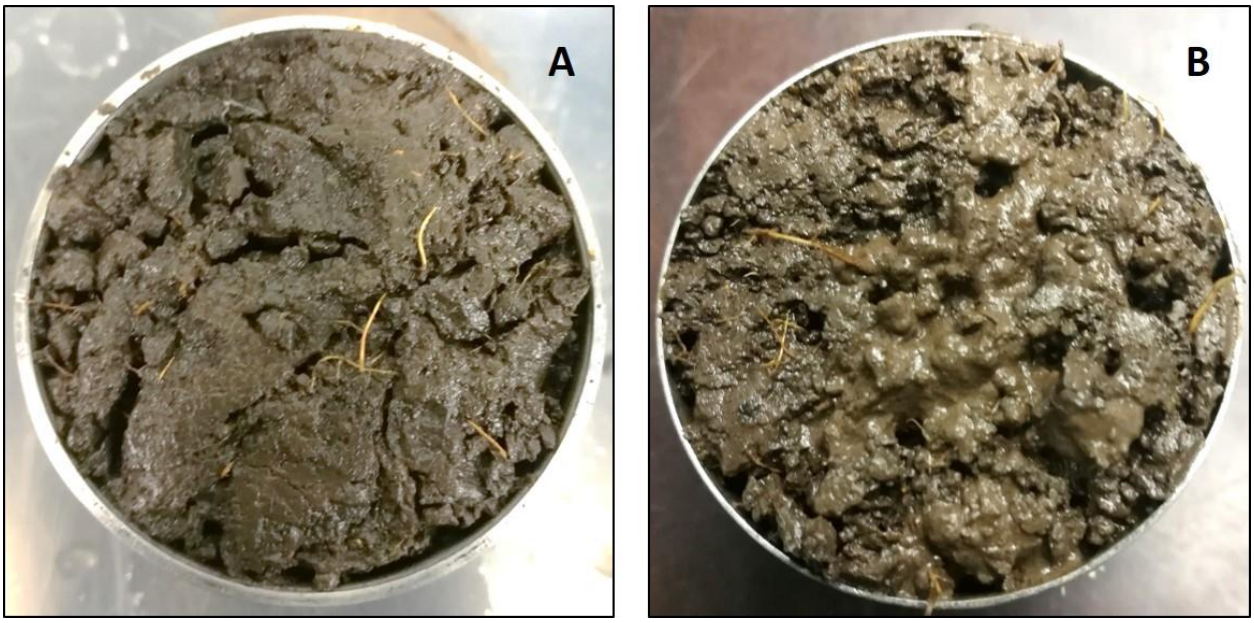

Figure A1. Example of soil samples with high saturated hydraulic conductivity (K_S) resulting from A) cracks, root channels, and gaps between soil and walls of the sample ring in silty clay soil at 5 cm depth in Overbrook station and B) macropores left by the activity of worms and root channels in a silty clay loam at 5 cm depth in Miami station. Measured K_S is 43098 cm d^{-1} for the soil in Overbrook station, and 9500 cm d^{-1} for the soil in Miami station.

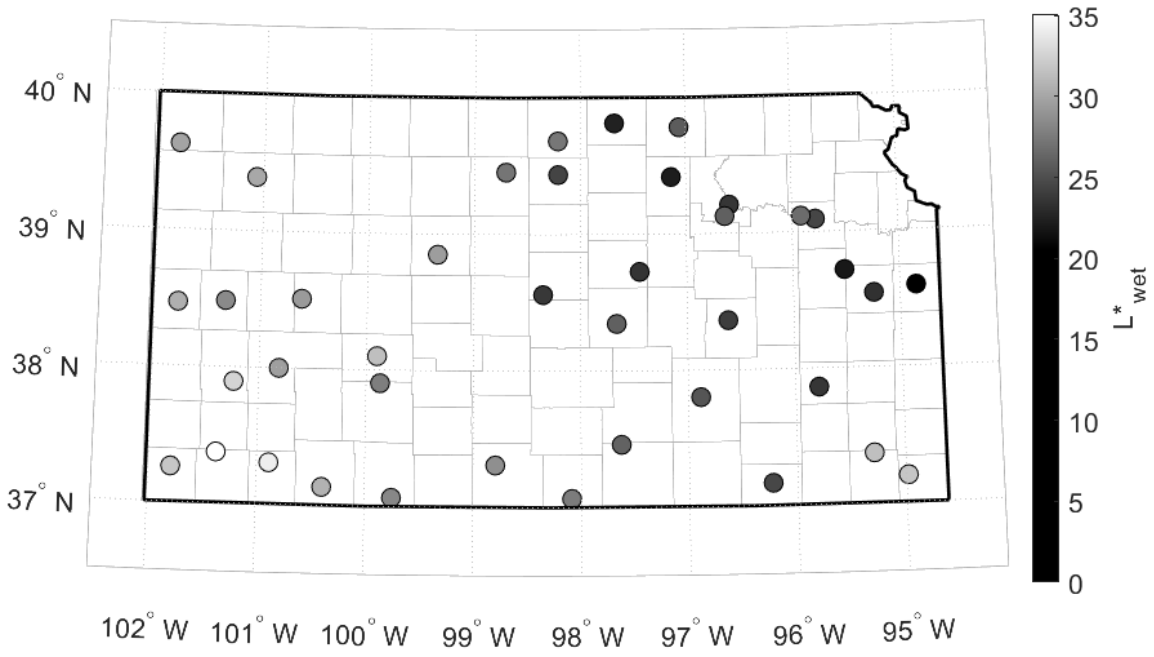

Figure A2. The pattern of soil blackness (L^*_{wet}) at the top 5 cm depth across the state of Kansas. The figure shows increasing soil blackness across the state of Kansas from west to east, following the organic matter gradient shown in Figure 2.7 in the text.

Appendix B - Supplemental Materials for Chapter 3

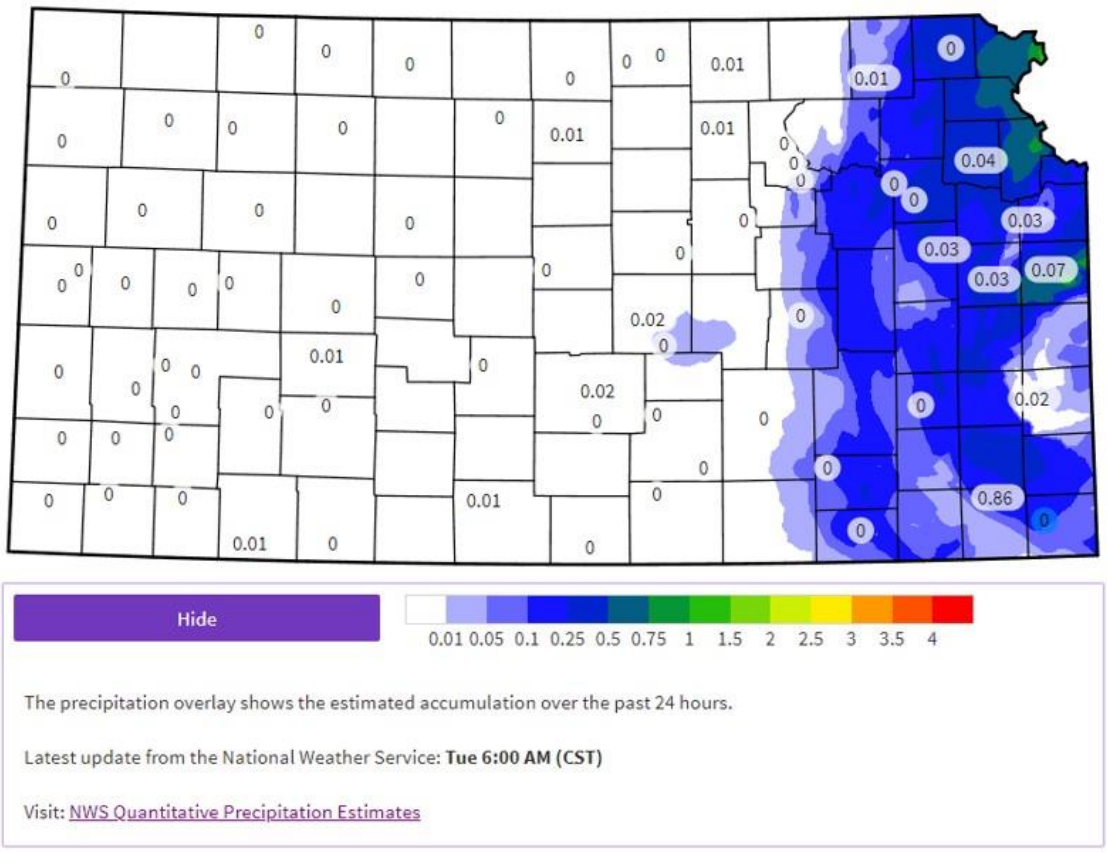

Figure B1. Map of precipitation daily totals from the US National Weather Service multi-sensor gridded precipitation product at 4-km spatial resolution and measured precipitation amounts at stations of the Kansas Mesonet on 12 October 2021. This figure provides supporting evidence that rain gauges and gridded precipitation products do not always agree at the point level. In this case, a total of nine rain gauges recorded no measurable precipitation in areas where the gridded precipitation product indicated precipitation. Source: Kansas Mesonet: https://mesonet.k-state.edu

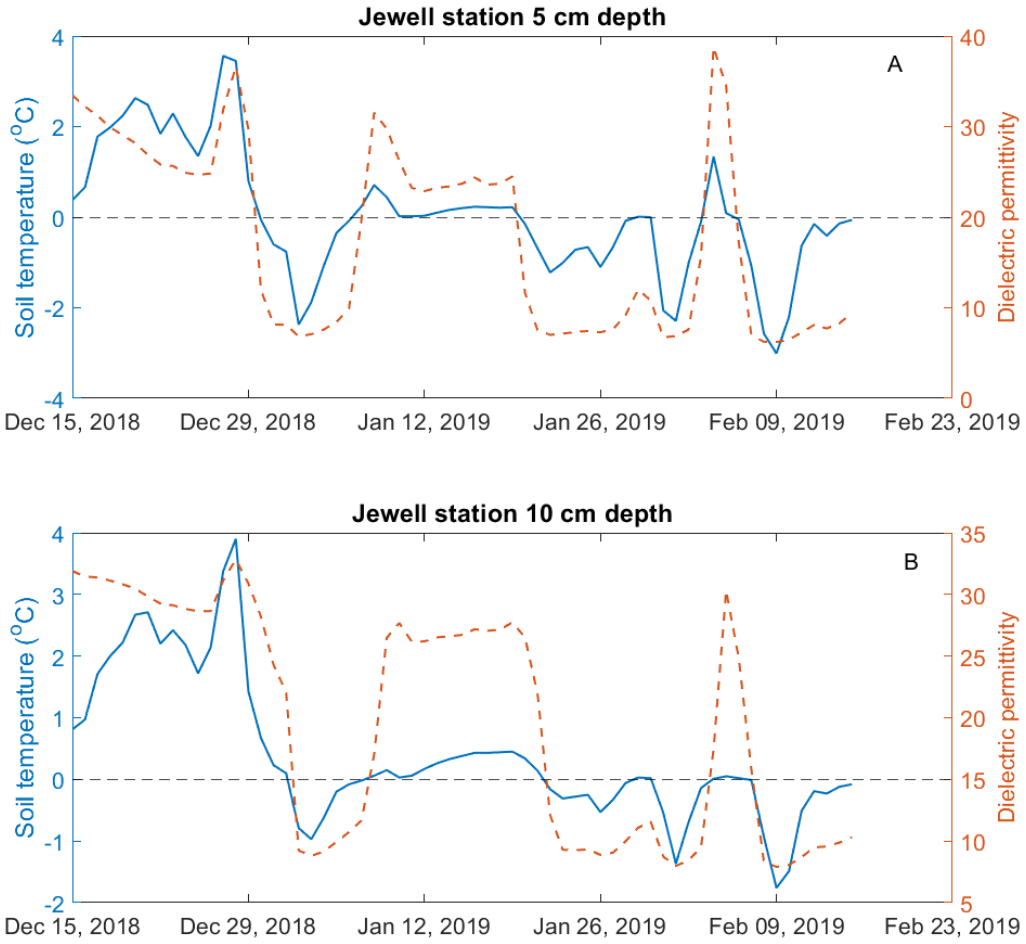

Figure B2. Changes in soil temperature (blue solid line) and the corresponding changes in apparent bulk dielectric permittivity (orange dashed line) at the A) 5 cm and the B) 10 cm soil moisture sensor at the Jewell station of the Kansas Mesonet from 15 December 2018 to 15 February 2019. This example illustrates that soil dielectric permittivity drops sharply as soil temperature approaches freezing conditions, and thus, soil moisture sensors that use dielectric permittivity as a proxy for volumetric water content are sensitive to near-freezing and freezing conditions. To be conservative, in our study we did not consider precipitation events and soil moisture observations that occurred with soil temperatures <1 Celsius.

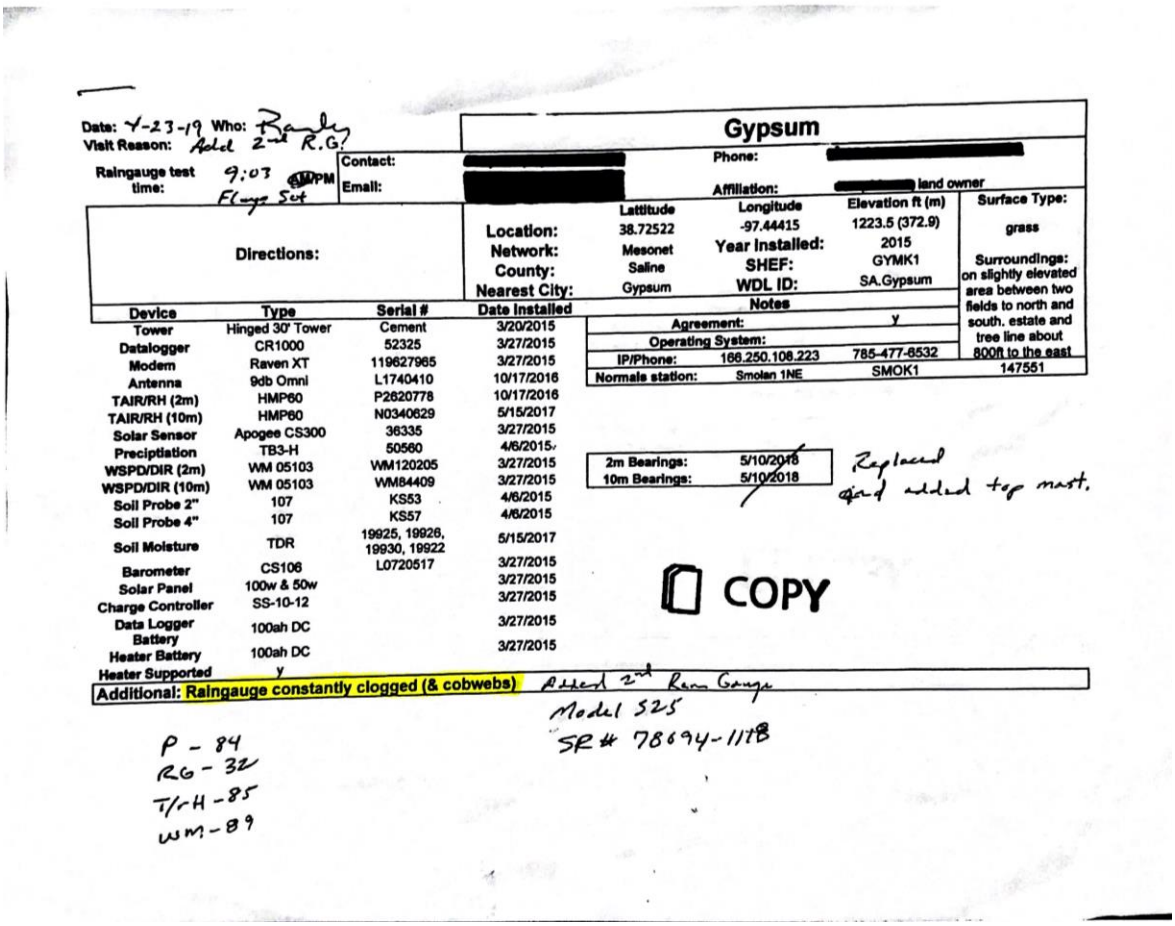

Date: 4-23-19 Who: Randy
Visit Reason: Added 2nd R.G.

Raingauge test time: 9:07 AM/PM
Flange Set

Contact: [redacted]
Email: [redacted]
Phone: [redacted]
Affiliation: [redacted] land owner

Gypsum

Directions:

	Latitude	Longitude	Elevation ft (m)	Surface Type:
Location:	38.72522	-97.44415	1223.5 (372.9)	grass
Network:	Mesonet	Year Installed:	2015	
County:	Saline	SHEF:	GYMK1	Surroundings: on slightly elevated area between two fields to north and south. estate and tree line about 800ft to the east
Nearest City:	Gypsum	WDL ID:	SA.Gypsum	

Device	Type	Serial #	Date Installed
Tower	Hinged 30' Tower	Cement	3/20/2015
Datalogger	CR1000	52325	3/27/2015
Modem	Raven XT	119627985	3/27/2015
Antenna	9db Omni	L1740410	10/17/2016
TAIR/RH (2m)	HMP60	P2620778	10/17/2016
TAIR/RH (10m)	HMP60	N0340629	5/15/2017
Solar Sensor	Apogee CS300	36335	3/27/2015
Preciptiation	TB3-H	50560	4/6/2015
WSPD/DIR (2m)	WM 05103	WM120205	3/27/2015
WSPD/DIR (10m)	WM 05103	WM84409	3/27/2015
Soil Probe 2"	107	KS53	4/6/2015
Soil Probe 4"	107	KS57	4/6/2015
Soil Moisture	TDR	19925, 19926, 19930, 19922	5/15/2017
Barometer	CS106	L0720517	3/27/2015
Solar Panel	100w & 50w		3/27/2015
Charge Controller	SS-10-12		3/27/2015
Data Logger Battery	100ah DC		3/27/2015
Heater Battery	100ah DC		3/27/2015
Heater Supported	y		

Notes

Agreement:		y
Operating System:		
IP/Phone:	166.250.108.223	785-477-6532
Normals station:	Smolan 1NE	SMOK1

2m Bearings:	5/10/2018
10m Bearings:	5/10/2018

Replaced and added top mast.

COPY

Additional: Raingauge constantly clogged (& cobwebs) Added 2nd Rain Gauge Model 525 SR# 78694-1178

P - 84
RG - 32
T/rH - 85
WM - 89

Figure B3. Station visit sheet showing technician notes about the clogged pluviometer at the Gypsum station on 22 April 2019. Private information about the landowner was removed for privacy.

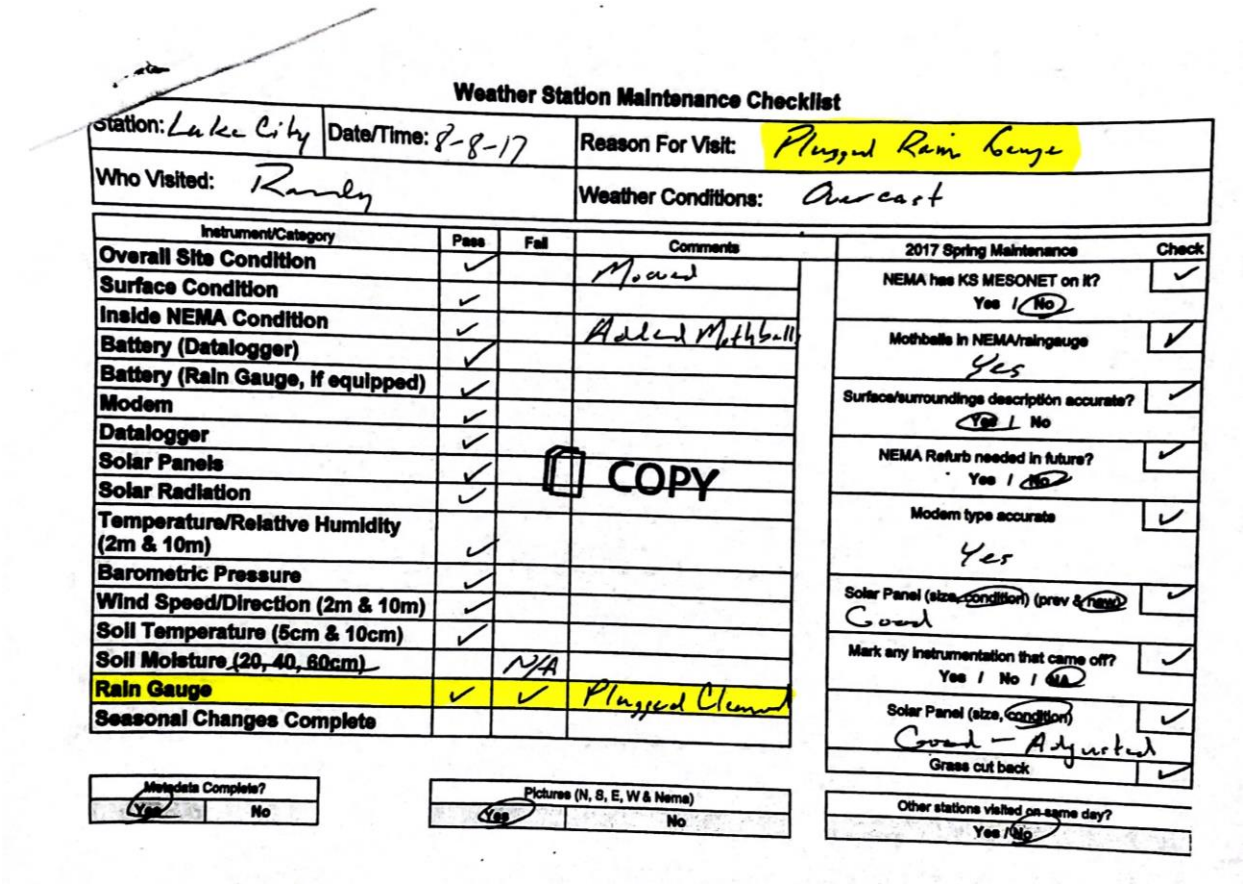

Weather Station Maintenance Checklist

Station: Lake City | Date/Time: 8-8-17 | Reason For Visit: Plugged Rain Gauge

Who Visited: Randy | Weather Conditions: Overcast

Instrument/Category	Pass	Fail	Comments
Overall Site Condition	✓		Mowed
Surface Condition	✓		
Inside NEMA Condition	✓		Added Mothballs
Battery (Datalogger)	✓		
Battery (Rain Gauge, if equipped)	✓		
Modem	✓		
Datalogger	✓		
Solar Panels	✓		
Solar Radiation	✓		
Temperature/Relative Humidity (2m & 10m)	✓		
Barometric Pressure	✓		
Wind Speed/Direction (2m & 10m)	✓		
Soil Temperature (5cm & 10cm)	✓		
Soil Moisture (20, 40, 60cm)		N/A	
Rain Gauge	✓	✓	Plugged Cleaned
Seasonal Changes Complete			

2017 Spring Maintenance	Check
NEMA has KS MESONET on it? Yes / (No)	✓
Mothballs in NEMA/raingauge: Yes	✓
Surface/surroundings description accurate? (Yes) / No	✓
NEMA Refurb needed in future? Yes / (No)	✓
Modem type accurate: Yes	✓
Solar Panel (size, condition) (prev & new): Good	✓
Mark any instrumentation that came off? Yes / No / (NA)	✓
Solar Panel (size, condition): Good – Adjusted	✓
Grass cut back	✓

Metadata Complete? (Yes) / No

Pictures (N, S, E, W & Nema) (Yes) / No

Other stations visited on same day? Yes / (No)

COPY

Figure B4. Station visit sheet showing technician notes about the clogged pluviometer at the Lake City station in July 2017.

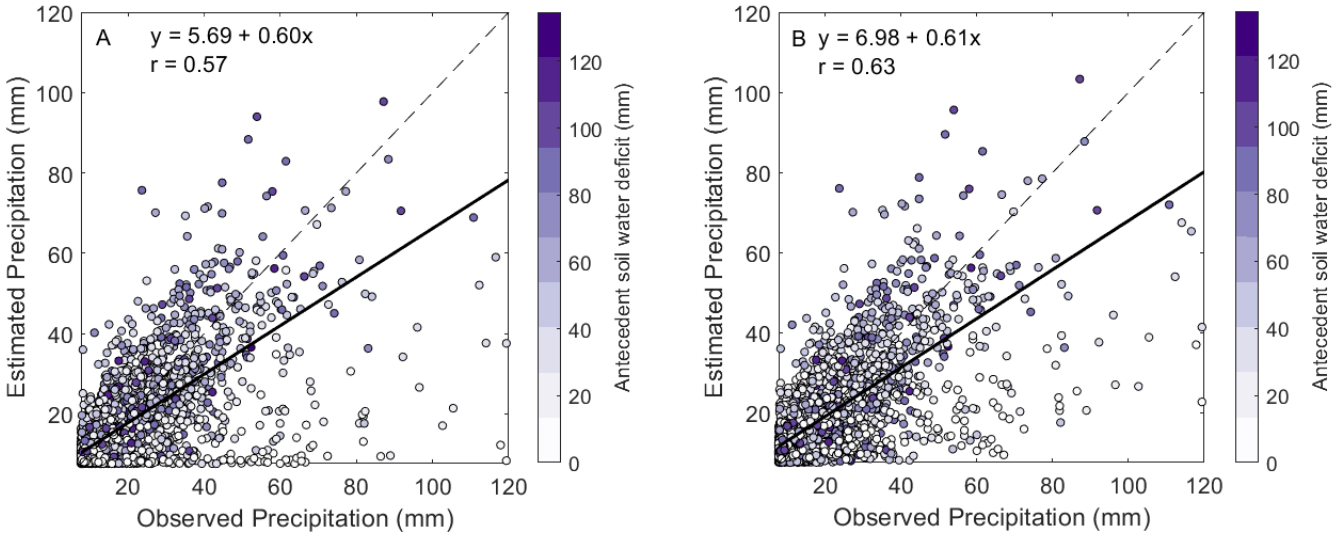

Figure B5. Comparison of observed and predicted precipitation amount using A) only the sum of hourly differences in soil water storage (ΔS), and B) sum of hourly differences in soil water storage + drainage (ΔS+D) for precipitation events exceeding 7.6 mm (N = 2497 events) across 28 stations of the Kansas Mesonet monitoring soil moisture from 15 May 2017 to 31 December 2020. For using only ΔS, RMSE =14.1 mm, MAE = 8.0 mm, and MBE = -3.0 mm and for using ΔS+D, RMSE = 13.0 mm, MAE = 7.7 mm, and MBE = -1.3 mm. The dash lines represent the 1:1 line and the solid lines represent fitted linear models (in both cases the linear model had $p<0.001$).

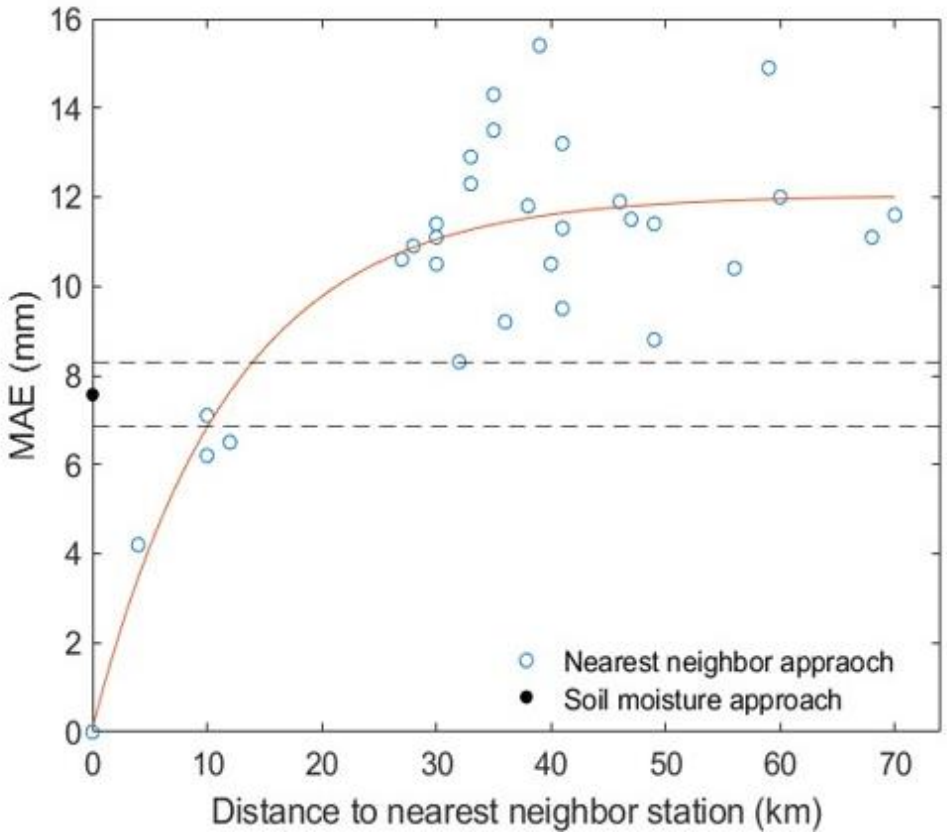

Figure B6. Alternative representation of MAE in Table 2. The black marker is the average of the soil moisture-based approach and the dashed lines represent the 2±SE of the mean. The intersection of the dashed lines and the red line is at 10 and 14 km. We force the interest to 0,0 since at the same point the error is just that of the instrument (negligible for this study). The black marker is at a distance of 10 meters from the station, which is similar to the layout of the stations, although hard to see in the figure due to the scale of the *x*-axis.

Supplemental code. An example code in CRBasic for implementing the proposed soil moisture approach onboard data loggers for quality controlling precipitation events in in situ networks.

```
Example Code
'CR1000
'Declare Variables
Public BattV
Public PTemp_C
Public VWC_5
Public VWC_10
Public VWC_20
Public VWC_50
Public Rain_obs
Public Rain_pred
Public Rain_flag As Boolean
Public SWS_previous
Public SWS_mm
Public SWS_change_mm
Const Interception = 7.6

'Declare Units
Units BattV = Volts
Units PTemp_C = Deg C
Units VWC_5 = m^3/m^3
Units VWC_10 = m^3/m^3
Units VWC_20 = m^3/m^3
Units VWC_50 = m^3/m^3
Units Rain_obs = mm
Units Rain_pred = mm
Units SWS_previous = mm
Units SWS_mm = mm
Units SWS_change_mm = mm

'Define Data Tables
DataTable(Table1,True,-1)
       DataInterval(0,1,Hr,10)
       Average(1,VWC_5,FP2,False)
       Average(1,VWC_10,FP2,False)
       Average(1,VWC_20,FP2,False)
       Average(1,VWC_50,FP2,False)
       Totalize(1,Rain_obs,FP2,False)
       Totalize(1,Rain_pred,FP2,False)
       Sample(1,Rain_flag,Boolean)
       Average(1,SWS_previous,FP2,False)
       Average(1,SWS_mm,FP2,False)
       Totalize(1,SWS_change_mm,FP2,False)
EndTable

'Define data tables
DataTable(Table2,True,-1)
       DataInterval(0,1,Min,10)
       Minimum(1,BattV,FP2,False,False)
EndTable

'Main Program
BeginProg
       'Main Scan
       Scan(1,Hr,1,0)

       'Default CR1000 Datalogger Battery Voltage measurement
       Battery(BattV)
```

```
    'Default CR1000 Datalogger Wiring Panel Temperature measurement
    PanelTemp(PTemp_C,_60Hz)

    'CS650/655 Water Content Reflectometer measurements 'VWC'
    SDI12Recorder(VWC_5,1,"0","M4!",1,0,-1)
    SDI12Recorder(VWC_10,1,"1","M4!",1,0,-1)
    SDI12Recorder(VWC_20(),1,"2","M4!",1,0,-1)
    SDI12Recorder(VWC_50(),1,"3","M4!",1,0,-1)

    'TE525MM/TE525M Rain Gauge measurement
    PulseCount(Rain_obs,1,1,2,0,0.1,0)

    'Use equation 2 to compute current total soil water storage
  SWS_mm = VWC_5*50+(VWC_5+VWC_10)/2*50+(VWC_10+VWC_20)/2*100+(VWC_20+VWC_50)/2*300

  'Compute the change in soil profile water storage
  SWS_previous = Table1.SWS_mm_Avg(1,1)
  SWS_change_mm=SWS_mm -  SWS_previous

  'Set change in storage < 1 mm to 0
  If SWS_change_mm <1 and Rain_obs = 0 Then
     SWS_change_mm = 0
     Rain_flag = False
     Rain_pred = 0

  ElseIf SWS_change_mm >=1 AND Rain_obs = 0 Then
    Rain_flag = True
    Rain_pred = SWS_change_mm + Interception

  ElseIf Rain_obs >0 and Rain_obs <7.6 Then
    Rain_flag = False
    Rain_pred = 0

  Else
    Rain_flag = False
    Rain_pred = SWS_change_mm + Interception

  EndIf

  'Call Data Tables and Store Data
  CallTable Table1
  CallTable Table2

 NextScan
EndProg
```